technische universität
dortmund

Role of Aqueous Two-Phase Systems in Modulating the Kinetics and Dynamics of Biological Processes

Dissertation

For the achievement of the academic degree of the
Doctor rerum naturalium
(Dr. rer. nat.)

submitted to
TU Dortmund University
Faculty of Chemistry and Chemical Biology

by

Sudeshna Banerjee
born in Raniganj, India

Dortmund 2020

technische universität
dortmund

Die Rolle wässriger Zweiphasensysteme bei der Modulation der Kinetik und Dynamik Biologischer Prozesse

Dissertation

zur Erlangung des akademischen Grades
Doctor rerum naturalium
(Dr. rer. nat.)

eingereicht bei der
Technischen Universität Dortmund
Fakultät für Chemie und Chemische Biologie

vorgelegt von

Sudeshna Banerjee
geboren in Raniganj, Indien

Dortmund 2020

Erklärung/Declaration

The work described in this Dissertation was performed from July 2016 to December 2019 at the Faculty of Chemistry and Chemical Biology, TU Dortmund University under the guidance of Prof. Dr. Roland Winter.
I hereby declare that I performed the work presented independently and did not use any other but the indicated aids.

Die in dieser Dissertation beschriebene Arbeit wurde von July 2016 bis December 2019 der Fakultät für Chemie und Chemische Biologie der Technischen Universität Dortmund unter der Leitung von Prof. Dr. Roland Winter durchgeführt.
Hiermit versichere ich an Eides statt, dass ich die vorliegende Arbeit selbstständig und nur mit den angegebenen Hilfsmitteln angefertigt habe.

Dortmund, January 2020
Sudeshna Banerjee

Dissertation submitted on:

Main Supervisor: Prof. Dr. Roland Winter

Examination Board

First Examiner: Prof. Dr. Roland Winter
Physical Chemistry, CCB, TU Dortmund

Second Examiner: Prof. Dr. Claus Czeslik
Physical Chemistry, CCB, TU Dortmund

Dedicated to my parents

ACKNOWLEDGEMENT

Firstly, I would like to express my sincere and deepest gratitude to my supervisor, **Prof. Dr. Roland Winter** for the continuous support throughout my doctorate research, for his patience, advices, enthusiasm as well as for numerous fruitful discussions. I would like to extend by gratefulness to him for giving me an opportunity to work in his lab due to which I gained exposure to several new research areas. I value his effort in correcting the draft of papers, conference posters and my thesis despite his busy schedule. I sincerely thank him for lifting me up during my failure in doctorate research and motivating me throughout to achieve the final goal. Thank you for showing the trust and faith on me and for being an excellent mentor.

I sincerely acknowledge **Andrea Jeworrek** for the constant friendly support and help with all kind of administrative problems during the three years. She always responded happily to every query of mine. I will cherish the funny moments spent with her inside and outside the lab. I am also very grateful to **Simone Möbitz** for quick ordering of the chemicals and helping me with the experiments in S1 lab. Many thanks to **Bertina Schuppan** for her help in the lab.

A special thanks to **Dr. Rosario Oliva** for helping me in every possible way in my experiments. I thank you for keeping your office door open and being available always whenever I needed scientific and practical advice. I learnt a lot from your scientific knowledge. I appreciate **Dr. Vitor Schuabb** for introducing me to the stopped-flow instrument. I thank **Michel Jaworek** for his help with the high-pressure stopped-flow instrument and **Hasan Cinar** for his help with the high-pressure phase contrast microscopy.

I sincerely thank **Prof. Dr. Claus Czeslik** for being there always for scientific discussions and his kind help in the experimental and instrumental difficulties in the lab. I also want to thank him for examining my thesis and agreeing to be my second supervisor. I wish to thank **Dr. Artem Levin** for his assistance with the stopped-flow instrument. My heartfelt thanks to **Loana Arns** who has helped me survive my three years in Germany. Be it scientific, administrative or things related to daily life, she has helped me in every way, and I thank you for the countless funny moments in the lab. I would also like to thank all other former and current members of our **PC I** group for a good and constructive working atmosphere with special mention to **Dr. Melanie Berghaus, Dr. Satyajit Patra** and **Dr. Mridula Dwivedi** for helping me in my research during the initial days. All members of the mechanical and glass workshop are acknowledged for their help. **Magiliny Manisegaran** is acknowledged for proof-reading and correcting the ‘Zusammenfassung’ part of my thesis.

I am thankful to **TU Dortmund University** for providing me the funding and resources for my doctorate research.

I am profoundly grateful to **Dr. Anirban Chakraborty** for emotional and mental support. I would also like to thank all my family and friends with special mention to **Atrayee, Sayani, Suraiya** and **Payel** for sticking with me during my tough times. Last but definitely not the least, I would like to express my sincere thanks to **my parents** for their unconditional love and support without which this thesis would not have been possible.

I thank **Almighty** for always being there with me.

Abbreviations

AAF-AMC	Ala-Ala-Phe-7-amido-4-methylcoumarin
AMC	7-amido-4-methylcoumarin
ANS	1-anilino-8-naphthalene
α-CT	α-chymotrypsin
Å	Angström
ATPS	Aqueous Two-Phase System
ADC	Apparent translational diffusion coefficient
a.u.	Arbitrary units
BSA	Bovine Serum Albumin
Cr	Crowding
CD	Circular dichroism
CM	Center of mass
Dex	Dextran
DMSO	Dimethyl sulfoxide
Da	Dalton
e.g.	Exempli gratia
etc.	Et cetera
E. coli	*Escherichia coli*
Eq.	Equation
ES	Enzyme-Substrate complex
FITC	Fluorescein isothiocyanate
FTIR	Fourier-transform infrared spectroscopy
Fig.	Figure
HSA	Human Serum Albumin
HOMO	Highest Occupied Molecular Orbital
HHP	High hydrostatic pressure
i.e.	Id est
ITC	Isothermal Titration Calorimetry
IC	Internal conversion
ISC	Intersystem crossing
LLPS	Liquid-liquid phase separation
LHCPL	Left-handed circularly polarized light

LUMO	Lowest Unoccupied Molecular Orbital
LLE	Liquid-Liquid Extraction
MD	Molecular dynamics
M.W	Molecular weight
min	Minute
OPL	Optical path length
OPD	Optical path difference
pH	Potential of Hydrogen
pI	Isoelectric point
PMT	Photomultiplier tube
RHCPL	Right-handed circularly polarized light
RNA	Ribonucleic acid
SAAPPpNA	*N*-succinyl-L-alanyl-L-alanyl-L-prolyl-L-phenylalanine-*p*-nitroanilide
SASA	Solvent accessible surface area
s	Second
SPT	Scaled-particle theory
SF	Stopped-Flow
Trp	Tryptophan
T	Temperature
TLL	Tie line length
UV/Vis	Ultraviolet–visible
VDW	Van der Waals
VR	Vibrational relaxation
wt%	Weight percentage
2D-IR	Two-dimensional infrared
$\boldsymbol{\gamma}$	Interfacial tension
°C	Degree Celsius

Table of contents

Abstract

Liquid-liquid phase separation (LLPS) phenomena have contributed immensely to the field of cell biophysics and cell biology in providing rational answers to the process of formation of membraneless organelles. These membraneless organelles play a vital role in understanding the origin of life in terms of cellular compartmentalisation. An increasing number of proteins and protein-nucleic acid mixtures has been shown to undergo LLPS at high concentrations forming two liquid phases - a protein-rich phase and a phase with diluted protein concentration. The tendency of LLPS to concentrate proteins comes with an added danger of aggregation, however, which is an issue in many human diseases such as amyloid formation in Alzheimer's disease or synuclein plaques in Parkinson's disease.

High Hydrostatic Pressure (HHP) is a sophisticated tool to yield novel information on the free-energy and conformational landscape of biomolecules. Further, Earth being a predominantly high-pressure region makes it imperative to use this tool to understand the adaptability of piezophiles. However, the combined effect of LLPS and HHP on biological reactions and cellular processes, such as enzyme kinetics and ligand binding, has yet not been experimentally determined. A part of the thesis explores the combined effects of an aqueous two-phase system (ATPS) formed by the synthetic polymers polyethylene glycol (PEG) and dextran invoking LLPS and pressure on the enzymatic hydrolysis reaction of the substrate AAF-AMC catalysed by the proteolytic enzyme α-CT. In general, ATPS affects the enzymatic reactions in a variety of ways, such as partitioning in different or the same phases, increasing the effective concentration of solutes and thus inducing an excluded volume effect. Pressure, on the other hand, can increase the reaction rate and, alter the substrate specificity and stereoselectivity of an enzyme by choosing the product with a smaller partial volume, increases conformational flexibility. In this work it was observed that HHP did not have any marked effect on the kinetic constants in the ATPS, which was not possible to explain by simple steric crowding. Additional contributions, such as changes in water activity and non-specific weak interactions with ATPS components have to be considered to explain the results obtained. These results are important for understanding the use of LLPS and ATPS in modulating an enzymatic reaction for biotechnological use.

The other part of this thesis focusses on the combined effects of pressure and ATPS on a ligand binding reaction, i.e., on the binding phenomenon between Bovine Serum Albumin (BSA) and 1-anilino-8-naphthalene (ANS) which was monitored through fluorescence spectroscopy. The results indicate that unlike buffer where the binding affinities to the three equivalent and independent binding sites of BSA could not be distinguished, the presence of ATPS gives rise

to two binding modes, thus allowing to differentiate between weak and strong binding of the three sites. This result can be explained by considering soft interactions between the binding sites on BSA with the crowder molecules, such as PEG and dextran. Upon pressurization, the binding affinities of all binding sites decrease, which can be due to the unfavourable effect of pressure on hydrophobic interactions as well as a volume change due to release of water molecules and creation of void volume upon binding. These results also demonstrate that pressure dependent studies are able to reveal differences in binding sites of ligands, owing to the high accuracy by which volume changes can be determined.

Zusammenfassung

Das Phänomen der *liquid-liquid phase separation* (*LLPS*) hat einen wesentlichen Beitrag zur Zellbiophysik und Zellbiologie geleistet, indem es Antworten auf den Bildungsprozess membranloser Organellen lieferte. Diese membranlosen Organellen spielen eine entscheidende Rolle für das Verständnis des Ursprungs des Lebens im Hinblick auf die Zellteilung. Es wurde gezeigt, dass eine zunehmende Anzahl von Proteinen und Protein-Nucleinsäure-Mischungen *LLPS* in hohen Konzentrationen eingehen, wobei zwei flüssige Phasen gebildet werden - eine proteinreiche Phase und eine Phase mit verdünnter Proteinkonzentration. Die Tendenz zur LLPS, könnte zusätzlich zur Aggregationen führen, die das Hauptproblem bei vielen Erkrankungen des Menschen ist, wie die Amyloidbildung bei Alzheimer oder Synucleinplaques bei Parkinson.

Die Nutzung hohen hydrostatischen Druckes (*High Hydrostatic Pressure*, *HHP*) ist eine hochentwickelte Methode zur Untersuchung der freien Energie und der Konformationslandschaft von Biomolekülen. Viele Regionen der Erde stehen vorwiegend unter hohem Druck. Daher spielt die Untersuchung dieses Parameters für das Verständnis vieler biologischen Systeme, wie z.B. die Anpassungsfähigkeit von Piezophilen, eine wichtige Rolle. Die kombinierte Wirkung von *LLPS* und *HHP* auf zelluläre Prozesse wie Enzymkinetik und liganden bindung, wurde jedoch noch nicht experimentell bestimmt. Ein Teil dieser Arbeit erforscht die kombinierten Effekte eines wässrigen Zweiphasensystems (*Aqueous Two-Phase System*, *ATPS*), das aus den synthetischen Polymeren Polyethylenglykol (PEG) und Dextran besteht, *LLPS* und Druckes auf die Hydrolysereaktion des Substrates AAF-AMC, welche durch das proteolytische Enzym α-CT katalysiert wird. Im Allgemeinen beeinflusst *ATPS* die enzymatischen Reaktionen auf vielfältige Weise, wie z.B. durch Aufteilung in verschiedene oder gleiche Phasen, durch Erhöhung der effektiven Konzentration der gelösten Stoffe, welle letztendlich auf einem ausgeschlossenen Volumeneffect beruht. Der Parameter Druck kann andererseits die Substratspezifität und Stereoselektivität eines Enzyms verändern, indem das Produkt mit einem kleineren partiellen Volumen ausgewählt wird, und er kann die Konformationsflexibilität erhöhen. In dieser Arbeit wurde beobachtet, dass *HHP* keinen Einfluss auf die kinetischen Konstanten im *ATPS*

hatte, was nicht durch einfaches sterisches Verdrängen erklärt werden kann. Zusätzliche Beiträge wie Änderungen der Wasseraktivität und unspezifische schwache Wechselwirkungen mit *ATPS*-Komponenten müssen berücksichtigt werden, um die erzielten Ergebnisse zu erklären. Diese Ergebnisse sind wichtig für die Verwendung von *LLPS* und *ATPS* zur Modulation einer enzymatischen Reaktion in biotechnologischen Anwendungen.

Der andere Teil dieser Arbeit befasst sich mit der kombinierten Wirkung von Druck und *ATPS* auf die Bindung an Bovine Serum Albumin (BSA). von 1-anilino-8-naphthalene (ANS), das hauptsächlich durch Fluoreszenzspektroskopie wurde. Die Ergebnisse zeigen, dass *ATPS* im Gegensatz zu Puffer, bei dem die Bindungsaffinitäten zu den drei äquivalenten und unabhängigen Bindungsstellen von BSA nicht unterschieden werden konnten, zu zwei Bindungsmodi führt. Bei den drei Bindungsstellen homme wurde zwischen einer schwachen und starken Bindung unterschieden werden. Dieses Ergebnis kann durch die Berücksichtigung schwacher Wechselwirkungen zwischen den Bindungsstellen des BSA mit den *Crowder*molekülen wie PEG oder Dextran erklärt werden. Unter dem Einfluss des Druckes nimmt die Bindungsaffinitäten an allen Bindungsstellen ab, was auf die ungünstige Wirkung des Drucks auf hydrophobe Wechselwirkungen sowie auf die Volumenänderung aufgrund der Freisetzung von Wassermolekülen und somit Bildung von *void volume* bei der Bindung zurückgeführt werden kann. Diese Ergebnisse zeigen, dass druckabhängige Studien die Unterscheidung der Bindungsstellen der Liganden aufgrund der Feststellung der Volumenänderung ermöglichen.

Index of figures

Index of tables

Chapter 1
Scientific Background

1.1 Macromolecular Crowding

1.1.1 Excluded volume effect

The intracellular environment has macromolecule concentrations ranging from 80-400 mg/mL [1,75,111] which represent up to about 40% of the cell volume, with considerably restricted amounts of free water [1,53,145,147,218,224,226]. Most biochemical works were carried out at *in-vitro* conditions, typically in a very dilute and well-stirred solution, a scenario very different from the *in-vivo* condition encountered in the cytoplasm of a biological cell. However, in the 80s, pioneering work by Allen P. Minton indicated the effect of such crowded media on various parameters of biochemical reactions, thereby coining the term "excluded volume effect" [143,144,146]. Since no macromolecules are present at very high concentrations, the medium is called crowded rather than concentrated [17,145,147]. Fig. 1.1 illustrates the crowding in the cytoplasm of an eukaryote and a prokaryote.

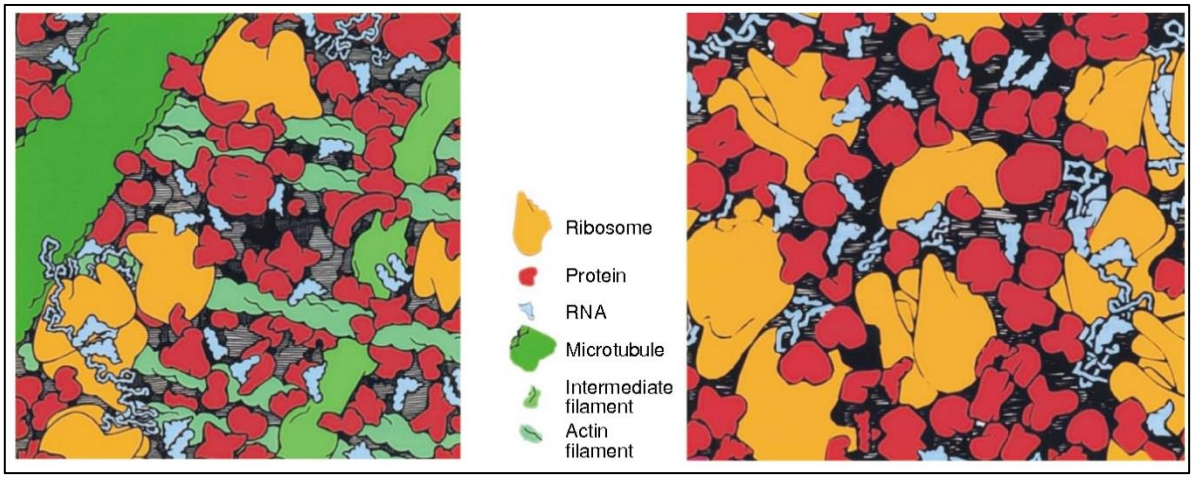

Figure 1.1. Macromolecular crowding in the cytoplasm of eukaryotic (left) and *E. coli* (right) cells. Each square illustrates the face of a cube of cytoplasm with an edge 100 nm in length. The sizes, shapes and numbers of macromolecules are approximately correct. Small molecules are not shown. Adapted from [224].

In such crowded media, the average distance between any two macromolecules can sometimes be smaller than the size of macromolecules themselves [137,138], which gives rise to steric repulsion leading to mutual impenetrability [139]. This observation was first described by Asakura and Oosawa [279] and later developed by Minton with his ‘Scaled-Particle Theory (SPT)’ of hard-sphere fluids [137,140,141]. According to this theory, the particles are considered as inert, hard spheres and the closest distance that can be approached by two particles is equal to the sum of their radii [138,146] as can be seen in Fig. 1.2. Thus, it generates a spherical excluded volume around each molecule which is inaccessible to the centre of all

other molecules [206]. The larger the size of the crowder, the less is the excluded volume effect due to the smaller number of molecules per unit volume. Synthetic polymers such as dextran, Ficoll, PEG and biomolecules such as proteins have been used to mimic the crowding scenario [201], with the most effective condition being those where the volume of both crowder and test molecule are comparable [80,142,241].

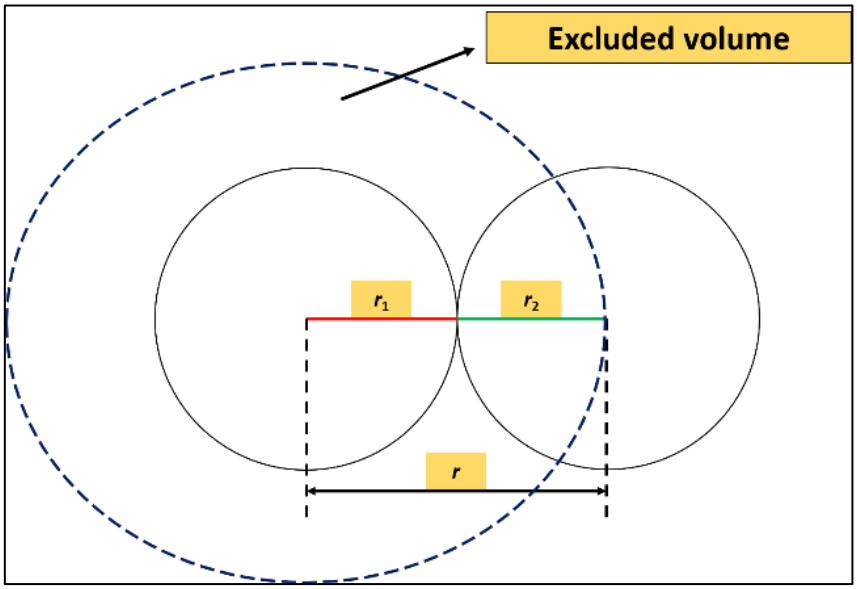

Figure 1.2. Excluded volume effect: the closest distance that can be approached by two molecules which are considered as hard spheres is equal to the sum of their radii $r_1$and r_2. Around each molecule there is a circle of radius r (= r_1+r_2) which is inaccessible to the centre of other molecules. Redrawn and adapted from [138].

Earlier findings suggested that small molecules like metabolites, ions, osmolytes were not affected by crowding [273]. However, studies by Sharp illustrated that not only large crowding molecules like proteins and nucleic acid, but also small molecules like ions and water do exclude [94,102]. Using the hard sphere model, he showed that large molecules are less effective crowders than water due to the loss in net entropy since one large crowder can replace many small water molecules [102].

The hard sphere model does not take into account the chemical nature of the crowders since the effect only depends on the volume occupied by them [114]. However, several studies have shown that these inert crowders with the same hydrodynamic volumes affect the biomolecule in different ways [167,168]. It was pointed out that these "inert" crowders are not truly inert in the sense that they interact with the biomolecules and cause some additional effects [167]. The model assumed the crowders to be of spherical shape which justifies largely the use of PEG, Ficoll as crowders [17,69]. Recently, cellulose derivate were used as crowders to study the

presence of rod-shaped biopolymers such as DNA [255]. These crowders behaved differently than the spherical ones owing to their large surface to volume ratio [195]. The model also describes crowding as an entirely entropic effect [206,224], as against some recent studies showing both entropic and enthalpic contributions [85,96,104].

1.1.2 Thermodynamics of macromolecular crowding

Crowding restricts the mobility of solute molecules, which leads to the decrease in entropy and an increase in free energy of the solute [50,136]. This increase in free energy increases the thermodynamic activity of the solute and affects various processes which are determined by the activity, like association reactions, protein folding and enzyme kinetics [10,251,273]. The standard free energy changes due to crowding (denoted by subscript Cr) compared to the bulk solution is depicted in Eq. 1 [57]

$$\Delta\Delta G^{\circ} = \Delta G^{\circ}_{\mathrm{Cr}} - \Delta G^{\circ}_{\mathrm{bulk}} \tag{1}$$

These changes in Gibbs free energy per mole (ΔG^0) is related to the equilibrium constant by the following equation (Eq. 2) [215]

$$K_{\mathrm{Cr}} = K_{\mathrm{bulk}} \exp(-\Delta\Delta G^{\circ}/RT) \tag{2}$$

Minton and Rivas dissected the crowding effect into enthalpic and entropic contributions by introducing a factor called crowding coefficient, Γ_{Cr}, which is a function of crowding-induced changes in enthalpy and entropy and is shown by Eq. 3 [110]

$$\ln\Gamma_{\mathrm{Cr}} = \ln(K_{\mathrm{Cr}}/K_{\mathrm{bulk}}) = -\frac{\Delta\Delta G^{\circ}}{RT} = -\frac{\Delta\Delta H^{\circ}}{RT}\left(\frac{1}{T}\right) + \frac{\Delta\Delta S^{\circ}}{R} \tag{3}$$

Macromolecular crowding also increases the effective concentration of a solute which is defined in terms of thermodynamic activity (a_i) [215]

$$K_{\mathrm{th}}(T,p) = \prod_i a_i^{\vartheta_i} = \prod_i \left(\mathrm{x}_i^{\vartheta_i}.\gamma_i^{\vartheta_i}\right) = K_{\mathrm{x}}K_{\gamma} \tag{4}$$

K_{th} is the thermodynamic equilibrium constant, ϑ_i is the stoichiometric factor, x_i being the mole fraction and γ_i is the activity coefficient of species *i*. For an enzyme reaction, the activity based kinetic constant, $K_{\mathrm{M}}^{\mathrm{a}}$, is approximately given by Eq. 5 [196]

$$K_{\mathrm{M}}^{\mathrm{a}}(T,p) = K_{\mathrm{M}}^{\mathrm{m}}\gamma_{\mathrm{S}} \tag{5}$$

$K_{\mathrm{M}}^{\mathrm{m}}$ is the apparent Michaelis constant and γ_{S} is the activity coefficient of the substrate. K_{th} and $K_{\mathrm{M}}^{\mathrm{a}}$ consider both ideal and non-ideal contributions to the total chemical potential and are concentration independent [215,222]. Incorporating activity coefficients into various models have led to a better understanding of the kinetics and equilibrium properties of enzymatic reactions [148,149,196,197].

1.1.3 Effect on viscosity and reaction rate

The solvent viscosity increases greatly due to the crowding which reduces the diffusion rate of biomolecules [38,151,161]. This increase in solvent viscosity depends on the chemical nature, concentration, size and molecular mass of a crowder [204]. Crowding affects viscosity both on a micro and macro scale. The modified Stokes-Einstein equation (Eq. 6) links the apparent translational diffusion coefficients (ADCs) with solvent viscosity and crowding [214]-

$$\mathrm{ADC} = k/R_G\ (1 + 2.5\Phi) \tag{6}$$

Where k is a constant for a given temperature, Φ is an obstruction factor reporting the fractional volume of solution occupied by cosolutes and R_G is the radius of gyration of the biomolecule. ADCs of metabolites decrease with increasing concentration of crowders [214]. This decrease in ADC affects the reaction rate. The formation of products from reactants generally involves various steps, such as diffusion of reactants and overcoming an activation energy to form a transition state. In dilute solutions, the latter step is usually rate determining since the diffusion process is generally fast. However, with an increase of crowding, the diffusion can be significantly reduced and thus, a reaction which is reaction-controlled in dilute solution can become diffusion controlled in crowded media. The rate constant of association between two molecules may be written as [57,93,260]

$$k = \frac{k_{\mathrm{D}}.k_{\mathrm{react}}}{k_{\mathrm{D}}+k_{\mathrm{react}}} \tag{7}$$

where k_{D} is the rate constant for diffusion control and k_{react} is the rate constant for reaction control. The effect of crowding on both rate constants is illustrated schematically in Fig. 1.3.

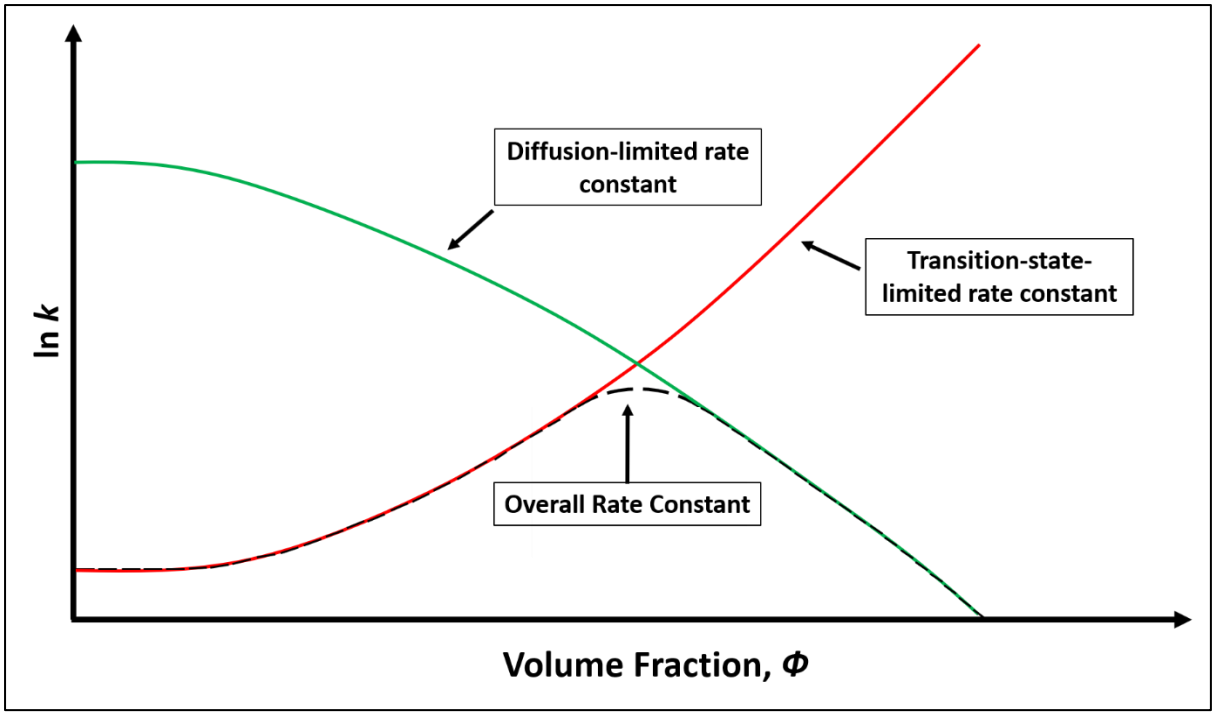

Figure 1.3. Crowder effects on bimolecular reactions. Schematic representation of a transition-state-limited rate constant (red curve), a diffusion-limited rate constant (green curve), and the overall rate constant (black curve) of a bimolecular reaction as a function of crowder volume fraction, ϕ. In the transition-state-controlled regime, a compact transition state leads to crowding-induced acceleration of the reaction, whereas collision and attractive interactions with the crowders controls the diffusion-controlled regime. The reaction rate is transition-state limited at low degrees of crowding and diffusion-limited at high degrees of crowding. Redrawn and adapted from Ref. [215].

As shown in the figure, in the diffusion-controlled regime, increased crowding is expected to decrease k_{D}, because it is proportional to the relative diffusion constant of the reactants [99]. Two major mechanisms are responsible for this decrease in diffusion rate in crowded media: collision with crowders and nonspecific reversible binding to the crowders [99]. The decrease is somewhat compensated by the increase in attractive interactions between reactants due to increase in effective concentration as a result of crowding [57,58]. In the reaction-controlled regime, the association rate constant is expected to increase due to a decrease in activation energy. The presence of crowders tend to make the transition state more compact compared to dilute solution and thus increase the k_{react} [57]. As a matter of compensation between these two opposing effects, reaction rates are generally reaction-controlled at low crowding concentration and diffusion-controlled at higher crowding concentration [34,99,273].

1.1.4 Soft interactions

Apart from steric exclusion between biomolecules and crowders, some non-specific or soft interactions also play a role in the stability of biomolecules in such crowded milieu

[136,137,167,227]. Many a times, the chemical interaction can be a dominating factor over hard-core repulsion [225,275]. At low crowder concentration, each crowder behaves as a monomeric unit and thus the entropically driven excluded volume effect dominates, but when the concentration of crowder increases, the enthalpic driven soft interactions makes the larger contribution [86,104,116]. However, it is usually difficult to differentiate the enthalpic and entropic contributions due to the presence of an excluded volume effect at both low and high crowder concentration. The strength of nonspecific interaction depends on the properties such as the shape of the crowding agent, macromolecule, its net charge, surface polarity, dipole moment etc., depending on that it can either be attractive or repulsive [15] thus enhancing or diminishing the excluded volume effect [96,103,209]. The activity coefficient is related to non-specific solute-solute interaction as shown in Eq. 8 [140]

$$\ln\gamma_i = \langle g_i \rangle / k_B T \tag{8}$$

where k_B is the Boltzmann constant, and $\langle g_i \rangle$ denotes the equilibrium average free energy of nonspecific interaction between the molecule of species *i* and all other molecules present in the medium.

1.1.5 Change in hydration

Water molecules form a shell-like structure in the vicinity of protein which is referred to as water of hydration [71,272]. Crowding agents such as Ficoll and dextran have shown to affect the biomolecules in a way similar to their monomers such as sucrose and glucose [96,99,216,261], thus suggesting an enthalpy-dependent and hydration-mediated mechanism [96,209]. MD simulations have shown an altered water structure mostly beyond the first hydration shell, a slowdown of the diffusion and a decreased dielectric constant of interstitial hydration water, suggesting highly constrained water in crowded environments [4,203]. As a consequence, the hydrodynamic properties of biomolecules and the strength of different intramolecular interactions may be affected and modulated. Crowders, such as PEG, are generally preferentially excluded from the protein domain, which produces an osmotic stress [71]. The catalytic activity of such osmotically stressed enzymes are altered due to the change in the number of bound water molecules by the enzyme, substrate and the enzyme-substrate complex, both in the ground and the transition state [61,71,205]. Techniques, such as ultrafast two-dimensional infrared (2D-IR) and terahertz spectroscopy have shown that the majority of water inside the cell is expected to have slow, collective hydration and only a small amount of intracellular water behaves bulk-like [174,193,229]. A decrease in the water activity is also

caused by a high concentration of biomolecules, osmolytes and salts, which may also affect the reaction equilibria of biomolecules [128,213].

1.1.6 The molecular nature of crowding

As mentioned in section 1.1.1, crowding studies are often carried out using synthetic polymers like PEG, dextran, Ficoll or natural crowders like proteins. This gives rise to two kinds of crowding- uniform and structured [157,168]. Uniform crowding refers to the condition where a single synthetic crowder is used to mimic the *in-vivo* condition and thus has a very narrow size distribution [157]. This fails to create the heterogenous cellular environment and provide accurate results for various biochemical processes since the composition, size and heterogeneity of crowder molecules have been shown to play an important role in determining the crowding effect [157,263]. Structured crowding, on the other hand, refers to the highly coordinated cellular environment formed by protein crowders. Some studies also pointed out that the proteins with their surface charges, site-specific interactions and an intricate surface topology behave as more biologically relevant crowders than synthetic polymers and thus, reflects the *in-vivo* situation more realistically through structured crowding [208].

1.2 Aqueous Two-Phase System (ATPS)

ATPSs were accidentally discovered by Martinus Willem Beijerinck in 1896 while mixing aqueous solutions of starch and gelatin [76]. However, they were put to real use by Per-Åke Albertsson for the extraction and purification of biomolecules [284,285]. Though ATPSs can be formed by mixing the aqueous solutions of a variety of components [200], polymer-polymer and polymer-salt are the most well studied and commonly used systems among them [76]. The advantages of using ATPSs over conventional liquid-liquid extraction (LLE) methods [90,152] include low cost, environment friendly, scale up process, continuous operation and protection of biomolecules from damage due to high water content, low interfacial tension and stabilising effect of polymers [48,72,76,267,277,285]. Affinity ligands further improve the recovery yield and purification level [12]. These ligands are covalently attached to polymer or the polymer is modified with hydrophobic groups [262].

1.2.1 Types of ATPSs

The most common types include polymer-polymer [e.g., poly(ethylene glycol) (PEG)-dextran (Dex)] or polymer-salt (e.g., PEG-Sulphate) systems. Other ATPSs include ionic liquids [258], short chain alcohols, poly-phase systems (three or four polymer phases), alcohol-salt systems and many more [12,44,48,76,134,200]. Alcohol-salt ATPSs are better than polymer systems due to low cost, low viscosity, easy constituent recovery and reduced settling time [284]. However, the poor compatibility of proteins with the alcohol-rich phase is a major disadvantage [45]. Ionic and non-ionic surfactants are also used to form micellar and reverse micellar ATPSs [12,62,162]. Another type of ATPS is formed by a single polymer in water and is referred to as smart polymer [6,24,48]. The separation is achieved by collapsing the polymer through temperature, pH, ionic strength or light [24,180].

1.2.2 Formation and kinetics of ATPSs

Immiscibility of polymer solutions are a common phenomenon [52,288]. When the aqueous solutions of polymer are mixed, they can form aggregates and start to separate into two phases due to steric exclusion [52,100]. A similar situation is observed in polymer-salt systems where the salt absorbs a large amount of water leading to aggregation and phase separation [100,262]. Generally, the movement of a drop during phase separation is determined by the balance between three force- gravitational, frictional and flotation [11]. While gravitational force depends on the density of the drop, flotation and frictional force depend on the flow properties of phases [11,278].

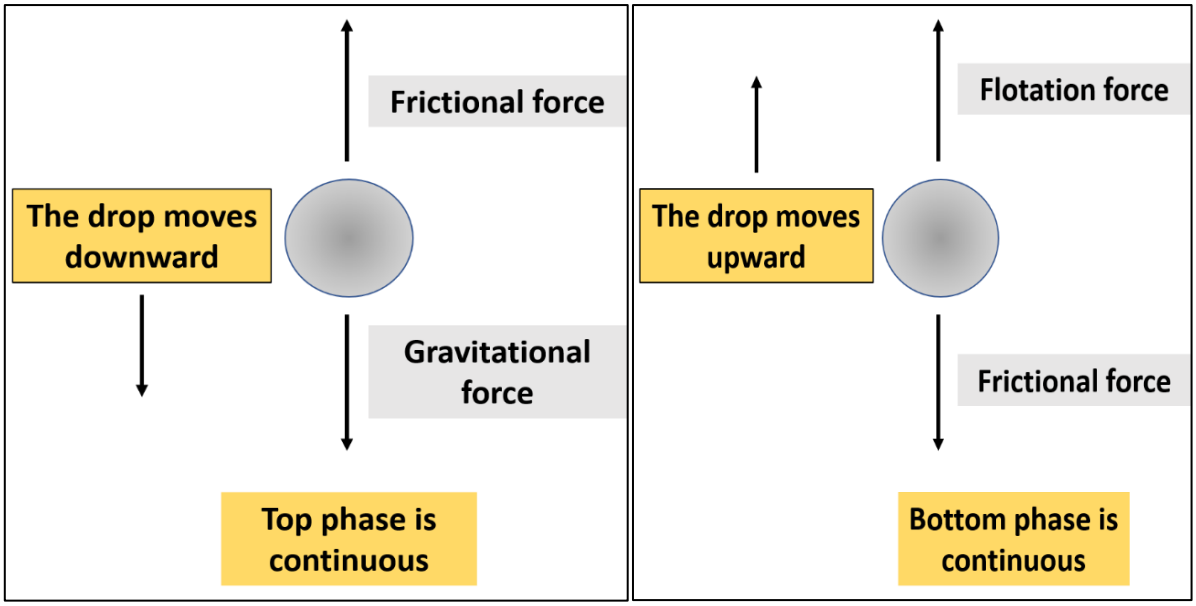

Figure 1.4. Diagram representing the forces effecting the movement of a droplet depending on which phase is continuous. Redrawn and adapted from [44].

Once the initial system is entirely mixed, three phases: top, bottom and dispersion phases are formed till the complete separation of top and bottom phases occur [11,278]. When the top phase is continuous, droplets of the bottom phase remain dispersed in this phase and slowly tend to settle down towards the horizontal interface so that the topmost drops form the settling front. The drops accumulate and coalesce at the boundary of the dispersion region and the bottom phase forms a coalescing front. It is depicted schematically by plotting the fraction of initial height (h_t) with time (Fig. 1.5). With time, h_t decreases and approaches zero when the phases are completely separated [11,278]. Phase separation times are dependent on which phase is continuous. A change in phase separation time has been observed during phase inversion, i.e., when the continuous phase changes to a dispersed phase and vice versa [19].

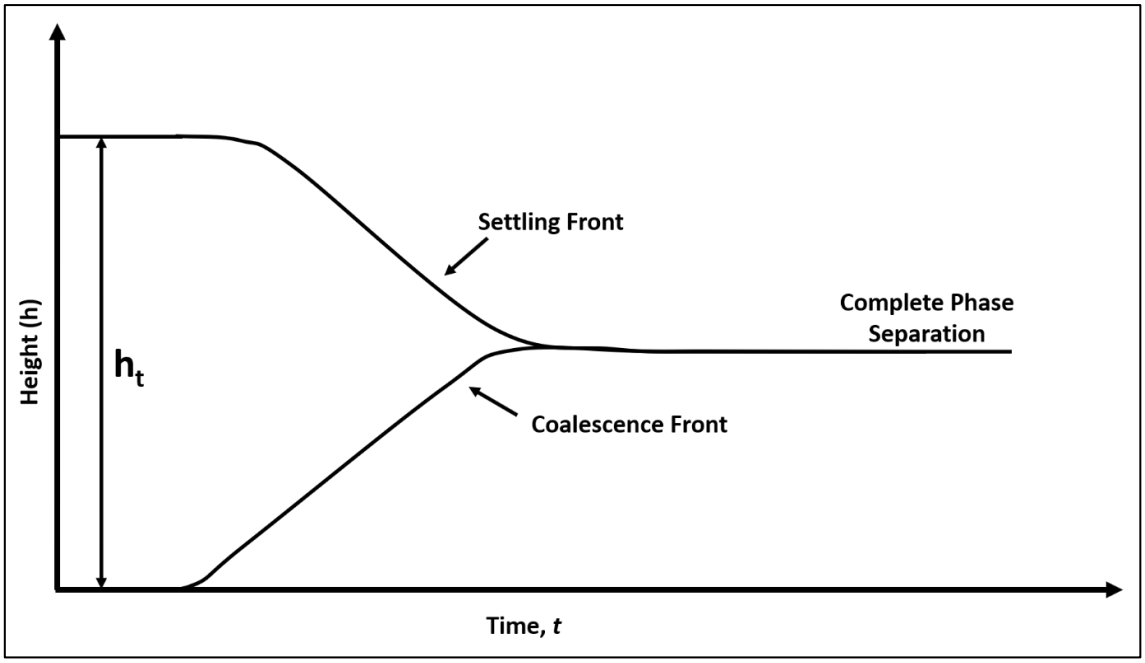

Figure 1.5. Batch separation profile representing the ATPS with dispersed bottom phase. The height of dispersion (h_t) decreases from the initial height to zero when the top and bottom phase are completely separated. Redrawn and adapted from [44].

1.2.3 Thermodynamics of phase separation

In the Flory-Huggins theory, an unbranched polymer chain is represented as a linear sequence of connected segments, each segment occupying a site of a lattice [36,37,190,191]. Each lattice site has *z* contacting faces with the adjacent sites [42,59,179]. Considering a single polymer molecule, the enthalpy of mixing is expressed as a function of changes in enthalpy due to the contact formation between the polymer segment and water at the expense of breaking bonds between like components [42,59,179]. This energy change per contact, Δw_{12}, is given as [42]

$$\Delta w_{12} = w_{12} - \frac{1}{2}(w_{11} + w_{22}) \tag{9}$$

where w_{12} is the change in enthalpy due to contact between component 1 (water) and 2 (polymer), w_{11} and w_{22} are the energies associated with 1-1 and 2-2 contact, respectively. This change in enthalpy per contact can be positive or negative depending on whether the interaction is repulsive or attractive, respectively. Thus, the total enthalpy of mixing, ΔH_{m}, for component 1 and 2 is given as [42]

$$\Delta H_{\mathrm{m}} = z\Delta w_{12} n_1 \phi_2 \tag{10}$$

where z is the lattice coordination number, ϕ_2 being the fraction of lattice occupied by polymer segments, i.e., $\phi_2 = n_2P_2/(n_1 + n_2P_2)$, P is the number of segments per polymer molecule, and n_1 and n_2 are the numbers of solvent and polymer molecules on the lattice, respectively. Eq. 10 is usually written as [42,59]

$$\Delta H_{\mathrm{m}} = k_B T \chi_{12} n_1 \phi_2 \tag{11}$$

where k_B is the Boltzmann constant, T is the absolute temperature and $\chi_{12} = z\Delta w_{12}/k_B T$. The parameter χ_{12} is known as Flory interaction parameter. The net entropy of mixing, ΔS_{m}, according to this theory is given as [42,59]

$$\Delta S_{\mathrm{m}} = k_B \ln W = -k_B(n_1 \ln \phi_1 + n_2 \ln \phi_2) \tag{12}$$

where W is the total number of distinguishable ways of arranging n_1 solvent molecules and n_2 polymer molecules on a lattice and ϕ_1 is the fraction of lattice sites occupied by the solvent. Thus, the free energy of mixing is given by [42]

$$\Delta G_{\mathrm{m}} = \Delta H_{\mathrm{m}} - T\Delta S_{\mathrm{m}} = k_B T(n_1 \ln \phi_1 + n_2 \ln \phi_2 + \chi_{12} n_1 \phi_2) \tag{13}$$

The major restriction applied for this theory is that it doesn't consider the volume change upon mixing and hence no pressure study on ATPSs can be explained by this theory.

1.2.4 Phase diagram

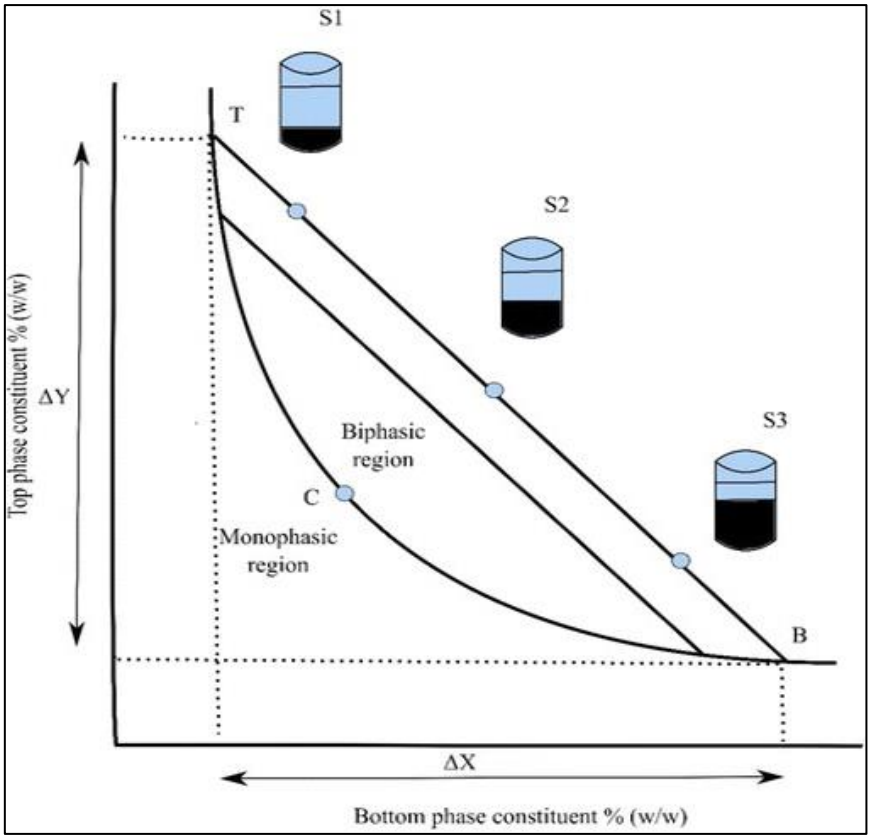

Figure 1.6. Illustration of the phase diagram formed by a salt and a polymer. Bottom phase, polymer or salt X % (w/w) is plotted on the abscissa and the top phase, polymer Y % (w/w) is plotted on the ordinate. The concentrations above the binodal curve (TCB) form the aqueous two-phase system. Adapted from [185].

A phase diagram is unique for each system under specified conditions (e.g., temperature, pH) and provides information about the concentration of components in the top and bottom phases [14,23]. The curve TCB is known as the binodal curve, which separates the one- and two-phase region. It is determined by cloud point titration, turbidometric titration and the node determination method [14,23,44,185]. Binodal curves are important in the way that they predict the concentration of components required for two-phase formation. The line joining the nodes on the binodal is known as tie line and represents the composition of both phases in equilibrium [14,52,185]. All points on one tie line will have the same equilibrium composition of the top (t) and bottom (b) phases, but the relative phase volume and phase mass and hence the overall composition will be different. The ratio of the weight of the upper and lower phases is given by the ratio of line segments ST/SB. The point C is referred to as the critical point, at which both the phases have identical composition. The value of tie line length (*TLL*) is zero at the critical point. The *TLL* is estimated by Eq. 14 [185]

$$\frac{V_{\mathrm{t}}\rho_{\mathrm{t}}}{V_{\mathrm{b}}\rho_{\mathrm{b}}} = \frac{SB}{ST} \tag{14}$$

where V and ρ represent the volume and density of the top (t) and bottom (b) phases, respectively. *TLL* can also be expressed (see Fig. 1.6) [185] as

$$TLL = \sqrt{\Delta X^2 + \Delta Y^2} \tag{15}$$

The tie lines are generally straight, and the slope (*STL*) is given by Eq. 16 [185]

$$STL = \frac{\Delta Y}{\Delta X} \tag{16}$$

The partitioning of a biomolecule in the ATPS is quantified by the partition coefficient (K) and is given as [14]

$$K = \frac{equilibrium\ concentration\ of\ partitioned\ biomolecule\ in\ top\ phase\ (C_{\mathrm{t}})}{equilibrium\ concentration\ of\ partitioned\ biomolecule\ in\ bottom\ phase\ (C_{\mathrm{b}})} \tag{17}$$

1.2.5 Thermodynamics of partitioning of a solute in the ATPS

Various models have been proposed to explain the partitioning behaviour in ATPSs [2,45,119,123,231,237,265]. Albertsson, a legend in this field, proposed a model which includes six different kinds of partitioning, each having a different driving force. He proposed that the overall partitioning may be as a result of the dominance of either one factor or due to conjugative effects of several factors. The overall K is given by Eq. 18 [32,185,267,284,285]

$$K = K_0 * K_{\mathrm{hfob}} * K_{\mathrm{el}} * K_{\mathrm{biosp}} * K_{\mathrm{size}} * K_{\mathrm{conf}} \tag{18}$$

where hfob, el, biosp, size and conf stand for hydrophobic, electrochemical, bio specific, size and conformational contributions to the partition coefficient, and K_0 includes other factors. In a stable two-phase system, the coexisting phases are in equilibrium and thus, the chemical potential (μ) of a solute i in both phases are equal i.e. $\Delta\mu = 0$ [264]. At equilibrium, μ can be expressed as a function of activity (a_i), particle surface area (A), interfacial tension (γ), particle charge (z) and electrical potential of the phase (ψ) as described in Eq. 19 [48,264]

$$\Delta\mu_i^0 + k_B T \ln\left(\frac{a_i^{\mathrm{t}}}{a_i^{\mathrm{b}}}\right) + A\Delta\gamma + \frac{z_i F \Delta\Psi}{N_A} = 0 \tag{19}$$

where F and N_A represent the Faraday and Avogadro constants and the subscripts t and b refer to the top and bottom phases respectively. Defining a_i as a product of concentration of solute ([c]) and activity coefficient (f_i), μ can be related to the partition coefficient K as [48,264]

$$-k_B T \ln K = \Delta\mu_i^0 + k_B T \ln\left(\frac{f_c^t}{f_c^b}\right) + A\Delta\gamma + \frac{z_i F \Delta\Psi}{N_A} \quad (20)$$

Eq. 20 shows three major factors affecting the K at infinite dilution (f_i approaches unity):

1) Interfacial tension between the two phases
2) Solute charge
3) Electrical potential difference between the two phases

1.2.6 Factors affecting the solute partitioning in ATPSs

(A) Molecular weight (M.W.) and concentration of polymer and protein

The aqueous solution of a polymer generally has two regimes – a diluted solution regime and a concentrated solution regime [41,119]. In the diluted solution regime, the polymer molecules are separated from each other by several layers of water. As the M.W. increases, the concentration range over which the solution stays in the diluted regime becomes narrower as the polymer starts occupying larger volumes and overlapping with each other to form mesh-like structure as described by Cabezas, leading to the concentrated regime [250]. This limiting concentration at which a polymer solution changes its regime is referred to as crossover concentration. The higher the M.W., the lower is the crossover concentration and vice-versa [113,247].

In a polymer-polymer system, high M.W polymers induce phase separation at lower concentrations due to a large difference in interfacial tension, viscosity and phase density [47]. Proteins also tend to partition to the phase enriched with the lower M.W. polymer due to steric exclusion and change in hydrophobicity [32,281,282]. For polymers such as PEG, decreasing the molecular weight at constant concentration decreases the number of ethylene oxide groups per PEG molecule, thus lowering the hydrophobic character [192,221]. Albertsson designed an equation for the PEG-Dex system, correlating partition coefficient K with polymer concentration and protein M.W. [45,48]

$$-\log_{10} K = aM^{2/3} \quad (21)$$

where a is a polymer concentration dependent constant and M is the protein's molecular weight.

Brønsted proposed a qualitative model to link K with the solute M.W. as shown in Eq. 22 [48]

$$K = \mathrm{e}^{-M\lambda/k_B T} \quad (22)$$

where λ is a parameter that considers solute and system characteristics.

(B) Charges, salts and pH

The electrical potential (ψ) resulting from the establishment of an electrical double-layer due to the differences in affinity of a solute towards either of the two phases of an ATPS can be calculated from Albertsson's model assuming that each ion can partition independently from the other [25,192,264,285]

$$\Psi = \frac{RT}{(z_+ + z_-)F} \ln\left(\frac{K_+}{K_-}\right) \tag{23}$$

here R is the ideal gas constant, z_+ and z_- are the total positive and negative charges and K_+ and K_- are the respective partition coefficients of positively and negatively charged ions formed from the solute as a result of differential affinity. Johansson proposed that this difference in partitioning tendency of a solute towards either of the two phases leading to an electrical double layer influences the protein partitioning [180].

The presence of salt, at very low concentrations, brings a drastic change in the cloud point of the polymers and helps in achieving better yields [25,47,55,56]. This salting-out effect is used to lower the cloud point and perform the extraction process of biomolecules at much lower temperature. The detailed effect of salt on protein partitioning is explained by the Hoffmeister series [6,95,105].

Using pH values above the isoelectric point of proteins (pI) induces negative surface charge and thus increases the affinity towards the positively charged phase (usually PEG) due to the positive dipole moment and vice-versa [122,237].

(C) Temperature and interfacial tension

Lower temperature (*T)* favours phase separation in polymer-polymer systems whereas the opposite is observed in polymer-salt systems [41,200]. Apart from effecting the density and viscosity of the phases, *T* is an important parameter in partitioning, as can be seen from all the equations mentioned above.

Interfacial tension (γ) is generally less for ATPSs as compared to organic solvent-water systems. In PEG-Dex system, an increase in M.W. of either PEG or Dex increases the interfacial tension but the effect is much stronger in case of PEG [45,285]. Comparison between systems with the same *TLL* showed an increase in γ with increase in *T*. However, when

systems with the same composition are prepared at different *T*, γ decreases with the rise in *T* [269]. Thus, γ changes with *T* depending on the *TLL*, i.e. the distance from the critical point [35,48].

(D) Density and viscosity

Density and viscosity are the main driving forces for the formation of two-phase systems and are related to the *TLL* [33]. Increase in the *TLL* increases the density difference between the top and bottom phases and increases the viscosity of the top phase [150,247].

1.3 High Hydrostatic Pressure (HHP)

The story of pressure studies on biomolecular systems began with the pioneering work of Nobel laureate Piercy Bridgman in 1914 [129], who reported the denaturation of egg white under HHP at room temperature. Despite this, pressure was long neglected by biochemists due to lack of a proper concept about the effect of pressure on biochemical reactions and the deficiency of instruments to test it. However, in recent decades pressure has become a powerful tool in studying the thermodynamic and kinetic aspects of bioprocesses and modulating them for the benefits of mankind such as in food processing industry [18,106,112,130,131,207,217]. Moreover, oceans cover 70% of the earth's surface with an average depth of 3.8 km and an average pressure of 38.5 MPa make the earth predominantly a high-pressure environment. Interestingly, living organisms (microbes) have been found to grow in extreme conditions such as marine hydrothermal vents with temperatures as high as 122 °C and pressures upto 130 MPa. Even more complex organisms have been encountered under abnormal conditions (1-4 °C, <100 MPa) and thus pressure can be considered as an elegant tool to study the adaptability of life in such harsh situations [20,28,181].

1.3.1 Thermodynamic description

(A) Effect of pressure on kinetic constants

Activity of several enzymes have been found to increase using higher temperatures and/or higher pressures [82,132,234]. The way in which both effect the activity is quite different. Though the higher temperature helps to overcome the activation energy of a reaction, the fear of denaturation of the enzyme at high temperature limits its use. Pressure, on the other hand affects the transition state of a reaction and favours states with lower volume than the reactants.

The activation volume, $\Delta V^{\neq}$, which is defined as the difference in volume between the activated state and ground state of the enzyme-substrate complex, is related to the activation Gibbs energy, $\Delta G^{\neq}$, as [66,159,270]

$$\mathrm{d}\Delta G^{\neq} = \Delta V^{\neq}\mathrm{d}p \tag{24}$$

where dp being the increase in pressure. The dependence of the rate constant, k, on pressure is described as [172]

$$\left(\frac{\partial \ln k}{\partial p}\right)_T = -\frac{\Delta V^{\neq}}{RT} \tag{25}$$

where R denotes the ideal gas constant and T temperature. According to the Le Châtelier's principle, an increase in pressure favours the reaction towards negative $\Delta V^{\neq}$ [276]. The modification in $\Delta V^{\neq}$ can be brought in by sole or cumulative effect of several factors like a change in enzyme or substrate conformation, a change in solvent properties like pH, viscosity, phase or a change in the rate-limiting step. Depending on the fine-tuning of these factors, $\Delta V^{\neq}$ can either be positive, negative or negligible [66,120,197]. The maximum effect of pressure on $\Delta V^{\neq}$ is observed in reactions involving high hydration changes in the components between the ground and transition state and thus it has been found that the activation volume is dependent on water content. This dependency of $\Delta V^{\neq}$ on hydration and pressure can be used to alter reaction pathways, e.g., to obtain a higher yield of a favourable product or to modulate the relative amount of two substrates which differ in sign with respect to their activation volumes [126,154].

(B) Effect on the equilibrium constant

The effect of pressure on a chemical equilibrium is given by Eq. 26 [270]-

$$\left(\frac{\partial \ln K}{\partial p}\right)_T = -\frac{\Delta V}{RT} \tag{26}$$

where ΔV is the reaction volume and K is the pressure-dependent equilibrium constant. The experimentally determined ΔV (ΔV_{exp}) generally includes several contributions for enzyme kinetics, such as binding of substrate, conversion and release of products, conformational changes, hydration and ionization [124]. As the pressure is applied over the entire system, it affects every step leading at the end to a decrease in volume with increase of pressure. E.

Ohmae et.al. suggested that the total volume change of a closed system can be described as [124]

$$\Delta V_{exp} = \Delta V_p + \sum_{i \neq p} \left(c_i / c_p \right) \Delta V_i \quad (27)$$

Where c_i and c_p are the concentrations of component *i* and protein respectively, ΔV_i is the partial molar volume change for component *i* and ΔV_p is the partial molar volume change of the protein. In 1959, Kauzmann proposed a model system consisting of only protein and water and neglecting any other kind of interactions to determine the partial molar volume of a protein in water, V_p, which is mathematically represented as [176,177]

$$V_p = V_{atm} + V_{cav} + V_{hyd} \quad (28)$$

where V_{atm} is the contribution from the Van der Waals volume of atoms , V_{cav} is the interatomic void spaces in a protein molecule and V_{hyd} denotes the hydration effect. Thus, ΔV_{exp} is represented as [243]

$$\Delta V_{exp} = \Delta V_{atm} + \Delta V_{cav} + \Delta V_{hyd} \quad (29)$$

ΔV_{atm} represents the change in the van der Waals volume of atoms plus the volume of interior voids, which are water-inaccessible. This means that such voids are smaller than 18 mL mol^{-1}. ΔV_{cav} symbolises the change in interatomic void spaces in a protein which depends on biomolecule's solvent accessible surface area (SASA) [70] and ΔV_{hyd} describes the volume change of solvent molecules involved in hydrating solvent-accessible surface groups of the protein with respect to the bulk. This term is usually negative as the volume of hydrated water is less than that of bulk water and thus an increase in hydration might lead to a decrease in overall partial molar volume of the system [244]. Chen et al. showed that ΔV_{atm} upon protein unfolding is relatively large and negative due to the voids, whereas ΔV_{hyd} is positive, leading to a relatively small, positive or negative change in the total volume upon unfolding [242]. Thus, the main driving forces for pressure-induced protein unfolding are the presence of packing defects located in the protein and their hydration behaviour [242].

1.3.2 Pressure effect on intramolecular interactions in protein

Pressure effects are mostly caused due to loss of void volume, packing defects or making and breaking of non-covalent interactions. The covalent bonds define the primary structure of a

protein and are pressure insensitive up to at least 10 kbar [29,130,207]. This section briefly explains the effect of pressure on several intramolecular interactions in proteins.

(A) Ionic interactions

Ion pairs play an important role in maintaining the tertiary and quaternary structure of protein. They are short range interactions (4 Å or less) between oppositely charged amino acid chains [29,107]. Sometimes they are hydrogen bonded and are also referred to as salt bridges. Dissociation of these salt bridges leads to electrostriction, a phenomenon where there is reduction in overall volume due to contraction of solvent molecules [92,289]. The contraction happens due to the rearrangement of dipolar solvent molecules (H_20) in the electric field around the exposed charge. As pressure favours negative ΔV or $\Delta V^{\neq}$, it favours electrostriction too [30,256].

(B) Hydration and void volume

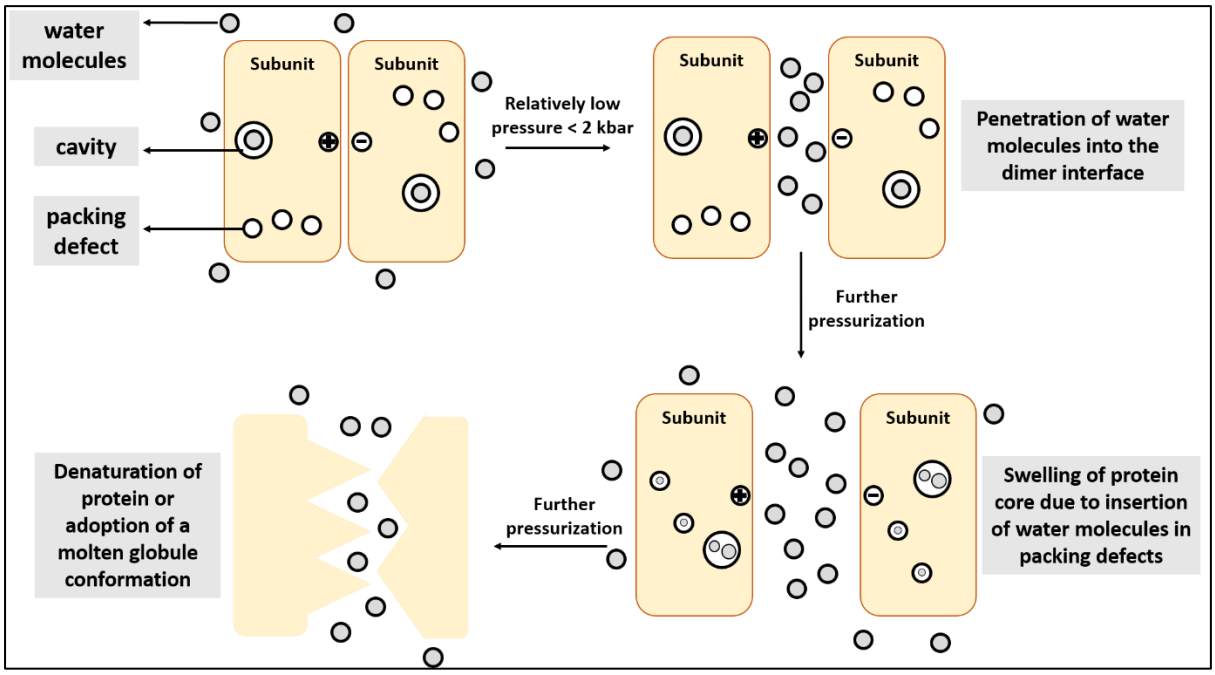

Figure 1.7. A native protein dimer contains packing defects and cavities both at the interface and within the subunits. Water generally fills the cavities and helps in smooth movement of side chains and polypeptide backbone. Upon application of relatively low pressure (< 2 kbar), the water molecules from bulk solvent start penetrating the dimer interface leading to the dimer dissociation by release of void volumes from cavities and packing defects present at the interface. This water exchange process is opposed by the decreased size of cavities upon pressurisation and favoured by the increase in conformational fluctuations with pressure. Further pressurisation leads to insertion of water into the packing defects inside the subunits which are generally water-inaccessible. This lead either to the swelling of the protein core and it's rupture (denaturation) or adoption of a molten globule conformations. Apart from protein unfolding, pressure induced hydration either leads to a decrease in compressibility due to electrostriction and loss of void volume or an increase in flexibility due to water penetration into the interior of the protein [29,130,207,266,271].

(C) Hydrophobic interaction

It plays the central role in the protein folding mechanism by directing the non-polar side chains to cluster into the protein core [176]. However, the pressure effect on this interaction remains unclear. In some cases, the hydrophobic interaction was believed to be stabilised by pressure due to a negative volume change resulting from the hydration of non-polar surfaces during protein unfolding [176]. This explanation was not enough to verify both the positive and negative volume changes that were recorded experimentally during protein unfolding [177,219]. This discrepancy between the predicted and experimentally determined values of volume change was addressed by Chen et al. who pointed out that the main disagreement might lie in the model used for determining the hydrophobic hydration [242] in which the protein unfolding was modelled as a transfer from non-polar solvent to aqueous solution. It was predicted that the large sizes of non-polar solvents as compared to water might have led to an overestimation of the volume change. They showed that upon using a transfer model from gas phase to water led to the positive volume change on protein unfolding [242].

(D) Hydrogen bonds

Owing to the negative volume change associated with the formation of hydrogen bonds in organic compounds, HHP has been known to promote hydrogen bond formation within proteins [256]. HHP increases protein hydration which increases the chances of formation of intermolecular hydrogen bonds at the expense of intramolecular hydrogen bonds. Furthermore, it was reported that pressure leads to a shortening of hydrogen bonds contributing to the compression of proteins [28,212,238].

(E) Van der Waal (VDW) forces

These forces are weak short-range interactions that arise due to fluctuations in polarizability in atoms or molecules. VDW forces contribute to the enthalpic and entropic components of hydrophobic interaction [107,183]. Weak VDW forces lead to several packing defects which in turn determine protein stability at HHP. However, pressure favours VDW forces as they tend to decrease the overall volume of the system by increasing the packing density of the hydrophobic core and thus decreasing the overall volume of the system. On the contrary, VDW forces may also lead to protein destabilisation at HHP (< 3 kbar) by establishing shorter and stronger bonds between amino acid residues and water which are promoted by pressure upon dissociation of oligomers [67,92,129,133].

1.4 Ligand Binding

Molecular recognition or binding is the underlying reason for the proper functioning of the cellular machinery. Several important cell functions, such as recognition of substrate by enzyme, translation of cellular signals and so on are controlled by molecular binding [283]. Most of the complexes formed as a result of binding between biomolecules are non-covalent complexes which are held by hydrophobic, ionic or hydrogen bonding [252]. In biochemical terms, binding is often described as non-covalent interaction between a larger molecule and a smaller molecule. The larger molecule is usually the macromolecule like protein, DNA, RNA etc., referred to as receptor, whereas the smaller molecule like a drug molecule is called the ligand. The ligands bind at specific sites on or near the surface of the receptor known as binding sites. These binding sites vary in strength and affinity for a ligand and thus the binding of a ligand to a receptor is governed by affinity and specificity [39,230]. High affinity binding is generally achieved by increasing the ligand's hydrophobicity whereas specificity relies on hydrogen bond interactions [254]. Biologically relevant interactions are highly specific. Binding of the ligand can either take place at a single site on the protein or on multiple sites. In case of multiple binding, if the binding of one ligand to one of the sites influences the binding of the other site with the ligand, this is known as allosteric binding [127], whereas if one binding interaction is independent of the other, it is referred to as non-allosteric binding [170].

1.4.1 Thermodynamics of binding

Most of the binding measurements such as equilibrium dialysis, dialysis or ITC are indirect in the way that they only measure the amount of ligand bound to the protein [166]. There are various models to explain the binding phenomenon, the simplest one being the binding of one ligand molecule to one site on the protein molecule. It is schematically explained below with P defining the protein and L the ligand:

$$\mathrm{P} + \mathrm{L} \rightleftharpoons \mathrm{PL} \tag{30}$$

where PL represents the non-covalent protein-ligand complex.

The equilibrium constant or association constant for the Eq. 30 is expressed as

$$K_{\mathrm{A}} = \frac{[\mathrm{PL}]}{[\mathrm{P}][\mathrm{L}]} = \frac{1}{K_{\mathrm{D}}} \tag{31}$$

where [PL] is the concentration of the bound complex, [P] and [L] are the concentration of free protein and free ligand, respectively. This equilibrium can also be expressed in terms of the dissociation constant $K_{D,}$ which is the inverse of K_A. The value of K_D defines the ligand concentration range over which the protein switches from bound to unbound [170]. The standard binding free energy (ΔG°_{bind}) is given by

$$\Delta G^{\circ}_{bind} = -RT\ln K_A = RT\ln K_D \quad (32)$$

Increasing affinity of binding is characterised by a decrease in ΔG°_{bind}, and specific binding is generally identified by a large negative ΔG°_{bind} for one particular ligand compared to another. Standard free energy changes upon binding vary from -50 kJ mol^{-1} for tightest interaction to -17 kJ mol^{-1} for weaker ones [170].

The average number of ligands bound to the protein at any given time is defined by the parameter $\bar{v}$ [189]

$$\bar{v} = \frac{concentration\ of\ bound\ ligand}{total\ protein\ concentration} = \frac{[PL]}{[P]+[PL]} \quad (33)$$

Generally, the fraction of sites in the protein that are occupied by ligand is quantitatively described by a factor θ, known as fraction saturation, as

$$\theta = \frac{\bar{v}}{n} = \frac{\Delta X}{(\Delta X)_T} \quad (34)$$

where the change with binding in some physical property X is linear in the extent of binding, $(\Delta X)_T$ is the total change produced when the macromolecules are saturated with L, and n is the total number of binding sites on the macromolecule that are available to the ligand. Since for a single site (n = 1), $\theta = \bar{v}$ and thus considering equilibrium (Eq. 30) and (Eq. 31), θ can be expressed in terms of K_A as [170]

$$\theta = \frac{K_A[L]}{1+K_A[L]} \quad (35)$$

The value of $\bar{v}$ approaches the value of n as the binding approaches saturation. Putting [L] = K_D, $\bar{v}$ = 0.5. Thus, when the protein is half saturated, the ligand concentration equals the dissociation constant. The plot of fractional occupancy as a function of ligand concentration at constant temperature is referred to as binding isotherm or binding curve [118,170]. Even

though K_D is a pure number, it can be equated with the ligand concentration which has molar units and the reason lies in the way K_D is expressed. The actual equation is [170]

$$K_D = \left[\frac{\frac{[P]}{[P]^\circ} \quad \frac{[L]}{[L]^\circ}}{\frac{[PL]}{[PL]^\circ}} \right] \tag{36}$$

Where [P]°, [L]°, [P.L]° are standard state concentrations and are numerically equal to 1 M. Thus, even though numerically Eq. 31 and Eq. 36 gives the same value of K_D, the units differ in both equations.

1.4.2 Scatchard plot

The Scatchard plot is a binding isotherm which correlates the K_D with the amount of ligand bound to the protein. It is mathematically represented as [8]

$$\frac{[L]_{Bound}}{[L]} = -\frac{[L]_{Bound}}{K_D} + \frac{[P]_{Total}}{K_D} \tag{37}$$

This plot is valid only when single site binding is considered [170]. Eq. 37 indicates that the ratio of bound ligand and total ligand concentration varies linearly with the concentration of bound ligand with a slope equal to the inverse of dissociation constant. This plot can be applied to impurified protein where the exact concentration of protein is not known [155]. One such important applications of the Scatchard plot is measuring the binding properties of the retinoic acid to its receptor, the retinoic acid receptor in cellular extracts without undergoing the trouble of purifying the receptor [170].

1.4.3 Entropy factor

Binding of the ligand to the protein decreases its entropy to a great extent by restricting its rotational and translational degrees of freedom [170]. This leads to the increase in binding free energy, rendering the process unfavourable. However, the effect can be compensated by forming a network of hydrogen bonds for polar ligands [170]. For non-polar ligands, hydrophobic interactions play a major role [115,246]. Hydrophobic interactions are also be used in drug designing and delivery since increasing the hydrophobicity of ligands generally increases the binding [245]. Unfortunately, increase in hydrophobicity also has side effects such as low water solubility and an increased tendency to adhere to various cellular component [98,169,187]. There is also another factor which contributes in favouring entropy increase. The

polar groups in a protein have tightly bound water molecules [118,246], which have less mobility compared to bulk water. Upon binding of a ligand, these water molecules are released which increases the overall entropy.

1.4.4 Multiple binding equilibria

In this case, $n > 1$ and there are many ways a ligand can bind to the receptor. One way to write the equilibria is depicted below [189]

$$\mathrm{P} + \mathrm{L} \rightleftharpoons \mathrm{PL} \qquad K_1 = \frac{[\mathrm{PL}]}{[\mathrm{P}][\mathrm{L}]} \tag{38}$$

$$\mathrm{P} + 2\mathrm{L} \rightleftharpoons \mathrm{PL}_2 \qquad K_2 = \frac{[\mathrm{PL}_2]}{[\mathrm{P}]\,[\mathrm{L}]^2} \tag{39}$$

$$\mathrm{P} + n\mathrm{L} \rightleftharpoons \mathrm{PL}_n \qquad K_n = \frac{[\mathrm{PL}_n]}{[\mathrm{P}]\,[\mathrm{L}]^n} \tag{40}$$

The general equation for $\bar{\nu}$ is given by the Adair equation [170]

$$\bar{\nu} = \frac{\sum_{i=1}^{n} iK_i\,[\mathrm{L}]^i\,[\mathrm{P}]}{\sum_{i=0}^{n} K_i\,[\mathrm{P}]\,[\mathrm{L}]^i} \tag{41}$$

The simplest case for multiple equilibria is assuming that all sites are equivalent and independent. Thus, the affinity of any binding site is not affected by whether or not other sites are occupied. The number of ways in which *n* sites may be divided into *i* occupied states and (*n*-*i*) unoccupied states is given by [170]

$$N_{i,n} = \frac{n!}{(n-i)!i!} \tag{42}$$

Combining Eq. 41 and Eq. 42, $\bar{\nu}$ for independent equilibria is given by [170]

$$\bar{\nu} = \frac{nK_0[\mathrm{L}]}{1+K_0[\mathrm{L}]} \tag{43}$$

Where K_0 denotes here the microscopic equilibrium constant which describes the affinity of a particular site. This equation is similar to Eq. 35 when $n = 1$.

Binding to non-equivalent sites does not include a cooperative effect but rather the difference in binding affinities between various binding sites, giving rise to some strong and some weak binding, depending on experimental conditions.

Chapter 2

Experimental Methods

2.1 Fluorescence Spectroscopy

Fluorophores absorb energy in the form of electromagnetic radiation with a certain wavelength. The energy of the photon excites a bound electron from the Highest Occupied Molecular Orbital (HOMO) to the Lowest Unoccupied Molecular Orbital (LUMO) which makes the total electron density more diffuse and easily polarizable. This leads finally to a larger bond length and weaker bond strength between two atoms in a diatomic molecule in the electronically excited state. Simultaneously, the energy potential curve i.e., the MORSE potential of the molecule in the electronically excited state shifts to a new equilibrium position of the nuclei [51].

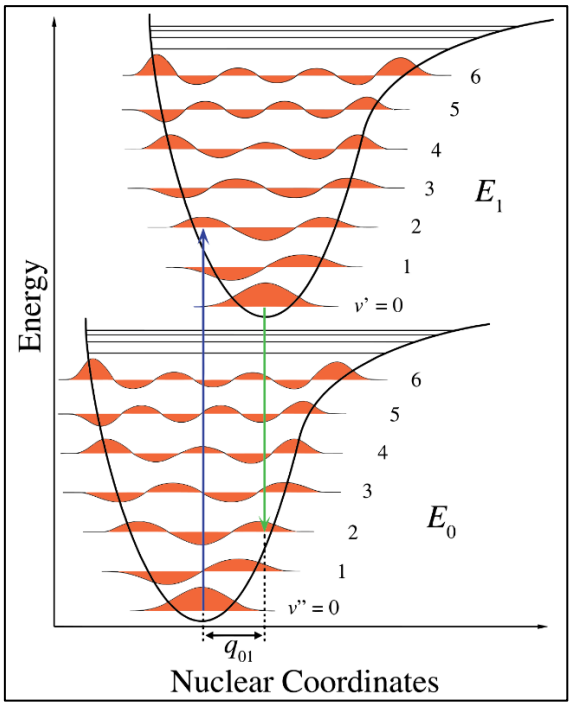

Figure 2.1. Morse-potential curve for a molecule in the singlet ground state E_0 and singlet excited state E_1 demonstrating the Franck-Condon principle. Adapted from [51].

The vertical transitions as can be seen in Fig. 2.1 can be explained by the BORN-OPPENHEIMER approximation and the FRANCK-CONDON principle. According to the BORN-OPPENHEIMER approximation, the electrons move much faster as compared to the nuclei due to the very high mass of protons or neutrons in comparison to electrons [51,276]. Thus, the electronic transitions are most likely to happen when the position and vibrational momenta of the nuclei are not changed (FRANCK-CONDON principle) [51,276]. This means, for a new vibrational transition to happen during an electronic excitation, the new vibrational level must be instantaneously compatible with the nuclear positions and momenta of the

vibrational level of the molecule in the originating electronic state. The intensity of this vibrational transition is proportional to the square root of the overlap integral between the vibrational wavefunctions of the two states that are involved in the transition [51].

The excited molecule can relax back to the ground electronic state in a number of radiative and non-radiative ways (Fig. 2.2) [276]. Firstly, the molecule relaxes back to the ground vibrational state of the excited electronic state. This process is known as vibrational relaxation (VR) and occurs within the first 10^{-11} s. The energy is released by collision with solvent molecules. The molecule can now relax to the ground electronic state either via non-radiative process such as internal conversion (IC) or Quenching or radiative process such as Fluorescence. Fluorescence is a radiative process where the molecule returns to the ground state from the first excited ground state by emitting a photon with a rate constant of 10^{8} s^{-1} as a result of spin pairing of electron (spin allowed). The vibrational state in the ground electronic state is relaxed till thermal equilibrium is reached which is governed by FRANCK-CONDON principle. The wavelength of the emitted photon is usually less i.e., red shifted (referred to as STOKE shift) compared to that of the absorbed photon [276]. Another pathway of electronic relaxation is intersystem crossing (ISC), where the electron changes spin multiplicity from singlet state to triplet state. Though the process is spin forbidden, the chances of ISC is high if the vibrational levels of the two states overlap or if the energy difference between the two states is small. ISC efficiency depends on the nature of the fluorophore and transition probabilities and is generally high due to the presence of heavy atoms [276]. The molecule can relax from higher vibrational levels of the triplet state to the lower vibrational levels of the same state by means of VR. It finally transits to the ground electronic state by emitting a photon and the process is termed as phosphorescence. It has a rate constant of 10^{-2} to 10^{2} s^{-1} and is slower than fluorescence. The relaxation energy can also be transferred to adjacent molecules by means of quenching.

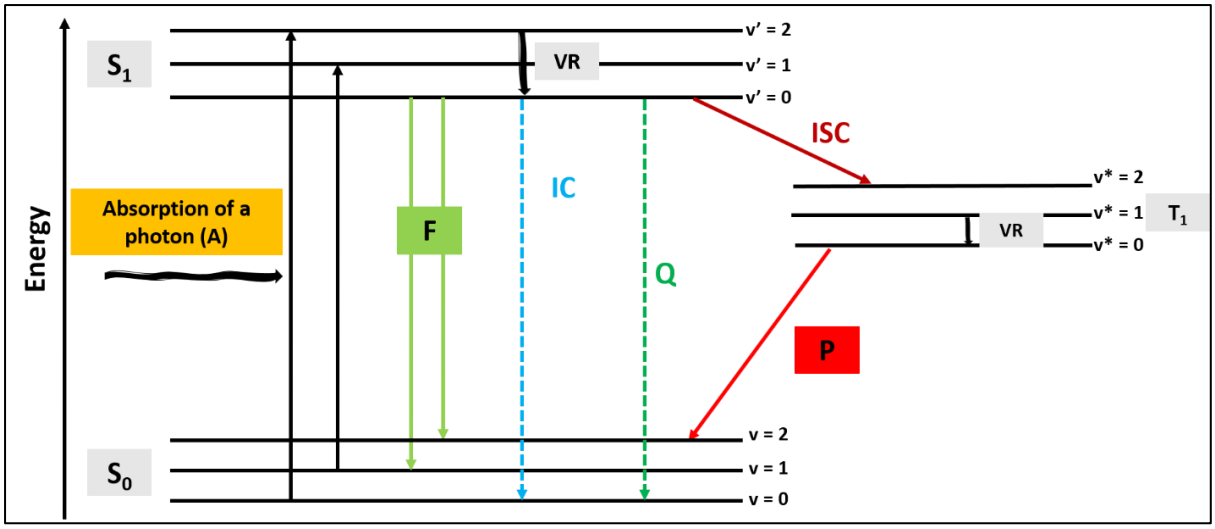

Figure 2.2. JABLONSKI diagram showing excitation and relaxation of a fluorophore. After absorbing (A) a photon, the molecule transitions from the singlet ground state (S_0) to the first (S_1) excited electronic singlet state with various vibrational energy states. The molecule relaxes from excited the vibrational state to the ground vibrational state through Vibrational Relaxation (VR). During relaxation from the excited electronic state to the ground electronic state, the energy is dissipated through multitude radiative and non-radiative processes, including internal conversion (IC), quenching (Q), fluorescence (F), intersystem crossing (ISC) and phosphorescence (P).

In general, the vibrational transitions in solution are not resolved, and the overlap of absorption and fluorescence bands is relatively large. This is mainly due to the inhomogeneity and polarity of solvent as well as the interactions between the fluorophores and solvent. This leads to the consequence that the position of the energy levels is influenced differently by the surrounding solvent. Fig. 2.3 illustrates the influence of a polar solvent on the fluorescence spectrum.

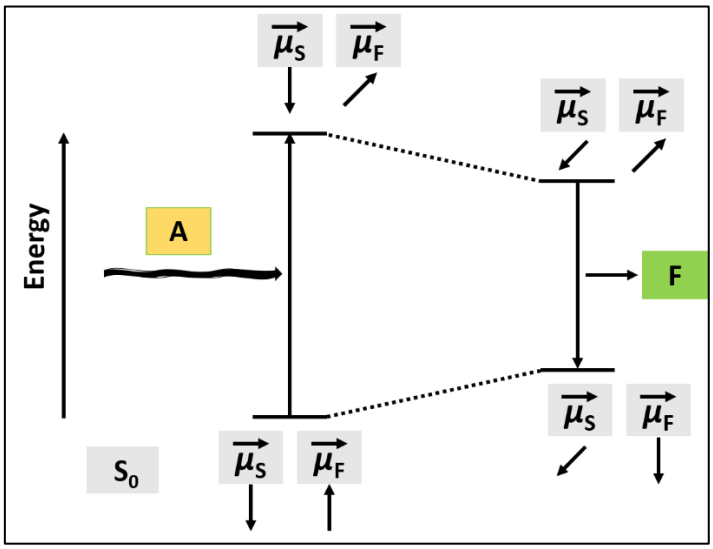

Figure 2.3. Schematic representation of the principle of solvent relaxation and the accompanying red shift of fluorescence. $\vec{\mu_S}$ representing the solvent dipole whereas $\vec{\mu_F}$ represents the fluorophore dipole.

The solvent dipoles ($\overrightarrow{\mu_S}$) orient antiparallel to the dipole moment of the fluorophore ($\overrightarrow{\mu_F}$) in the ground state. Upon absorption of radiation, the electric dipole moment of the fluorophore changes in strength and orientation. The solvent molecules then try to adapt to the new equilibrium which takes about 10^{-10} s to complete. Thus, the S_1 state is stabilized and is lowered energetically. After the photon has been emitted, the fluorophore again has its original dipole moiety, but the surrounding solvent molecules are no longer energetically aligned for this purpose at this time. As a result, the resulting new ground state is energetically destabilised compared to the equilibrium ground state. The result of this interaction of the fluorophore with the solvent molecules is a redshift of the fluorescence radiation in the spectrum (see Fig. 2.3). The greater the polarity of the solvent, the greater the redshift in general.

2.1.1 Fluorescence instrumentation

The schematic representation of a fluorescence spectrometer is shown in Fig. 2.4. The design of the apparatus is such that the detector is placed at a 90 ° angle to the light source and a monochromator between the sample and detector. As a result, not only the emission spectrum can be exactly resolved but the signal to noise ratio can be significantly improved, allowing the use of very low sample concentration.

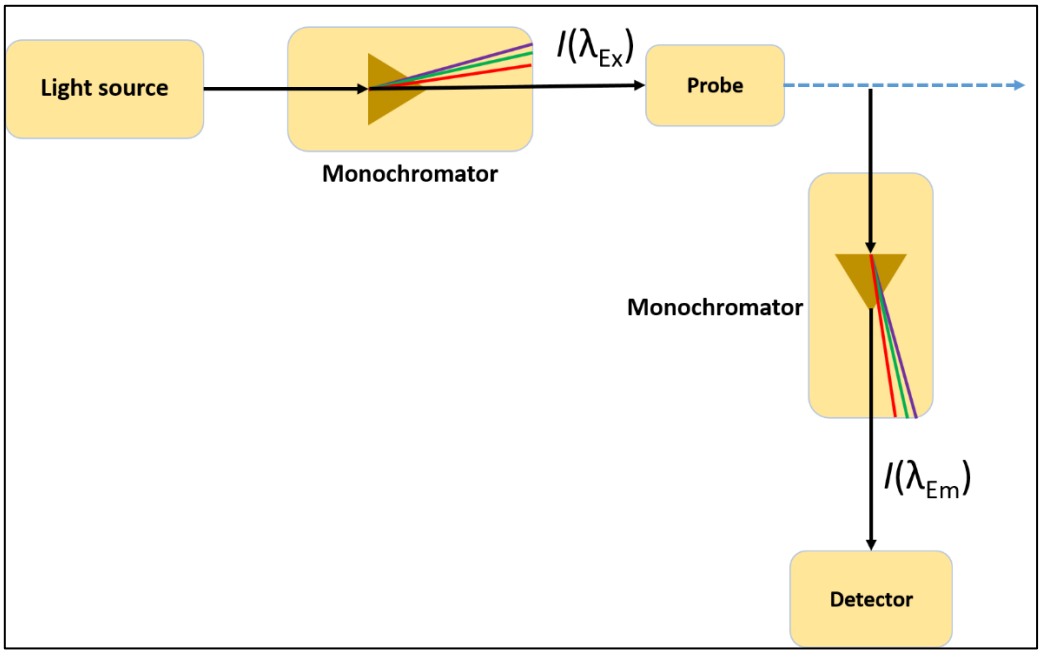

Figure 2.4. Schematic structure of a Fluorescence spectrometer.

All the fluorescence measurements that have been included in this thesis (Chapter 3 and Chapter 4) were carried out on a K2 fluorescence spectrometer from ISS:

- Labeling: K2
- Manufacturer: ISS (Champaign, Illinois, USA)
- Light source: xenon arc lamp
- Temperature control: external water bath - Julabo F 32
- Pressure indicator: TecSis P3298B093001 (electrical)

The instrument uses a xenon arc lamp as the source of excitation light. Such lamps are generally useful because of their high intensity in wavelengths range between 250 and 1100 nm. The emitted light is focused with the help of lenses on the entrance slit of the excitation monochromator. A monochromator accepts incoming light and disperses it into the various colors of the spectrum using prisms or diffraction gratings (Fig. 2.5). In the K2 spectrometer, the spectral region is in the range of λ = 200-800 nm with allowance of $\Delta\lambda$ = 0.25 nm. Both monochromators are equipped with a set of interchangeable slits. The slit handles are marked with the width of the slits: 2, 1, 0.5 mm. The monochromatic light is then stirred over a mirror, which is present in the corner of a two-way polarizer, directly on a beam splitter. The beam splitter reflects part of the excitation light to the reference cell and the rest part to the sample cell. In the sample space two different cells may be used. Firstly, the standard quartz glass cuvette for temperature-dependent measurements at atmospheric pressure can been used. For pressure dependent measurements a commercially available high-pressure cell (ISS) is used. The sample is filled into a quartz glass vial, sealed with Dura-Seal film and an O-ring free of air bubbles and placed in a stainless-steel cell filled with water. The cell is closed and connected to a capillary, which is connected to a hydraulic pump in order to build up pressure in the pressure medium (water). In the right emission channel, light emitted by the sample is spectrally divided by the emission monochromator in the optical path. The emission monochromator grating is maximized for fluorescence light detection in the region λ = 350-800 nm. Optical filters are used to compensate for the non-ideal behavior of monochromators. The detection of the emission can be made by the two photomultipliers, on the left and on the right side of the sample area. The fluorometer uses photomultiplier tubes (PMT) as detectors. A PMT is regarded as accurate source, the current being proportional to the light intensity. Although a PMT responds to individual photons, these individual pulses are generally detected as an average signal. Polarizer's are present in the both excitation and emission light paths. Generally, polarizers are removable so that they can be inserted only for the measurement of

fluorescence anisotropy or when it is necessary to select for particular polarized components of the emission and/or excitation (Fig. 2.5).

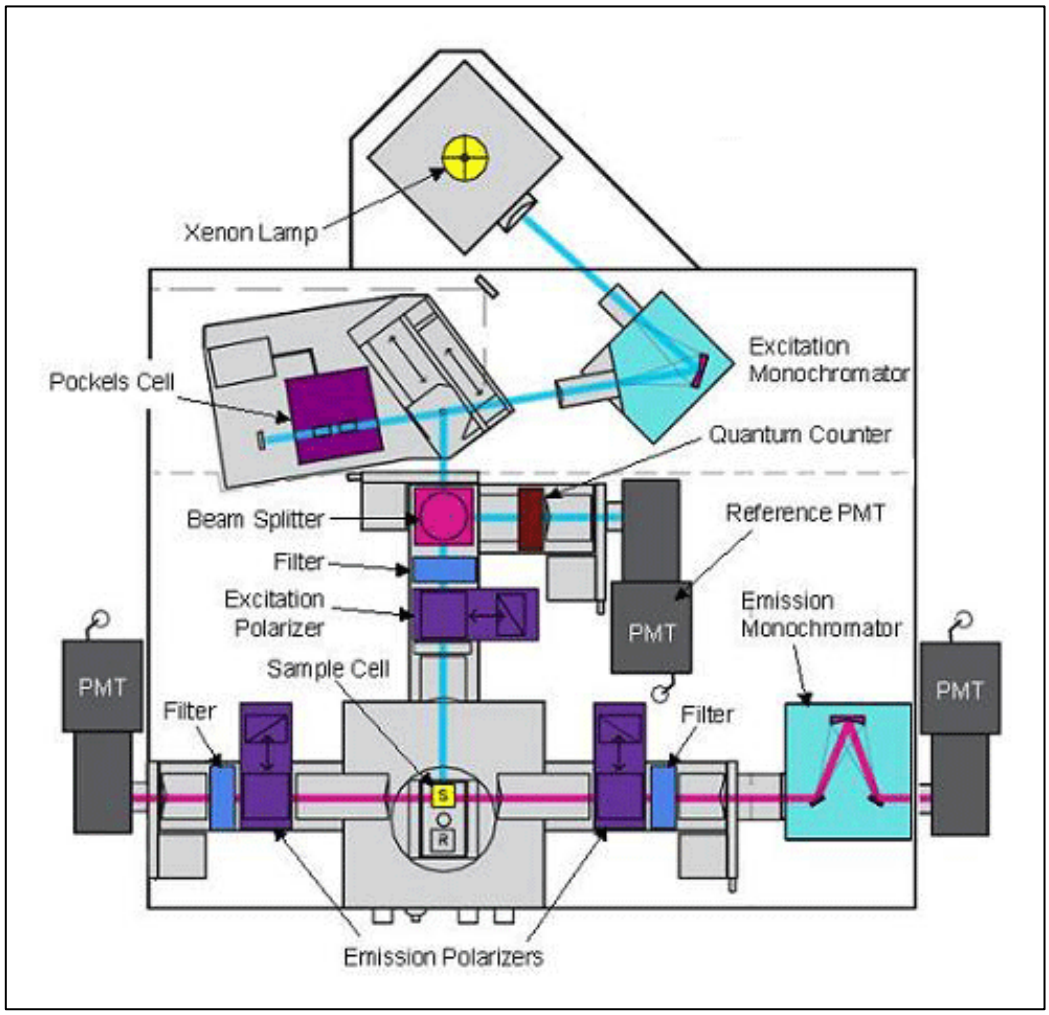

Figure 2.5. Schematic illustration of the K2 fluorescence spectrometer. Adapted from ISS.com.

High pressure cell: ISS (Champaign, Illinois, USA)

- Sample volume - 1 mL
- Window - sapphire; Sample vial - quartz glass
- Pressure control - Nova Swiss (hydraulic press)

Fluorescence spectroscopy is one of the most important methods in biology. Apart from investigating the structure and dynamics of proteins, lipids, nucleic acids using fluorescence, several other parameters can be determined such as-

1) Protein-ligand interactions
2) Rotational and translational diffusion
3) Internal dynamics and conformational changes
4) Kinetics
5) Change in environment of the fluorophore

2.2 Stopped - Flow Method

Several experimental techniques have been developed over years to monitor chemical reactions in real time scale. Fast reactions (in the time scale of milliseconds to seconds) are generally studied using flow techniques which involve automated mixing of components [173,276]. The difference in time between mixing of components and recording the first data point is called dead time. Manual mixing of components has a dead time of a few seconds which is not problematic for slow reactions as the progress of reaction is not significant in this time range, but for fast reactions, the whole reaction may be completed in a few seconds. Thus, for fast reactions, rapid mixing is an essential part.

There are various flow techniques – the stopped flow method, the continuous flow technique and the quenched flow technique to name a few. The continuous flow method is normally used to study initial rates and inhibition values [173]. In this case, the two reactants, each filled in a pneumatically driven syringe, are injected into the mixing chamber (Fig. 2.6(A)). After mixing homogeneously, the solution is passed from the mixing chamber to a long tube, the observation chamber, and measurements are taken by various detection units, mostly spectrophotometers situated at various points along the tube. Since the flow rate of reactants is constant, each point in the tube corresponds to a discrete point in time. It provides high level of accuracy in determining the time-dependent reaction mixture composition since many data points can be collected at one sample point as the reaction mixture passes through it several times. The disadvantage of this technique is the use of a large volume of reagent which is needed to maintain the continuous flow. This problem can be solved by the stopped-flow method. In this method, reactants are held in separate syringes that are prevented from free flow by syringe pumps (Fig. 2.6(B)). The reaction is initiated by the movement of a plate, driven by the expansion of compressed gas, which pushes the piston of the syringes and thus releasing the reactants into the mixing chamber. There is an additional pistol at the end of observation chamber, the stop syringe, which hits a stop plate or block once the homogeneously mixed solution reaches the observation chamber from the mixing chamber and a continuous flow has

been attained. This restricts the volume usage and only a small defined volume of reactants are necessary to carry out the measurement. The dead time for stopped flow instruments is generally in the range of 1-2 milliseconds and thus allows monitoring the reaction as a function of time. The disappearance of reactants or the formation of products can be monitored using fluorescence, circular dichroism, absorption or small-angle scattering [173]. This method is helpful for deducing the underlying kinetic mechanism by varying the concentration of reactants and determining the rate constants as a function of temperature and/or pressure. Double-mixing stopped flow instruments consist of four syringes as against two syringes for single-mixing stopped-flow instruments and thus are helpful in studying the reaction of intermediates with other compounds.

(A)

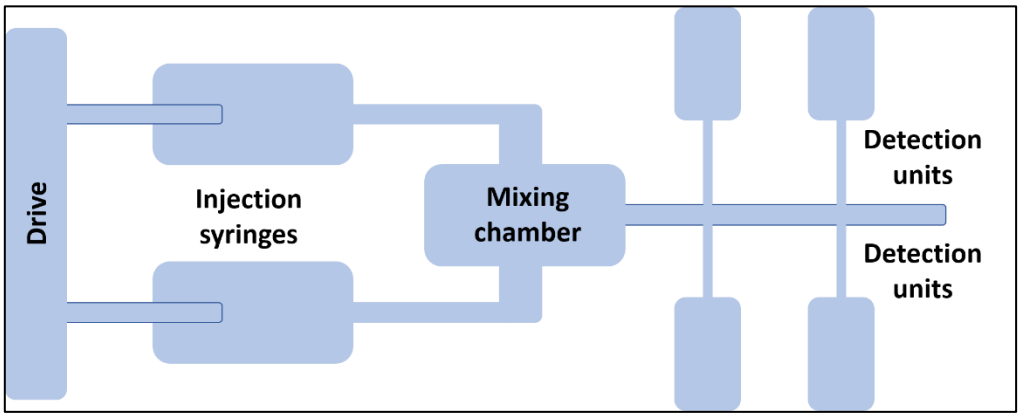

(B)

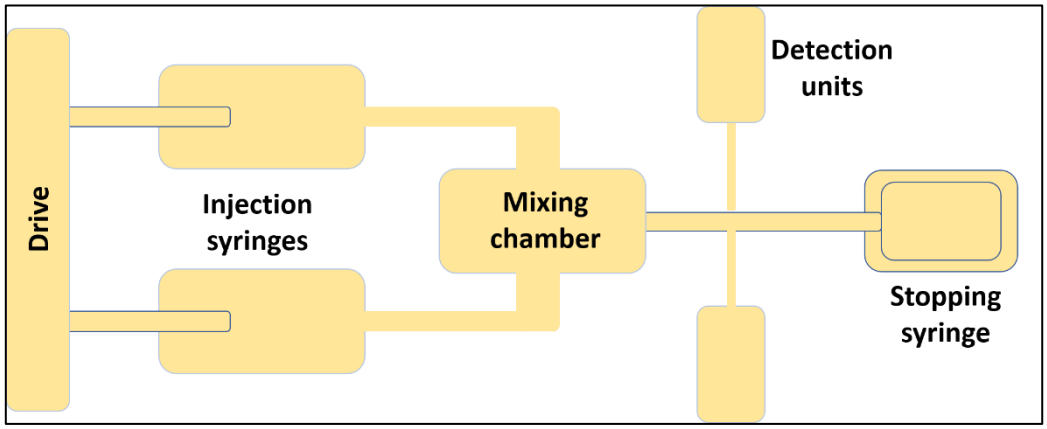

Figure 2.6. Flow techniques: (A) Schematic of a continuous-flow capillary mixing apparatus with several detection units. (B) Schematic of a stopped-flow capillary mixing apparatus with one stationary detection unit.

All the experiments included in this thesis were performed using the SF-61DX2 Stopped-Flow spectro-fluorimeter which comprises four major sections: a sample handling unit, two electronics units and a collection of optics for excitation and detection (Fig. 2.8). This instrument can be used in single mixing mode to rapidly mix two reagents, or in a double mixing mode where two reagents are first mixed and then a third reagent is added after some time. The body of the sample handling unit is majorly constructed in stainless steel. All sample flow circuit components are contained within a thermo-stable enclosure; a Pt100 temperature probe is fitted within this enclosure for temperature-dependent measurements. The sample flow circuit consists of four DRIVE/FILL valves, the STOP/WASTE valve and observation cell. The four syringes and associated DRIVE/FILL valves are grouped into pairs; each pair of syringes is driven by a common drive plate (Fig. 2.7). Samples are loaded onto the drive syringes of the sample handling unit and are mixed using the pneumatic cylinder which provides the drive using the stepper motor. The samples are mixed in the mixing chambers and the flow is stopped by a stop syringe. The stop syringe is restricted by a rigid stop block or the STOP/WASTE valve, causing rapid deceleration of the solutions and triggering of the data acquisition system.

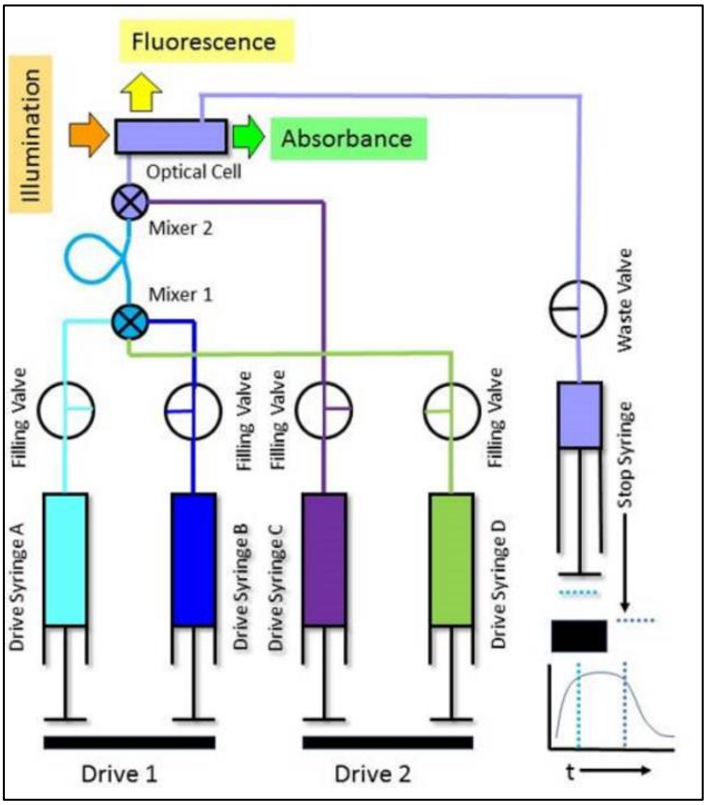

Figure 2.7. Double mixing stopped-flow instrument showcasing the sample handling unit. Adapted from [49].

The instrument uses a xenon lamp as the light source. The light passes through the monochromator and the selected wavelength then falls on the beam splitter. The beam splitter divides the incident light before it reaches the observation cell, so that approximately 80 % converges onto the cell, while the remaining 20 % is diverted at a right angle to the side coupler. A PM-61s photomultipler is attached directly to this side coupler for reference channel detection. Both absorption and fluorescence can be detected using this instrument. For absorbance measurements, the detecting photomultiplier is mounted opposite the incident light entrance whereas for fluorescence the photomultiplier is placed at an angle of 90 ° with respect to the incident light entrance (Fig. 2.7)

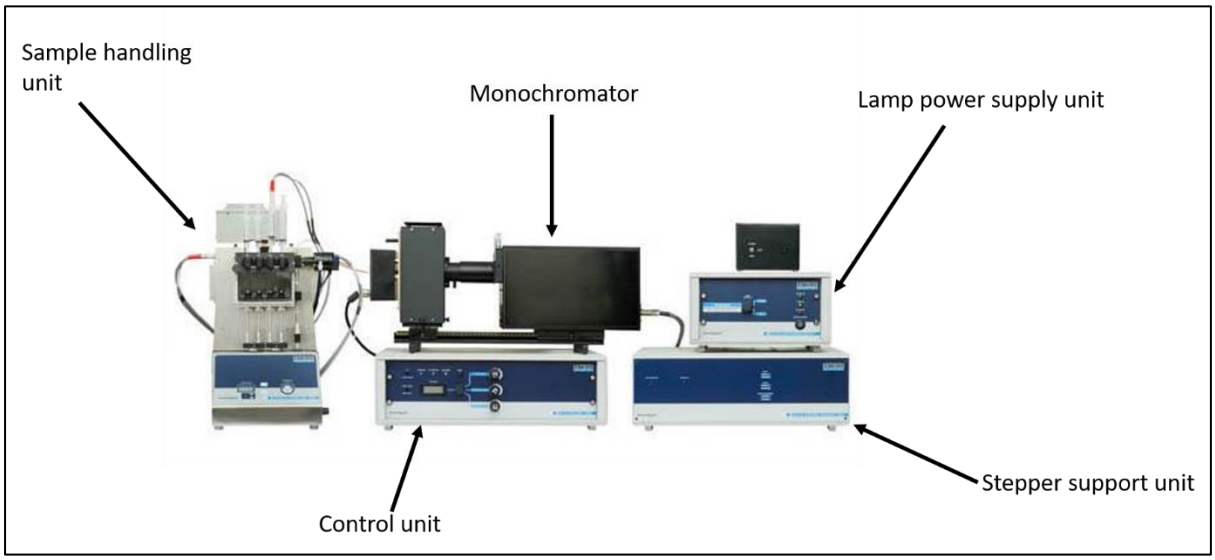

Figure 2.8. Benchtop layout of SF-61SX2 of Hi-Tech Scientific. Adapted from [49].

2.3 UV/Vis Spectroscopy

Absorption in the UV-Vis region (190 nm to 400 nm) gives rise to electronic transitions, promoting electrons from the ground n (non-bonding) or π orbitals (HOMO) to the excited π* orbital (LUMO) and thus favours molecules with delocalized π electrons i.e. aromatic and conjugated aliphatic species [101,276]. The part of the molecules that absorbs light is known as chromophore such as conjugated π-bond systems (azo-compounds, retinal). Usually, an absorption spectrum pictures the dependence of absorption by a molecule as a function of wavelength of the irradiating light.

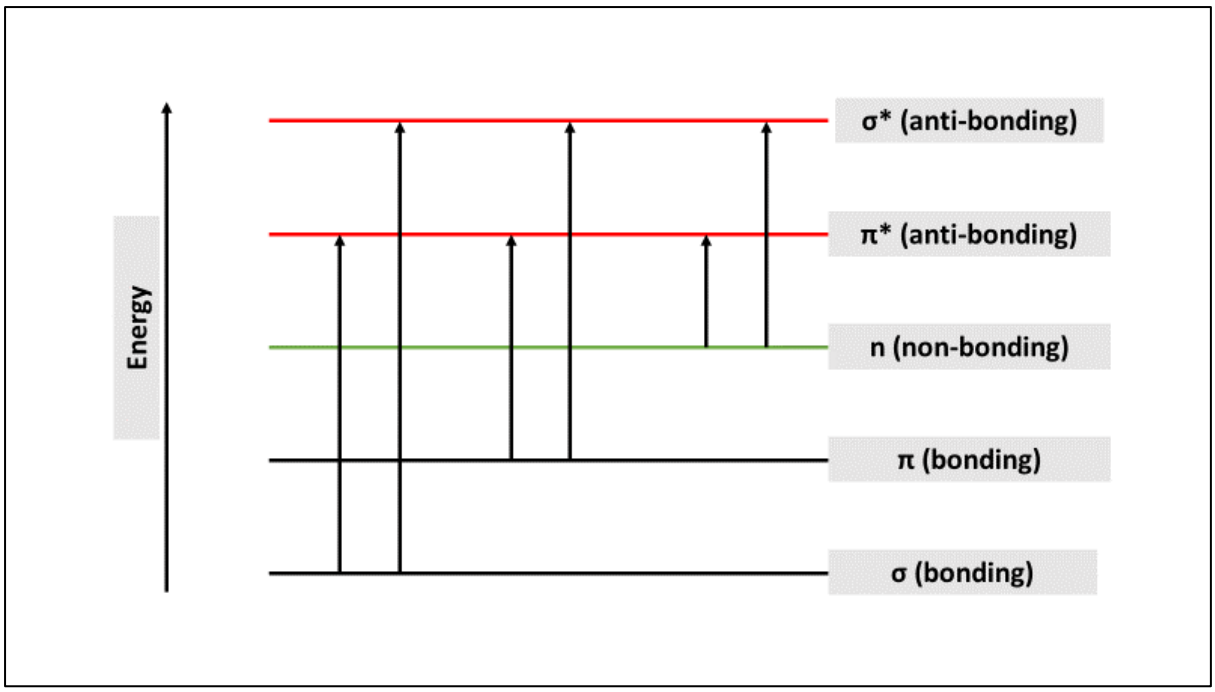

Figure 2.9. Schematic representation of the possible electronic transitions in a molecule upon excitation with UV-Vis radiation.

For each system, the energetic position of the molecular orbitals is precisely defined and thus, also the energy needed for excitation. The larger the distance between two energy states, the higher is the energy required and thus, the smaller is the wavelength of the radiation required for the transition. Hence, when a white light (entire UV/Vis spectrum) is illuminated on a probe, all the electronic transitions corresponding to the appropriate energies are excited and these wavelengths are absorbed from the spectrum. These particular wavelengths are then absent in the spectrum detected and the sample appears in the complementary color.

2.3.1 UV-Vis spectrophotometer

This instrument is used to measure the absorption of UV /Visible radiation by a sample either at a particular wavelength or by performing a scan over the entire range (190 nm to 400 nm) in the spectrum. The basic structure of a UV- spectrophotometer consist of a light source, a monochromator, a sample cell and a detector. The ultraviolet radiation is generated using a deuterium arc lamp, a tungsten lamp is used for visible light and a Xenon arc lamp for UV/Vis light. The monochromator consists of a diffraction grating used for splitting the light into its component colours of different wavelength and for selecting the wavelength of interest. UV/Vis spectrophotometry is generally used to measure absorbance for liquids, although solid

and gas samples can also be measured. Samples are typically placed in transparent cell known as cuvettes. Generally fused silica or quartz glass cuvettes are used due to their transparency throughout the UV/Vis region, whereas glass and most plastic cuvettes limit their usage due to their absorption in the UV. The detector is usually a photomultiplier that generates secondary electrons from the photons entering it through the photoelectric effect. These secondary electrons are accelerated in an electric field and amplified to a measurable photo current that is proportional to the light intensity [101,173]. The two most common types of absorption spectrometer are single and double beam spectrometers (Fig. 2.10).

(A)

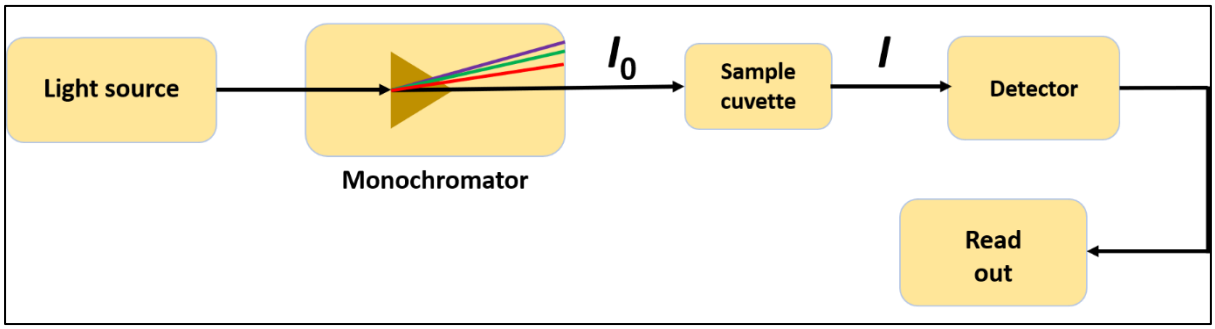

(B)

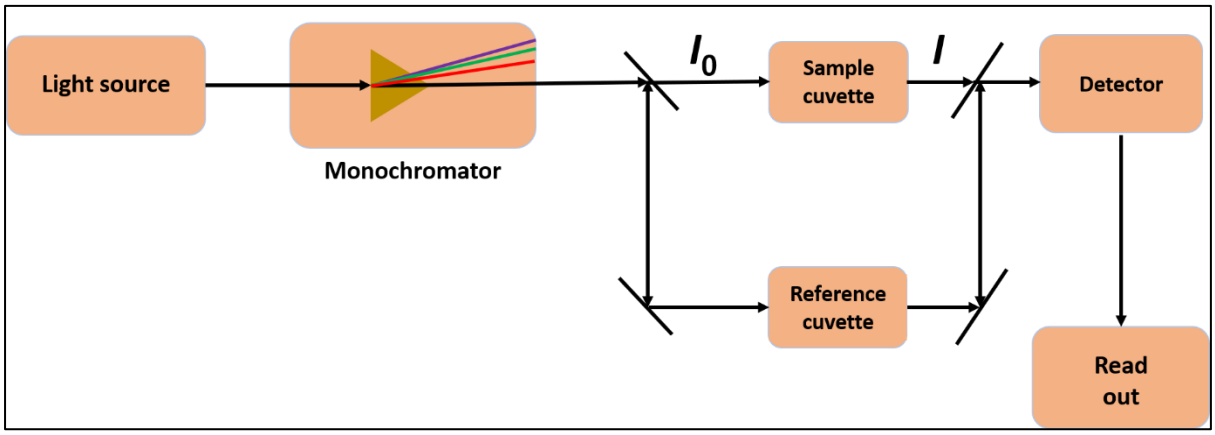

Figure 2.10. Schematic representation of (A) Single and (B) Double beam spectrophotometers where I_0 represents the incident radiation and I represent the emitted radiation intensity.

In a single beam spectrometer, the absorbance of the sample (A) is measured from the intensity of incident (I_0) and transmitted radiation (I). In another measurement, the solvent contribution to A is measured by putting only the solvent, in which the sample is dissolved, in the cuvette. This is called blank or reference which is subtracted from A to obtain the actual value. This technique differs from double beam spectrometers where the incident light is split before the

sample. One part of the light is passed through the cuvette containing the sample and the other part passes through the reference cuvette containing the solvent only. The difference between the sample and reference cell directly gives the actual absorbance value. The most common way to quantify Absorbance (A) is given by the Lambert-Beer Law which states that the absorbance (A) of a molecule is directly proportional to its concentration (c) and path length (l) [101,276]–

$$A = \varepsilon l c \tag{44}$$

where ε is the molar extinction coefficient which is a measure of the efficiency with which a molecule absorbs electromagnetic radiation and is wavelength dependent. If the concentration of a sample is unknown, it can be determined from the slope of the measurement of a dilution series of a known concentration.

The UV-Vis measurements are carried out on two different devices. On one hand the temperature-dependent measurements at atmospheric pressure are carried out by the UV-Vis-spectrophotometer from Shimadzu:

- Labeling: UV-1800
- Manufacturer: Shimadzu Deutschland GmbH
- Light source: Combination of WI halogen and D2 deuterium lamps
- Temperature control: External water bath - Julabo F 32

The standardized set-up is used and a commercially available sample cell Quartz cuvette with a volume of 1 mL and a layer thickness of 10 mm is used. On the other hand, the pressure-dependent turbidity measurements are carried out on the UV-Vis spectrometer from the PerkinElmer company.

- Labeling: Lambda 25
- Manufacturer: PerkinElmer
- Light source: Combination of WI halogen and D2 deuterium lamps
- Temperature control: External water bath - Julabo F 32
- Pressure indicator: TecSis P3298B093001 (electrical)

A high-pressure cell manufactured in-house (Fig. 2.11) has been used. Two quartz windows are screwed into a cylindrical jacket. An O-Ring in the cell seals between the stainless steel and the window. The sample volume is determined by the distance between the quartz

windows. The space between the windows can be filled with a syringe via another vertical hole. Then the same syringe is connected via a capillary to a hydraulic pump to build up pressure in the sample solution.

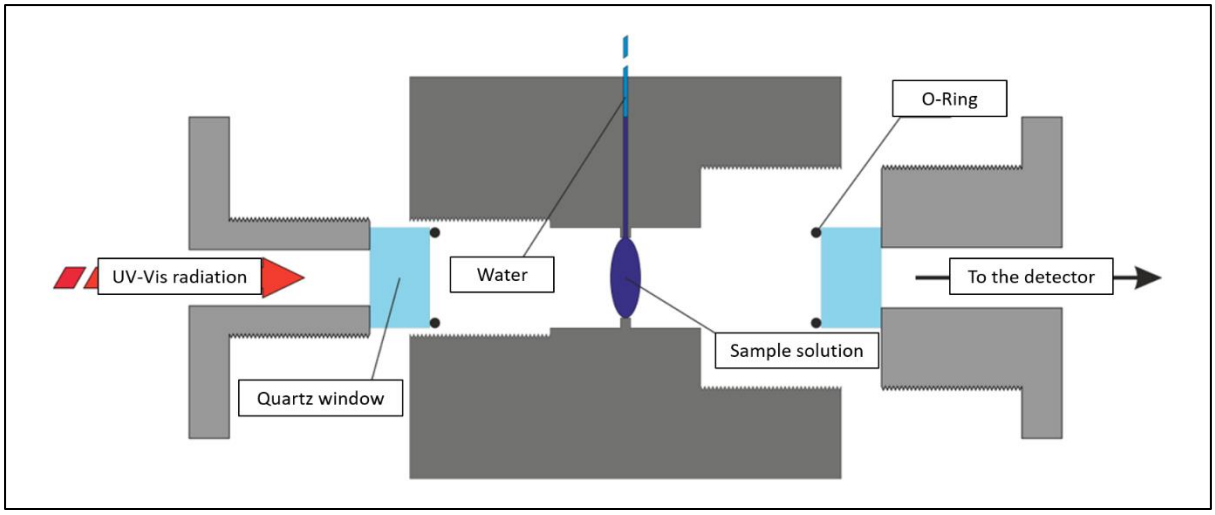

Figure 2.11. Schematic representation of the cross section of the high-pressure cell used for the UV-Vis spectroscopy. Redrawn and adapted from [163].

UV-HP cell: made in the lab (Prof. Dr. Roland Winter) (Fig. 2.11)

- Sample volume ≈ 300 μL
- Window - quartz
- Layer thickness - 4.3 mm (window to window)
- Pressure control - Nova Swiss (hydraulic press)

2.4 Circular dichroism spectroscopy (CD)

Absorption of light by a molecule takes place due to the interaction of the transition dipole of the molecule with the electric field vector of the light. When the vibration of electric field vectors is confined in one plane and parallel to one unique direction, it is referred to as Linearly polarized light [77,173]. The plane is generally known as polarization plane. The magnitude of the vector is modulated keeping the direction constant. For circularly polarized light, the tip of the electric vector depicts a helix as shown in Fig. 2.12.

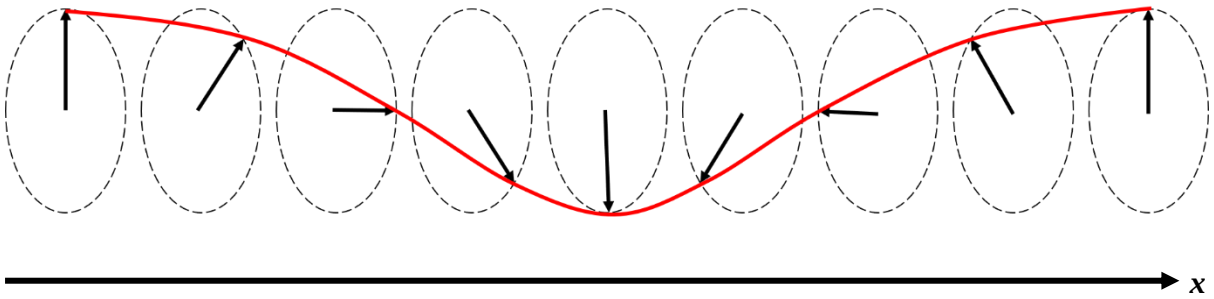

Figure 2.12. In circularly polarized light, the electric field vector is modulated in direction not in amplitude. The tip of the vector describes a helix (red line). Redrawn and adapted from [173].

Movement of the vector in the clockwise direction gives rise to right-handed circularly polarized light (RHCPL) and movement in the opposite direction forms left-handed circularly polarized light (LHCPL). If the refractive indices of a sample for RHCPL and LHCPL are different i.e., $n_{\mathrm{L}} \neq n_{\mathrm{R}}$, the transmitted light still remains linearly polarized, but the polarization plane is rotated with respect to the polarization plane of the incident light by an angle α. This phenomenon is called circular birefringence. On the other hand, if RHCPL and LHCPL are absorbed differently i.e., $A_{\mathrm{L}} \neq A_{\mathrm{R}}$ and $\varepsilon_{\mathrm{L}} \neq \varepsilon_{\mathrm{R}}$, the transmitted light is elliptically polarised with ellipticity θ as shown in Fig. 2.13. This is known as circular dichroism (CD). Thus, the direction of the electric field vector is changed keeping its magnitude constant [77,156,173].

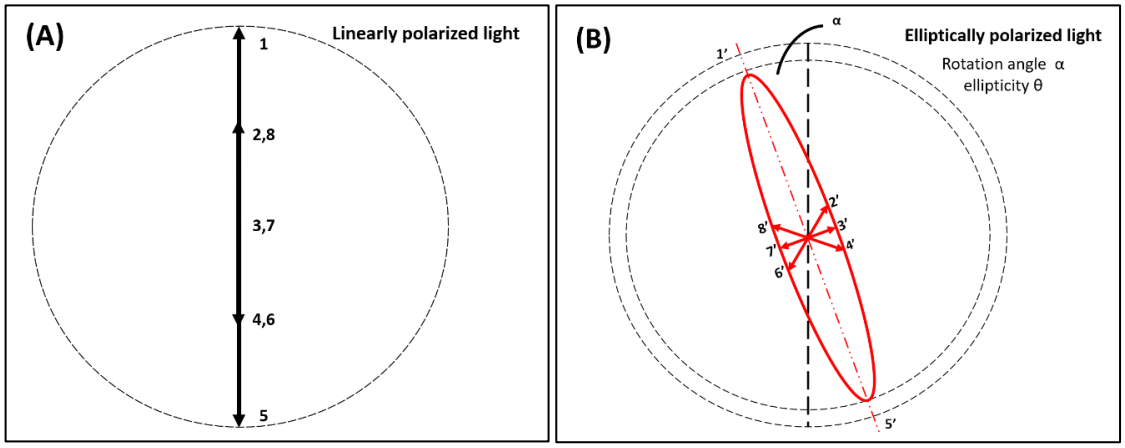

Figure 2.13. (A) linearly polarized light where the oscillation of the electric field vector is confined to one direction, here in the vertical direction. (B) when the RHCPL and LHCPL are absorbed differently and their refractive indices are different, it gives rise to elliptically polarized light and the plane of the ellipse is rotated by the angle α. Redrawn and adapted from [173].

CD spectroscopy is used to measure the interaction of polarized light with optically active (i.e., asymmetric) molecules. Asymmetry arises from chiral molecules such as the peptide backbone

[-(O)C-N(H)-] of proteins, a non-chiral molecule covalently attached to a chiral molecule (aromatic amino acid side chains) or a non-chiral molecule in an asymmetric environment (e.g., a chromophore bound to a protein). Proteins are CD-active due to the presence of at least one chiral centre in all amino acids except glycine. The resulting CD signals are sensitive to the secondary and tertiary structure of protein. The secondary structures of proteins interact preferentially with one circular polarization, allowing one to follow the changes in protein structure using CD spectroscopy.

By definition, CD is measured by the differential absorbance between RHCPL and LHCPL. Thus, from the Beer-Lambert law it can be written as

$$\Delta A = A_{\mathrm{l}} - A_{\mathrm{r}} = \varepsilon_{\mathrm{l}} cl - \varepsilon_{\mathrm{r}} cl = \Delta\varepsilon cl \tag{45}$$

where l is the path length and c is the concentration of the chiral solute. However, CD data are mostly not expressed in terms of $\Delta\varepsilon$ but in terms of molar ellipticity, i.e., $[\theta]_{\mathrm{molar}}$, which has the units of deg cm^2 dmol^{-1} and the relation between these two are expressed in Eq. 46 [63]

$$[\theta]_{\mathrm{molar}} \approx 3300\Delta\varepsilon \tag{46}$$

$[\theta]_{\mathrm{molar}}$ is related to ellipticity θ as [63]

$$[\theta]_{\mathrm{molar}} = \frac{100\theta}{cl} \tag{47}$$

The factor 100 is used for historical reasons. Thus, both θ and $[\theta]_{\mathrm{molar}}$ are proportional to the difference in extinction coefficient $\Delta\varepsilon$.

CD spectra of proteins and peptides are usually measured in two spectral regions. In the far-UV region (180-260 nm), the measured bands represent the electronic transitions of the amide bonds of the protein backbone. The sign, magnitude and position of these bands strongly depend on the arrangements of the peptide bonds. Thus, studies in this region give information about the secondary structure element of the protein. The CD spectra in near-UV region (250-350 nm) accounts for the packing of the side chains of aromatic amino acids and disulphide bonds. It depends on the local environment of the aromatic amino acids and on their orientation with respect to the backbone, thus providing information about the tertiary structure of the protein.

2.4.1 Far UV CD spectra and protein secondary structure

The most abundant elements of secondary structures of proteins are α-helices and parallel and anti-parallel β-sheets [63,79,156]. All proteins can be grouped into five classes according to their secondary structures:

1) All α proteins that show a strong double minimum at 222 nm and 208 ±2 nm and a strong maximum at 191±2 nm.
2) All β proteins showing a single negative at 216 ±3 nm and a single positive maximum between 190 nm and 200 nm whereas a highly distorted β-sheet or β-sheets made up of short irregular β-strands show a strong negative band near 200 nm, similar to the unordered form [63,156].
3) α/β proteins the have intermixed segments often alternate along the polypeptide chain.
4) α+β proteins have α-helices and β-sheets often in separate domains.
5) Denatured or unordered proteins have little ordered conformations and show a strong negative band near 200 nm and some weak bands between 220 and 230 nm, which can have either positive or negative signs.

For α+β and α/β proteins, the ellipticity of α-helices predominate that of β-sheets. In some cases, a single broad minimum band may appear between 210 and 220 nm because of the overlapping of the CD signal of various α-helices and β-sheets. For α+β proteins, the 208 ±2 nm band ellipticity is higher than the 222 nm band, and the reverse is true for α/β proteins [79,156].

2.5 Phase contrast microscopy

Phase contrast microscopy was first described by the Dutch physicist Frits Zernike in 1934. It is a contrast-enhancing optical technique that converts phase shifts in light passing through a transparent specimen into corresponding changes in amplitude, which can be visualized as differences in image contrast. One of the major advantages of using this technique is that living cells can be examined in their natural state without previously being killed, fixed and stained. This helps in inspecting ongoing biological processes which is generally not possible in brightfield microscopy.

2.5.1 Working principle and instrumentation

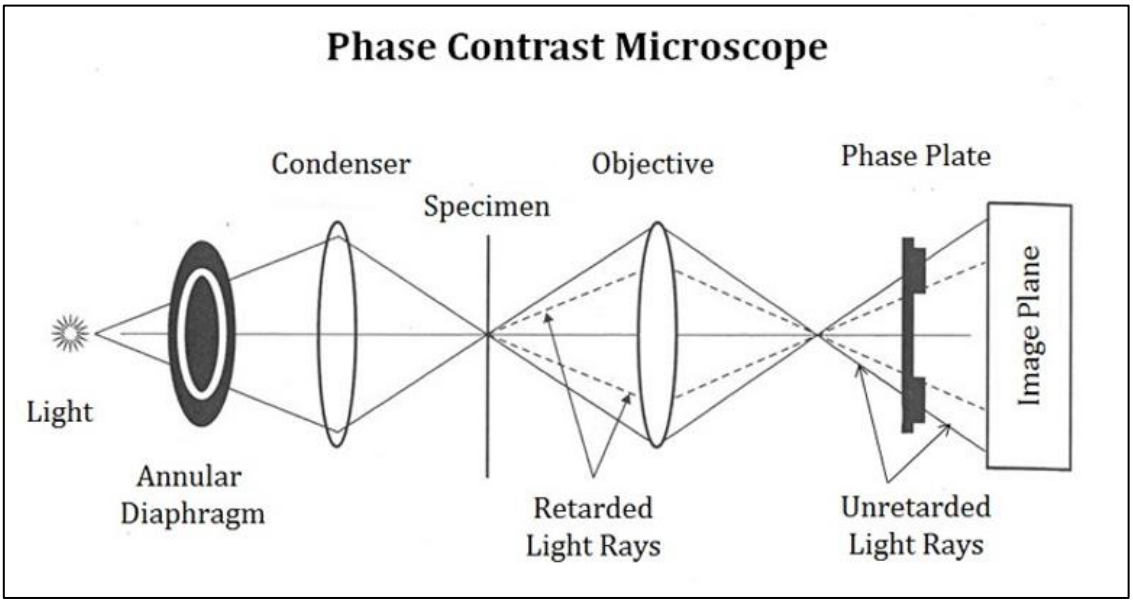

Figure 2.14. Schematic representation of a modern upright phase contrast microscope showcasing the optical path . Adapted from [125].

For an upright phase contrast microscope, ring-shaped partially coherent light is produced by a tungsten-halogen lamp. It is then directed through a collector lens and focused on a specialized annulus, also known as condenser annulus, positioned in the front focal plane of the condenser. The condenser annulus is constructed as an opaque flat-black (light absorbing) plate with a transparent annular ring. Light passing through the annulus illuminates the specimen and either gets scattered by the specimen or remains unaffected by the specimen and forms the background light (**S-wave**). Undeviated and diffracted light (**D-wave**) collected by the objective is separated by a phase plate and focused at the intermediate image plane to form the final phase contrast image observed in the eyepieces. A phase plate is constructed in or near the objective plane in order to selectively alter the phase and amplitude of the surrounding (or undeviated) light passing through the specimen.

The S-wave and D-wave after passing through the sample is focused at the image plane where they combine through interference to produce a resultant particle wave (**P-wave**). The mathematical relationship between the various light waves generated in phase contrast microscopy can be described as [125]

$$P = S + D \tag{48}$$

According to classical optics, the optical path length (OPL) through an object is the product of the refractive index (n) and the thickness (t) of the object as described by the relationship [125]:

$$\text{Optical Path Length (OPL)} = n \times t \tag{49}$$

The optical path length is also described as optical path difference (Δ) which is defined as

$$\text{Optical Path Difference (OPD)} = \Delta = (n_2 - n_1) \times t \tag{50}$$

where n_2 is the refractive index of the specimen and n_1 is the refractive index of the surrounding medium. The optical path difference results from the product of two terms: the thickness of the specimen, and its difference in refractive index with the surrounding medium. The difference in the wavefront between the specimen and surrounding medium is termed the phase shift (δ) and is related to OPD in radians as [197,248]:

$$\delta = 2\pi\Delta/\lambda \tag{51}$$

While observing an unstained sample, the scattered light is generally weak, and phase shifted by -90 ° with respect to the background light. This results in nearly the same intensity for the S-wave and P-wave and hence low image contrast. In phase contrast microscopy, the image contrast is increased in two ways [125]:

1) By generating constructive interference between the D-wave and S-wave in the region containing the specimen by phase-shifting the background light by -90 ° using the phase plate.
2) By reducing the amount of background light that reaches the image plane.

Chapter 3

Modulation of Enzymatic Activity by Aqueous Two-Phase Systems and Pressure – Rivalry between Kinetic Constants

3. Modulation of Enzymatic Activity by Aqueous Two-Phase Systems and Pressure – Rivalry between Kinetic Constants

Abstract

Macromolecular crowding inside the cell effects various physio-chemical processes such as enzyme kinetics, protein folding and its stability in a variety of ways. Aqueous two-phase systems (ATPSs), a variety of liquid-liquid phase separation (LLPS), have recently been proved to be a great medium not only for studying the crowding effect but also to research about the mechanism for the formation of membrane-less organelles. Pressure, on the other hand, is a powerful tool to understand the free-energy and conformational landscape of biomolecules. In this chapter, the combined effects of ATPS and pressure on an enzymatic hydrolysis reaction has been studied. The results imply that simple steric crowding is not enough to explain the enzyme kinetics in a crowded medium such as ATPS. Other factors, like a change in water activity, need also to be considered.

The work herein described has been published in the following peer-reviewed research article and subsequently reprinted in parts with the permission of the journals. Contributions of co-authors are either dinstinctly marked.

R. Oliva*, S. Banerjee*, H. Cinar, and R. Winter. Modulation of enzymatic activity by aqueous two-phase systems and pressure - rivalry between kinetic constants. *Chemical communications* **56** (2020) 395-398

was published online on December 2nd, 2019 and the DOI is 10.1039/C9CC08065A. In this chapter, the publication is partially reproduced in sections (3.1-3.3.7) and (3.5.3-3.6) with the permission from the Royal Society of Chemistry (Order license ID- 113573-1). The used text paragraphs and figures were reformatted to the format of the thesis (e.g. text font, reference numbering, figure numbering). Some phrases in active voice were changed to those in passive voice. In addition, the supplementary figures were moved to the main text and splitted to improve the quality of reading.

Author contribution: S.B. and R.O. designed the research, S.B. and R.O. performed research, H.C. performed the pressure-dependent phase contrast and turbidity measurements, S.B., R.O. and H.C. analysed the data, S.B., R.O. and R.W. interpreted the results and R.O. and R.W. wrote the paper with refinement by all co-authors.

*Both the authors contributed equally to the work.

3.1 Introduction

In recent years, the demand for biocatalytic processes has continuously increased as they often present better options to chemically catalysed routes [65]. However, the underlying process parameters of enzyme-catalysed reactions using temperature, pH and cosolvents as variables are often restricted and lead to limited enzyme stability as well as low reaction rates and yields [178,184]. Quite often, these parameters are also difficult to predict. However, to yield insights into the origin behind solution conditions of enzymatic reactions, a thermodynamic approach to predict the influence of cosolvents on the reaction kinetics on enzymatic reactions has been addressed recently [68,172]. The approach is based on molecular interactions in the form of activity coefficients of the substrate and of the enzyme in the multi-component solution. This allowed us, for example, to quantitatively predict the effect of cosolvents on the kinetic constants, i.e. the Michaelis constant, K_M, and the catalytic constant, k_{cat}, of an α-chymotrypsin-catalysed peptide hydrolysis reaction [68,172].

To expand the window of process parameters, application of high pressure has been proposed, as pressure may stabilize the enzyme at higher temperatures and modulate reaction rates [129,158,160,228,287]. Pressure is also a useful tool to modulate intermolecular interactions between molecules and thus serves as an important physical probe for changing the free-energy and conformational landscape (e.g., conformational substates) of proteins and enzymes [66,83,91,108,109,120]. Generally, by favouring states with a smaller partial molar volume, pressure shifts an equilibrium towards the state with smaller overall volume, in accord with Le Châtelier's principle [66]. The quantitative description of the effect of pressure on any chemical equilibrium and reaction rate (e.g., an enzymatic reaction) is given by

$$\left(\frac{\partial \ln K}{\partial p}\right)_T = -\frac{\Delta V}{RT} \quad , \quad \left(\frac{\partial \ln k}{\partial p}\right)_T = -\frac{\Delta V^{\neq}}{RT} \tag{52}$$

where K is the pressure-dependent equilibrium constant, k is the rate constant of the reaction, and ΔV and $\Delta V^{\neq}$ are the associated reaction and activation volumes, respectively. Hence, any reaction that is accompanied by a negative $\Delta V^{\neq}$, i.e., if the transition state has a smaller volume than the reactants partial volume, will be accelerated under pressure, and vice versa, and the K and k values can be expected to exponentially depend on pressure [66,132,158,228].

Furthermore, a huge fraction of organisms in the Earth's biosphere is thriving at a depth in excess of 1000 m and is therefore exposed to pressures of 100 bar and more, reaching the 1000

bar level at the sea floor in the Mariana trench and even higher pressures in the subseafloor crust which is abundant with life forms as well [186,233]. Hence, high hydrostatic pressure (HHP) studies on biomolecular systems (piezophiles) are also prerequisite for understanding life in the deep sea, an environment which is also the potential birthplace of life on Earth [233].

The effect of liquid-liquid phase separation (LLPS) as observed in aqueous two-phase systems (ATPSs) in modulating enzymatic reactions is hardly explored as well [7,43,175,232]. Liquid condensates (also denoted as coacervates) in ATPSs can locally concentrate reactants to accelerate reactions [46,268]. Further, different partitioning of enzyme and substrate in the coexisting phases and condensate-reactant interactions can modulate enzymatic reaction parameters. The use of studying the effect of ATPSs on enzymatic reactions is also of particular interest as it has become evident in recent years that the interior of the biological cell, which is crowded with biomacromolecules, contains also multiple coexisting liquid-like phases of distinct composition, [232,259,286] allowing dynamic localization and sequestering of molecules as well as reactions within these membrane-less subcellular compartments.

The best studied ATPS is the synthetic polyethylene glycol (PEG)-dextran system [43,175]. Proteins usually partition into its dextran-rich droplets because of favourable interactions with the more hydrophilic dextran-rich phase. This ATPS where the enzymes concentrate into one phase serves as a good in vitro model system for artificial liquid membrane-less organelles [175,235]. Many factors can influence the enzyme activity in these dense droplet phases, both favourably and unfavourably, such as changes in the structure and conformational dynamics of the active site of the enzyme, changes in the chemical activity of enzyme and substrate, or decreased diffusion in the dense droplet phase [286].

3.2 Aim

The combined effects of LLPS and high hydrostatic pressure (HHP) for modulating the kinetic constants of enzymatic reactions is still terra incognita. So far, the effect of pressure has been studied on pure LLPS systems, only [239,240]. Hence, the combined effect of ATPS and HHP on a representative enzyme reaction, i.e. the hydrolysis of the substrate Ala-Ala-Phe-7-amido-4-methylcoumarin (AAF-AMC) catalysed by α-chymotrypsin (α-CT) was studied in this project. The α-CT is a proteolytic enzyme of the mammalian digestive system which cleaves the amide bond at the C-terminus of an aromatic residue [71]. In this reaction, the enzyme hydrolyses the peptide bond at the C-terminus of the Phe residue leading to the release of the fluorescent reporter group 7-amido-4-methylcoumarin (AMC). The hydrolysis of AAF-AMC

catalysed by α-CT follows the Michaelis-Menten kinetics, and the AMC release can be followed by exciting it at 370 nm and recording the fluorescence emission at 460 nm as function of time, without interferences from the substrate [54].

3.3 Materials and Methods

3.3.1 Materials

Lyophilized powder of the enzyme α-chymotrypsin (α-CT) from bovine pancreas, the substrate Ala-Ala-Phe-7-amido-4-methylcoumarin (AAF-AMC), the pure product 7-amido-4-methylcoumarin (AMC), PEG of molecular weight 4.6 kDa, another substrate *N*-succinyl-L-alanyl-L-alanyl-L-prolyl-L-phenylalanine-*p*-nitroanilide (SAAPPpNA) and dimethylsulfoxide (DMSO) were purchased from Sigma Aldrich Chemical. Dex 10 kDa was purchased from Carl Roth. The rhodamine B-labeled Dex 10kDa (neutral) was purchased from Thermo Fisher Scientific. All the chemicals were used directly without any further purification. Solutions were prepared in pressure stable Tris buffer (0.1 M Tris-HCl and 10 mM $CaCl_2$, pH 7.8) and deionized water was used for buffer and other sample preparations.

3.3.2 Sample preparation

A stock solution of α-CT was prepared by dissolving the enzyme in buffer. The exact concentration of the solution was determined by measuring absorbance at 280 nm by means of UV/Vis spectroscopy (UV-1800 spectrometer from Shimadzu Corporation) and using a molar extinction coefficient of 51000 M^{-1} cm^{-1}. Similarly, the stock solutions of the substrate AAF-AMC (30 mM) and of the standard AMC (50 mM) were prepared by dissolving them in DMSO. A strong dilution in buffer was made for both the stock solutions to determine their concentration. The concentrations were also determined by measuring their absorbance using an extinction coefficient of $\varepsilon(325)$ = 16000 M^{-1} cm^{-1} for AAF-AMC and $\varepsilon(370)$ = 7600 M^{-1} cm^{-1} for AMC [21]. The dansyl-labeled α-CT was prepared by dissolving the dye in acetone. Then, the dye solution was added to the protein solution under stirring and stored at 4 °C for 2 h. After the reaction, the excess dye was removed by using a Sephadex G-25 HiTrapp Desalting column from GE Healthcare.

For the stopped-flow experiment, the enzyme α-CT and substrate SAAPPpNA were dissolved both in buffer and ATPS. A 400 μM stock solution of the substrate and a 2 μM stock solution of the enzyme were prepared. Their exact concentrations were determined by using UV/Vis spectroscopy (UV-1800 spectrometer from Shimadzu Corporation) and using a molar

extinction coefficient of 51000 M^{-1} cm^{-1} for α-CT at 280 nm and 14000 M^{-1} cm^{-1} at 315 nm for SAAPPpNA [158,253]. For all the measurements, the substrate concentration was kept constant at 400 μM before loading into the stopped-flow system (200 μM after mixing with the enzyme solution). The enzyme concentration was varied from 16 nM - 2 μM (8 nM – 1 μM after mixing).

3.3.3 Fluorescence Spectroscopy – Kinetics

The enzyme kinetics was recorded using a K2 fluorometer from ISS, Inc. (Champaign, IL, USA) which is equipped with a xenon arc lamp as light source. The excitation and emission wavelengths were set at 370 nm and 460 nm, respectively with the slit width set at 8 nm for both excitation and emission monochromators. The hydrolysis reaction of AAF-AMC catalysed by α-CT was monitored by recording the increase in fluorescence intensity due to the formation of product (AMC) at 460 nm as a function of temperature without any interference from the substrate AAF-AMC. The temperature in all cases was kept constant at 20 °C using a circulating water bath and sufficient time was provided for equilibration of sample chamber. In all the experiments, the enzyme concentration was kept constant at 10 nM. The substrate concentration was varied from 20 μM to 135 μM. The final volume of the solution was 1500 μL. The desired concentration of the enzyme and the substrate were obtained by diluting the stock solutions with either buffer, ATPS or Dex 30 wt% solution, as needed. In case of the pressure dependent measurements, the HHP cell system from ISS and quartz cuvettes were used. The pressure was controlled by means of a manual pump and water was used as pressurizing fluid. A pressure range from 1 bar to 2000 bar was explored. The enzyme and substrate were mixed, vortexed and then put in the sample cell which was sealed with DuraSeal™ laboratory stretch film and placed into the high-pressure vessel. Since the whole assembling process took nearly 4 minutes, this time was taken into account in the data analysis. Since it is not possible to correlate directly the intensity of the released AMC to concentration, a calibration of the instrument was performed. Four solutions of different concentrations (4 μM, 2 μM, 1 μM, 0.5 μM) were prepared from the AMC stock solution in buffer, ATPS and 30 wt% Dex. Recording their intensities, a calibration curve was obtained which was then used to convert the fluorescence intensity to the concentration of released product.

This hydrolysis reaction follows the Michaelis-Menten kinetics [71] and thus the catalytic activity of α-CT has been characterised by determining the Michaelis-Menten constant (K_M) and the turnover number (k_{cat}). Linear fitting of the data was done in the region where the

fluorescence intensity changes with time and the slope of the fitted line gave the value of initial rates (v_0) of the reaction. The data obtained were then analysed by the Lineweaver-Burk equation [234]

$$\frac{E_0}{v_0} = \frac{1}{k_{\mathrm{cat}}} + \frac{K_{\mathrm{M}}}{k_{\mathrm{cat}}} * \frac{1}{[\mathrm{S}]} \tag{53}$$

where E_0 is the total enzyme concentration and $[\mathrm{S}]$ is the total substrate concentration. Plotting E_0/v_0 against $1/[\mathrm{S}]$ gives the value of Michaelis-Menten constant (K_{M}) and turnover number (k_{cat}). The reported values of K_{M} and k_{cat} are the average of at least 3 independent measurements.

3.3.4 Steady-State Fluorescence spectroscopy

Fluorescence emission spectra of dansyl-labeled α-CT were acquired by using a K2 fluorometer from ISS, Inc. (Champaign, IL, USA). Measurements were performed at a constant temperature of 20 °C and using a 1 cm path length quartz cuvette. Similar to the sample preparation mentioned in section (3.3.2), dansyl-labeled α-CT was dissolved in buffer, ATPS or 30 wt% Dex as needed. The emission spectrum was recorded in the range 450-600 nm upon excitation at 325 nm. The position of the emission maxima was evaluated by calculating the spectrum center of mass (CM) [135].

3.3.5 Pressure Dependent Turbidity

Pressure dependent turbidity measurements were carried out on a PerkinElmer Lambda 25 spectrophotometer with a home built high-pressure optical cell. Sapphire with a diamond of 20 mm and a thickness of 10 mm was used as window material. Pressure was applied using a high-pressure hand pump and was measured by a pressure sensor (Burster Präzisionsmesstechnik, Gernsbach). Water was used as pressurizing medium.

3.3.6 Pressure Dependent Microscopy

Phase contrast and fluorescence microscopy experiments were also carried out using an Eclipse TE2000-U (Nikon Inc.) optical microscope with a Nikon CFI Plan Apo Lambda 10x objective coupled to an TIS DMK 23UX249 camera. Rhodamine B-labelled Dex, AAF-AMC and dansyl-labeled α-CT were used for fluorescence microscopy. For pressure-dependent microscopy studies, a home-built high-pressure microscopy cell was used. The pressure was

generated using a high-pressure hand pump using water as the pressure-transmitting fluid. Flat diamond windows were used as optical window materials on both sides.

3.3.7 Circular Dichroism Spectroscopy

Far-UV and Near-UV circular dichroism were recorded on a Jasco J-715 (Jasco Corporation, Tokyo, Japan). Far-UV spectra of α-CT (30 μM) were recorded in the range 260-195 nm using 0.01 cm path length quartz cuvette. The Near-UV spectra were acquired in the range of 320-260 nm. The concentration of α-CT was 15 μM and the path length of the cuvette used was 0.1 cm. Enzyme was dissolved both in buffer and ATPS to record the spectra. For each sample, a background blank (ATPS or buffer) was subtracted. The spectra recorded are a result of 6 accumulations. The spectra in both Near and Far-UV were normalized per mole of residue [22].

3.3.8 Stopped-Flow Experiments

The enzymatic hydrolysis reaction was carried out using the stopped-flow (SF) system (SF-61SX2 of Hi-Tech Scientific) which uses a xenon-lamp as light source. The increase in absorbance at 410 nm was monitored due to the product formation (*p*-nitoaniline). For all the experiments, the temperature was kept constant at 20 °C using a circulating water bath. The stopped-flow instrument consists of two syringes, one for the enzyme solution and the other for the substrate and a waste collection component. The dead time of the instrument is 10 ms. Before each measurement, the samples were kept for 10 min for complete equilibration. The absorbance was recorded for 2 min after the rapid mixing process. For measuring the change in absorbance during the mixing of PEG and Dex to form the ATPS, stock solutions of PEG (25.5 wt%) and Dex (11 wt%) were prepared so as to attain the critical concentration consisting of 12.7 wt% PEG and 5.5 wt% Dex (see section 3.4) after mixing.

3.4 Determination of binodal curve for the PEG-Dextran system

The binodal curve was determined using PEG of M.W. 4.6 kDa and Dex of M.W. 10 kDa, both dissolved in Tris buffer. The structure of the PEG and Dextran molecules are shown in Fig. 3.1.

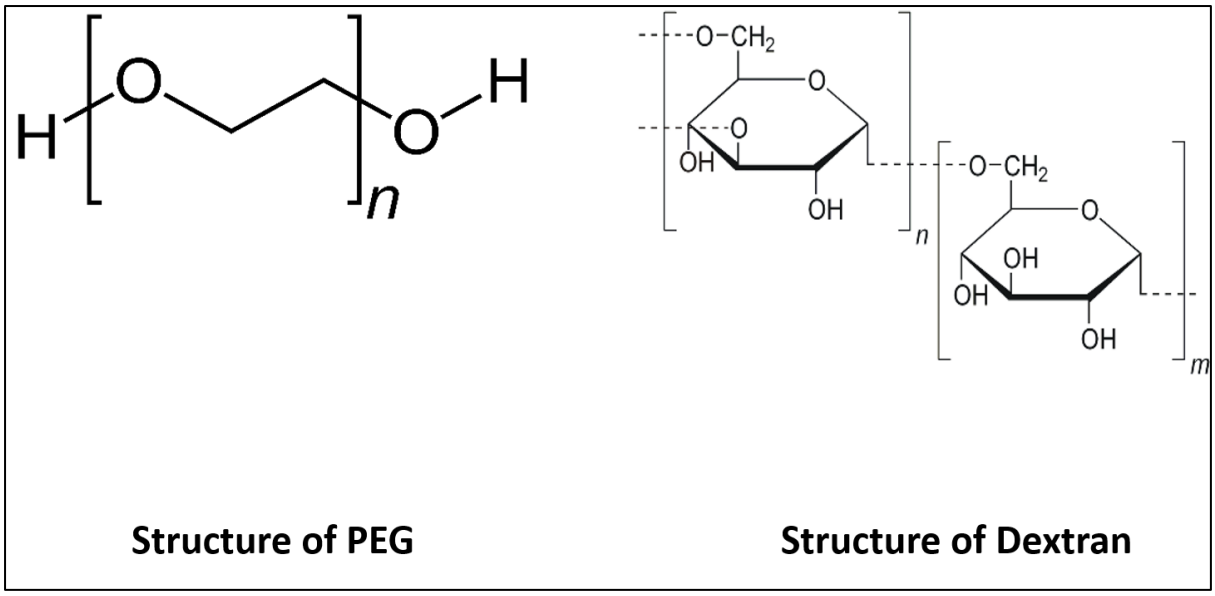

Figure 3.1. Schematic representation of the structures showing PEG and Dextran.

The aqueous solutions of PEG and Dex when mixed above a certain weight percent at constant temperature form two co-existing phases [43,175]. These certain weight percent points are referred to as critical concentrations. It is very important to determine the binodal curve to be able to locate the homogeneous region and the phase-separated region which is prerequisite in carrying out experiments in ATPS. The experimentally determined binodal curve is depicted in Fig. 3.2 -

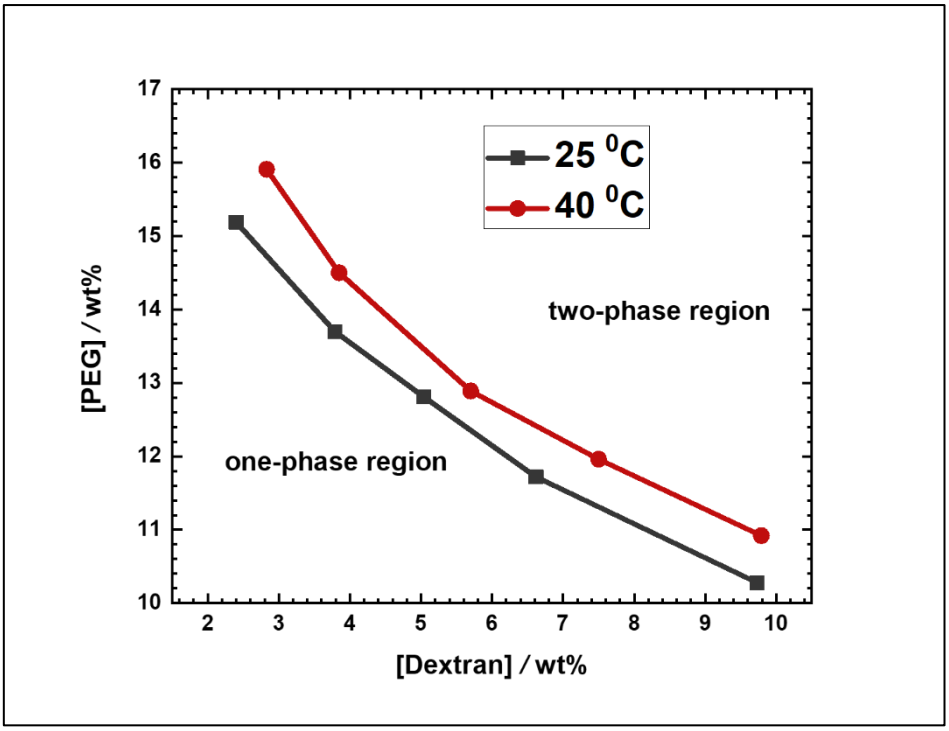

Figure 3.2. Binodals of Dex (M.W 10 kDa) and PEG (M.W 4.6 kDa) in Tris buffer at 25 °C (black squares) and 40 °C (red dots). The critical concentration of 12.7 wt% PEG and 5.5 wt% Dex lies in between the two binodals. The lines are just guide to the eyes.

This binodal curve was determined using cloud-point titration [23]. Six different stock solutions of PEG of M.W 4.6 kDa in Tris buffer were prepared (10, 12, 14, 16, 18, 20 wt%). Around 2 g of each stock solution was added to six different conical flasks and their exact weight was noted. Stock solution of Dex 20 wt% of M.W. 10 kDa prepared in Tris buffer was added to each one of them dropwise while maintaining a constant temperature of 25 °C till the first could-point or turbidity appeared. The total weight of the solution was recorded and the difference from the initial weight gave the amount of Dex required for the onset of the two-phase region at 25 °C. The conicals were then sealed with paraffin and put in a water bath at 40 °C for at least two hours. The solutions turned transparent on heating and the same procedure was repeated for obtaining the cloud points at 40 °C. The phase behaviour depends on the molecular weight of the polymers and their size distribution. Thus, they must be determined for each batch of polymer used in the lab. As can be seen from the Fig. 3.2, the polymer solution located below the binodal is a homogeneous solution whereas the one located above is phase separated. Though PEG and Dex are both water-soluble, PEG is more hydrophobic than Dex [23]. The critical concentration comprising 12.7 wt% PEG 4.6 kDa and 5.5 wt% Dex 10 kDa was chosen for the experiment which partitioned into a PEG-rich top phase and a Dex-rich bottom phase at 25 °C. The reason for this choice was the position of this critical concentration

in between the binodals of two different temperature. The phase diagram (Fig. 3.2) indicates that this critical concentration falls into the one-phase region for the binodal at 40 °C whereas it remains phase separated at 25 °C. This property could be used to shift the polymer solution between the two- and one-phase region by changing the temperature [175]. According to the reported phase diagram and procedures to determine the constituents' concentration [220], the Dex-rich phase is composed of about 30 wt% Dex and about 3 wt% PEG. The PEG-rich phase consists of about 14 wt% PEG and 2.5 wt% Dex.

3.5 Results and Discussion

3.5.1 UV data

To examine the effect of ATPS on an enzymatic reaction, SAAPPpNA was used as substrate and α-CT as the enzyme. The model enzymatic system is shown schematically below.

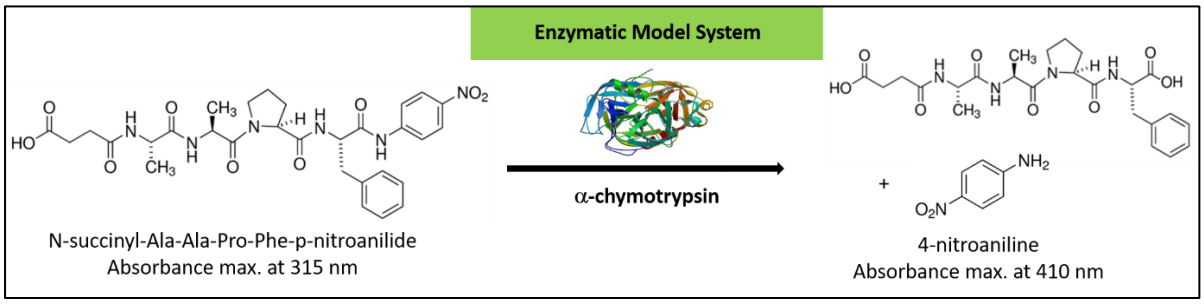

The aim of the project was to reveal the combined effects of ATPS and pressure on the hydrolysis reaction of SAAPPpNA catalysed by α-CT. Thus, as an initial step, UV spectroscopic measurements were carried out to follow the reaction as a function of time (Fig. 3.3).

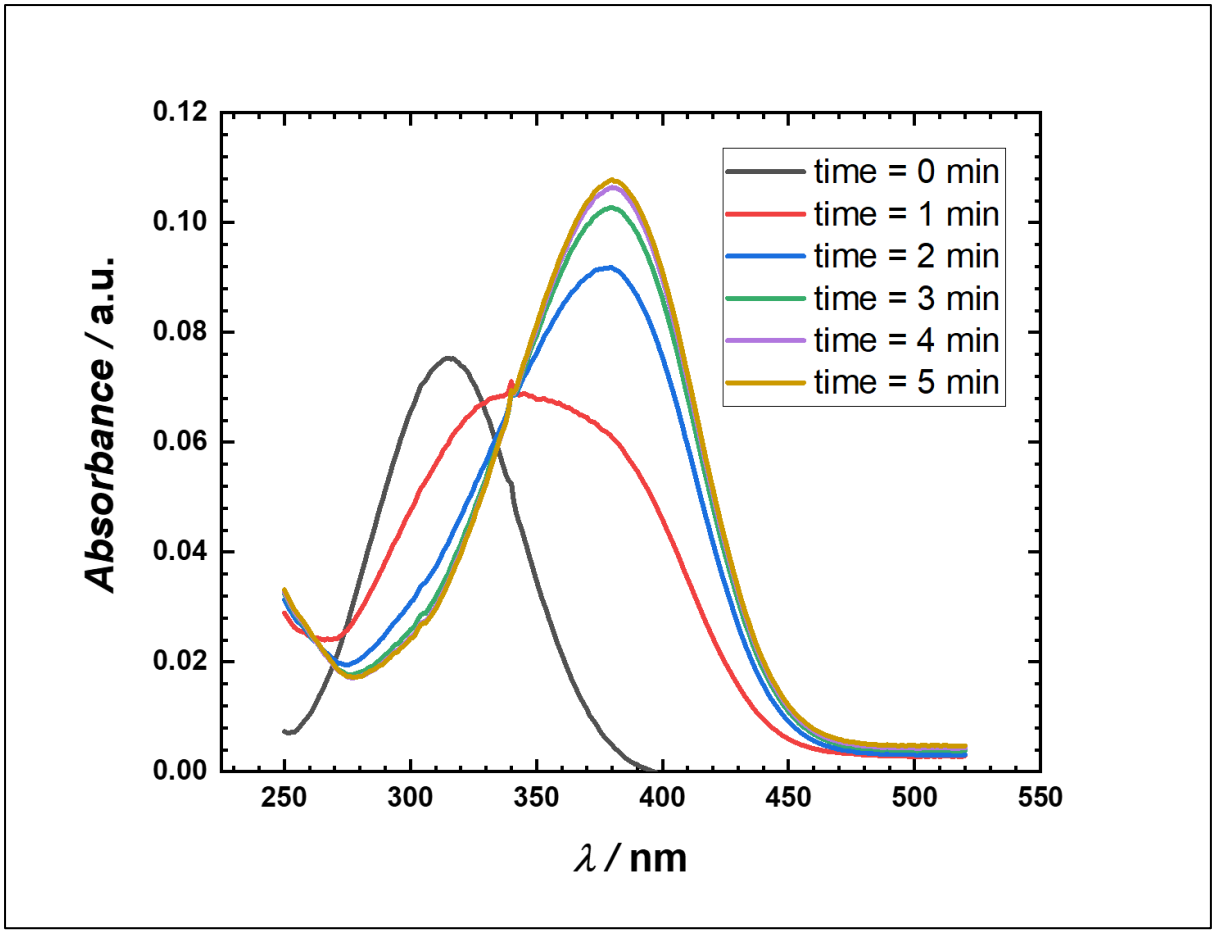

Figure 3.3. UV/Vis data depicting the progress of hydrolysis of SAAPPpNA by α-CT for the formation of 4-nitroaniline over a span of wavelengths from 250 nm to 520 nm at different time intervals.

From the Fig. 3.3 it can be inferred that with time the absorbance of the substrate (SAAPPpNA) peak decreases at 315 nm and that of the product (4-nitroaniline) peak at 410 nm increases indicating the formation of product with time. This increase in absorbance of the product peak ceases after nearly 5 min signalling complete hydrolysis of SAAPPpNA.

This artificial ATPS system is highly crowded with polymers such as PEG and Dex and thus, has higher chances of scattering due to their large molecular size. To check the scattering of ATPS at the excitation wavelength of the substrate (315 nm) and product (410 nm), individual UV measurements were conducted for the ATPS alone, and the ATPS and substrate with the substrate concentration being fixed at 200 μM and ATPS with varying concentrations of enzyme (8 nM, 100 nM and 1 μM) (Fig. 3.4).

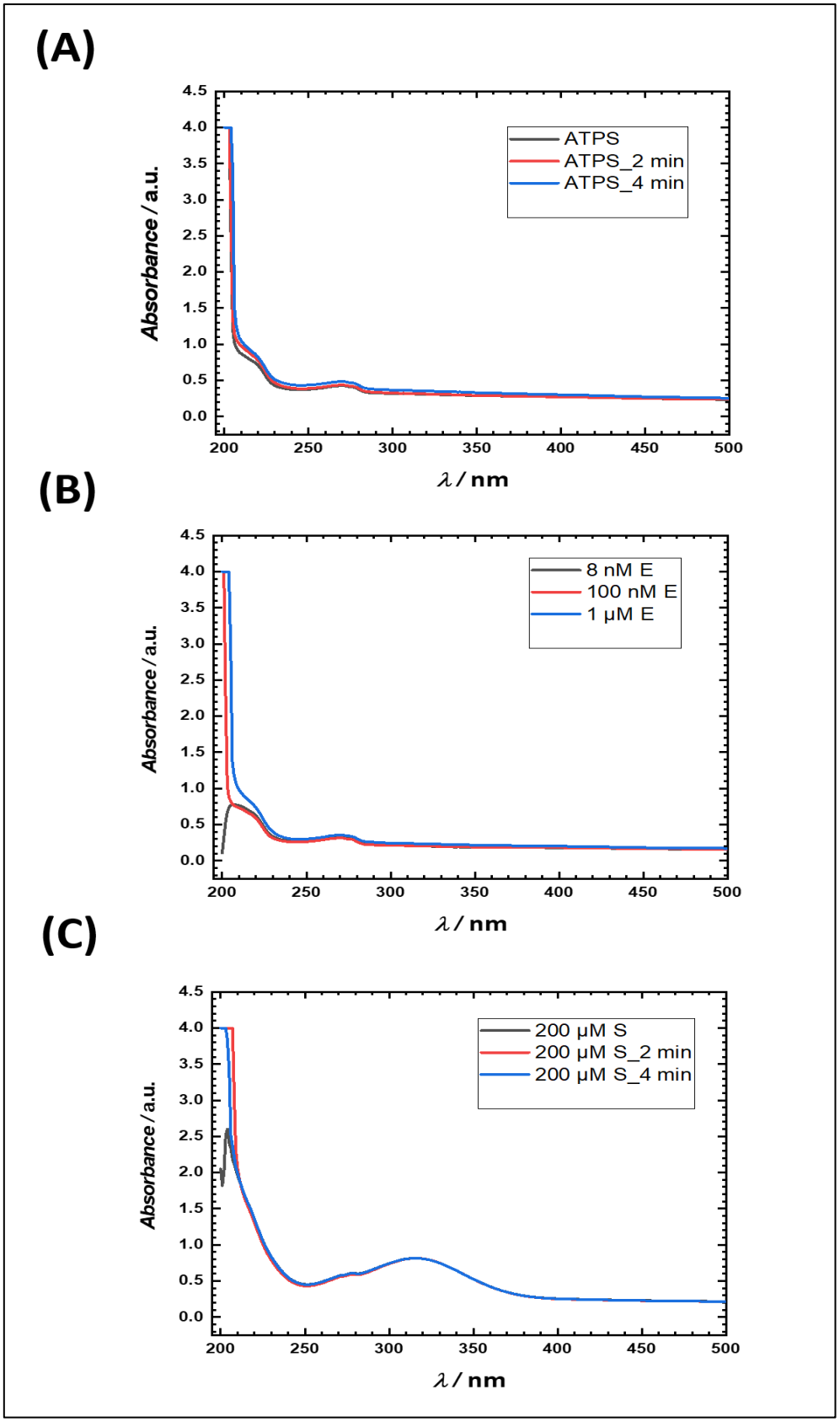

Figure 3.4. Wavelength-dependent absorbance data for (A) ATPS, (B) for varying concentrations of α-CT (E) in the ATPS and (C) for 200 µM SAAPPpNA (S) in ATPS. In fig. (B) and (C), the absorbance values were recorded at different time intervals: immediately after putting the sample into the UV/Vis spectrometer (black line), after 2 min (red line) and after 4 min (blue line).

ATPS alone (A) and ATPS with varying enzyme concentrations (B) did not show any peak at 315 nm and 410 nm, suggesting no scattering effect at these wavelengths. The ATPS with 200 µM substrate (C) showed the usual peak at 315 nm. All these observations made sure that the hydrolysis reaction of SAAPPpNA catalysed by α-CT could be followed by monitoring the increase in absorbance at 410 nm caused due to product formation, *p*-nitroaniline, without any scattering interference from the ATPS. To confirm this finding, some more UV measurements were performed with 200 µM substrate concentration and varying concentrations of α-CT in the ATPS (Fig. 3.5).

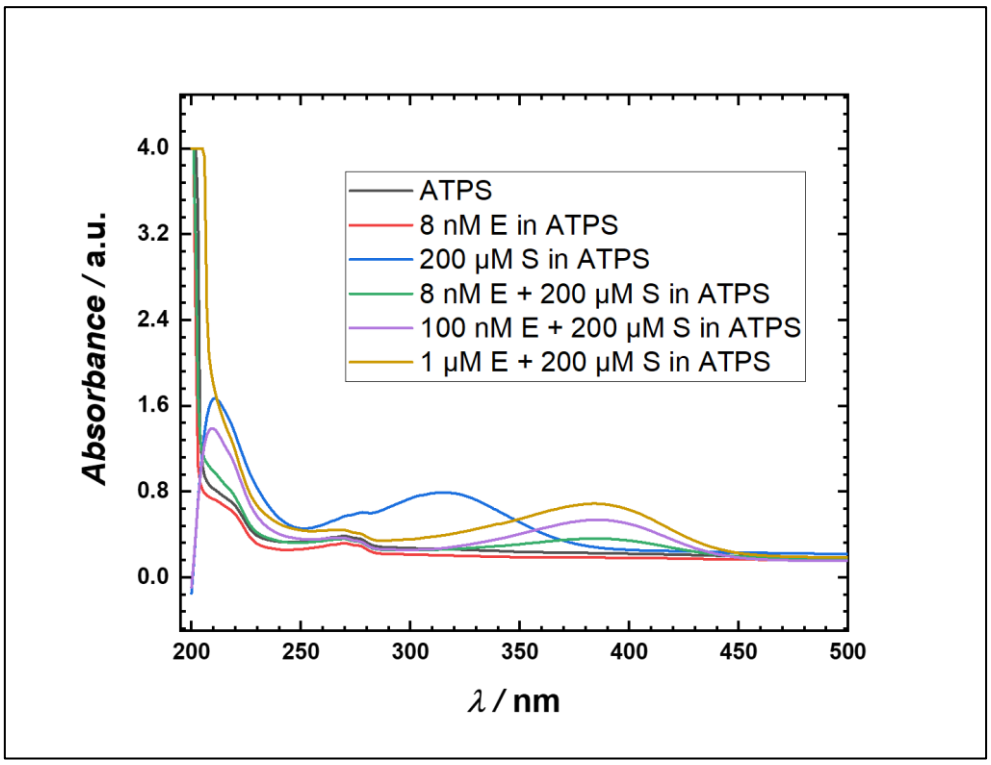

Figure 3.5. Wavelength-dependent absorbance data for the ATPS alone (black line), 8 nM α-CT(E) dissolved in ATPS (red line) and 200 µM SAAPPpNA (S) dissolved in the ATPS (blue line). Green, purple and yellow lines represent the absorbance upon product formation at 410 nm by mixing 200 µM S with 8 nM E, 100 nM E and 1 µM E respectively.

As can be seen from Fig. 3.5, even with varying enzyme concentrations, there is no change in the respective substrate and product peaks at 315 nm and 410 nm. Fig. 3.5 also indicates the general trend that with the increase in enzyme concentration, the amount of product formation is higher and hence the absorbance at 410 nm has increased. All these data confirm the possibility of monitoring the kinetics of this hydrolysis reaction by following the product

formation at 410 nm without disturbance of light scattering contribuions to the spectral region recorded.

3.5.2 Stopped flow data

The hydrolysis reaction of SAAPPpNA catalysed by α-CT was found to be very fast, i.e., the reaction was completed in a very short amount of time (300 s). This was the reason for the choice of using a stopped-flow instrument to monitor the kinetics of the hydrolysis reaction. Since, the dead time of the instrument used (Section 3.3.8) is 10 ms, it should be possible to record any change in kinetics for fast reactions i.e., any change occurring in absorbance after 10 ms with this instrument. However, the data acquired by stopped-flow methodology didn't match with the UV data due to severe light scattering induced by the turbulent mixing in the stopped-flow apparatus, which masked changes in absorption due to product formation.

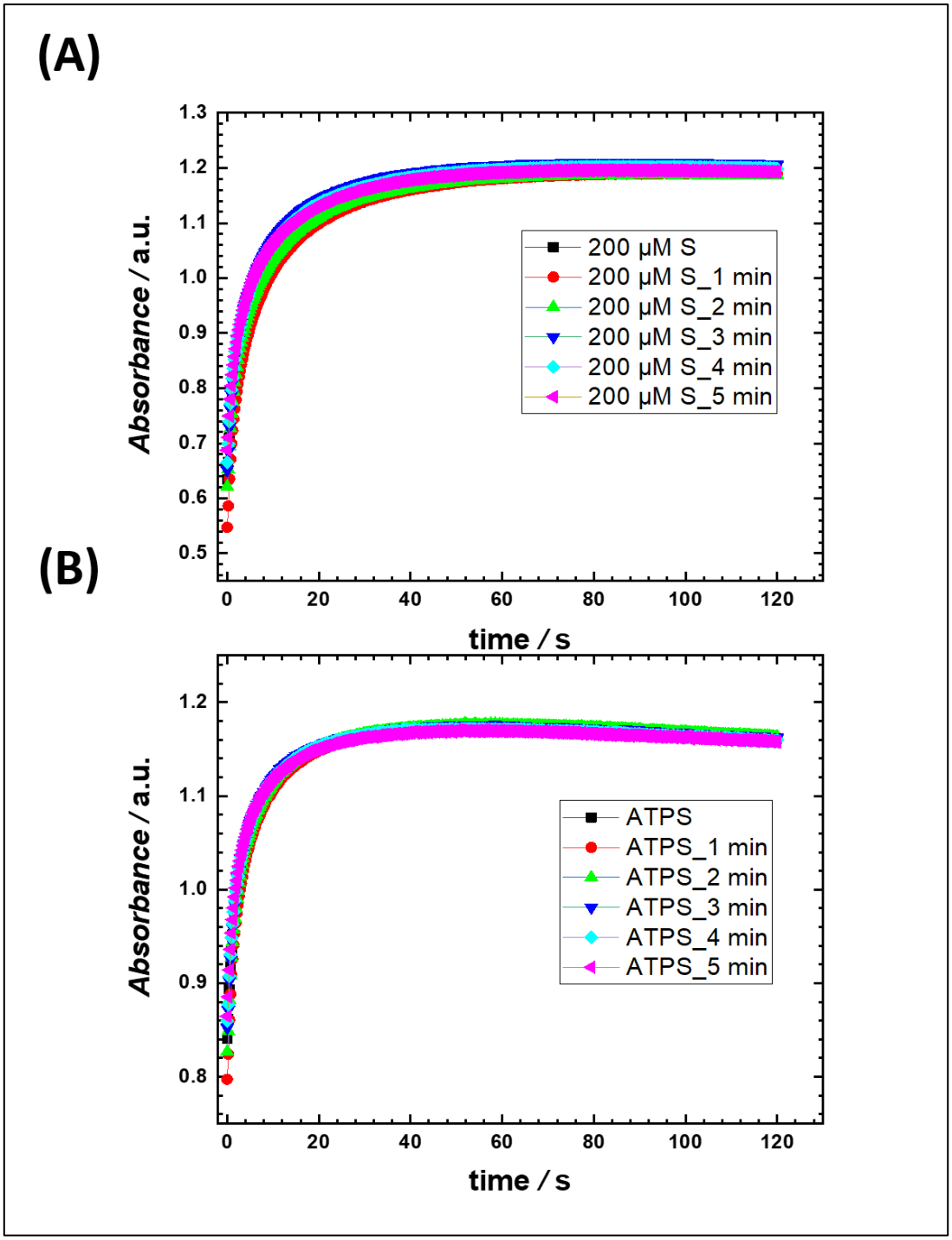

Figure 3.6. Time-dependent absorbance data at 410 nm due to the mixing of (A) ATPS and (B) 200 µM substrate (S) dissolved in ATPS, at various time intervals: recording of absorbance after mixing the reagents from two syringes immediately (black squares), after 1 min (red dots), after 2 min (green triangles upward), after 3 min (blue triangles downward), after 4 min (blue squares) and after 5 min (purple triangles).

Absorbance was recorded at 410 nm as a function of time upon formation of the ATPS (Fig. 3.6) by mixing PEG and Dex stock solutions to finally obtain the critical concentration (12.7 wt% PEG and 5.5 wt% Dex). It was observed that the ATPS alone gave a considerable value

of absorbance at 410 nm due to the scattering effect. Addition of 200 µM of SAAPPpNA to the ATPS (Fig. 3.6) did not bring any significant change in the shape of the absorbance curve recorded or the relative absorbance values, the reason for this being the turbulent mixing of the PEG and Dex stock solution in the stopped-flow system, which led to the formation of a droplet phase giving rise to strong scattering unlike in the whole UV/Vis spectral region. The scattering due to the ATPS alone at 410 nm is so strong and the lifetime of the droplets formed so long that it masks the actual absorbance values of product formation, as can be seen from Fig. 3.7.

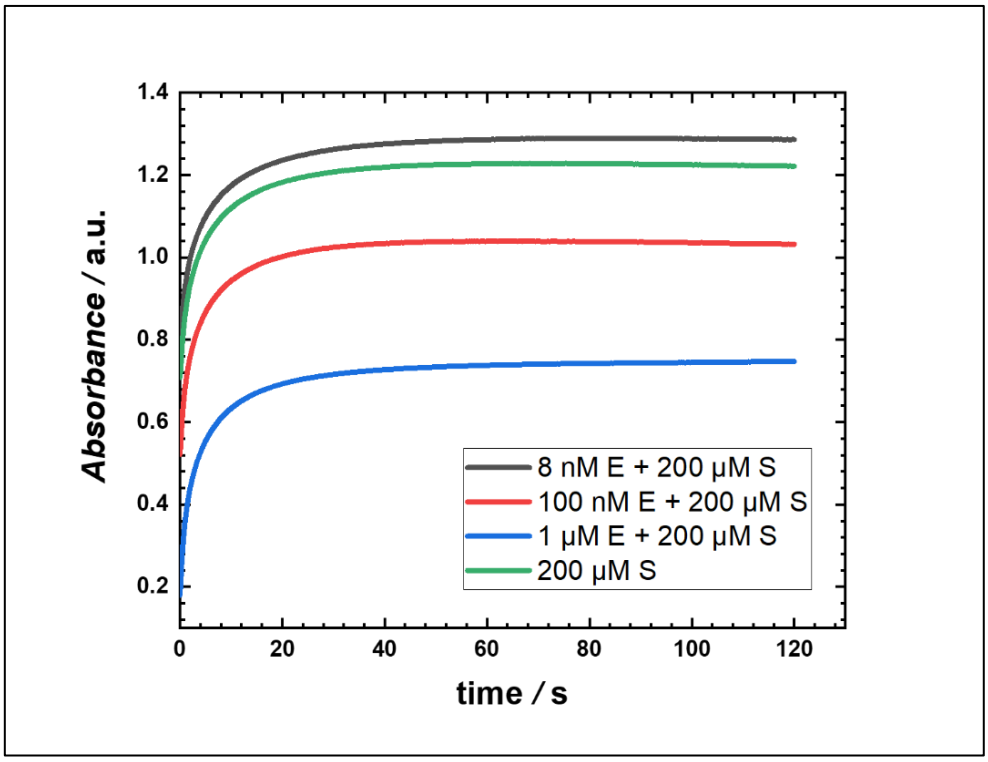

Figure 3.7. Absorbance data at 410 nm for product (p-nitroaniline) formation during the hydrolysis of 200 µM SAAPPpNA with 8 nM α-CT (black line), 100 nM α-CT (red line) and 1 µM α-CT (blue line) in ATPS. The green line represents the absorbance of only 200 µM SAAPPpNA dissolved in ATPS at 410 nm.

Generally, increasing the enzyme concentration increases the product formation and hence its absorbance at 410 nm. However, a reverse trend has been observed in this case as can be seen from Fig. 3.7. Increase in enzyme concentration from 8 nM to 1 µM decreased the absorbance accordingly and the absorbance of 200 µM SAAPPpNA alone dissolved in ATPS was detected to be much higher than the product absorbance obtained by mixing 200 µM SAAPPpNA with 100 nM α-CT and 1 µM α-CT. Thus, it can be concluded that these absorbance values are not true due to the major contribution of scattering generated from the ATPS, only.

The settling time for an ATPS depends on several factors and thus varies greatly from one system to another [44]. The formation of a new set of droplets upon turbulent mixing also changes the settling time and hence the absorbance values (Fig. 3.8), overriding absorbance changes due to product formation.

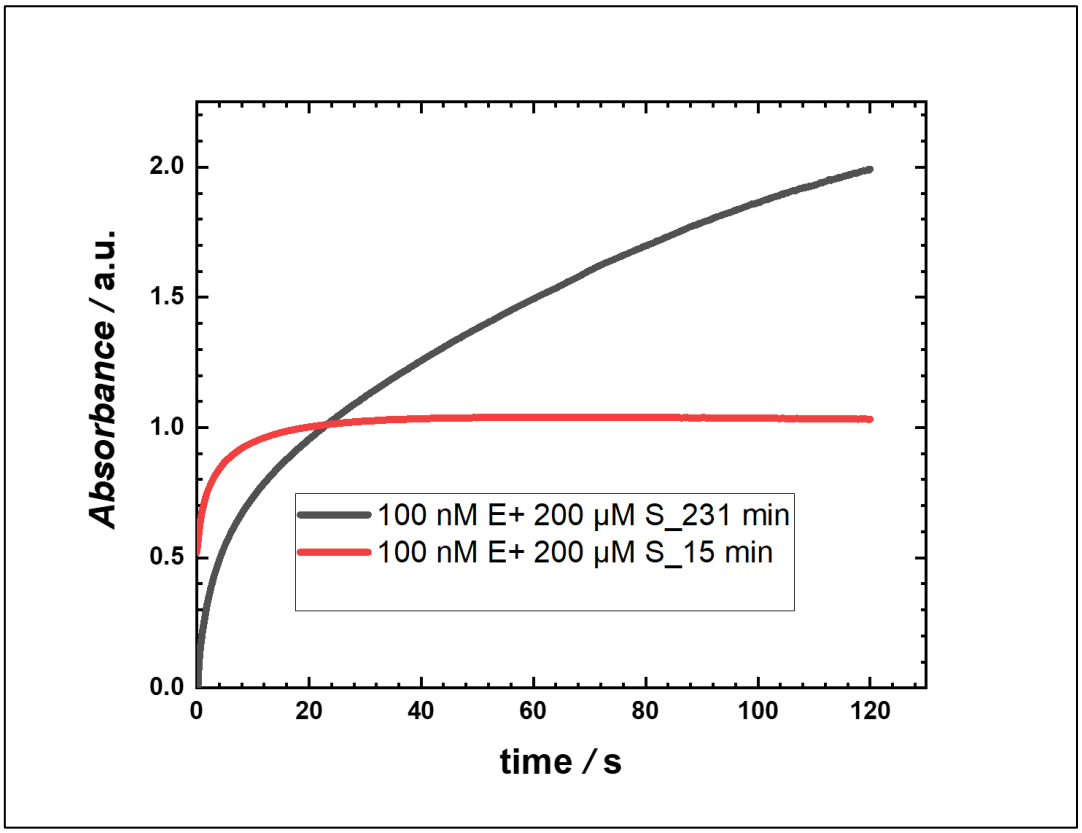

Figure 3.8. Time-dependent absorbance data at 410 nm due to the formation of the product p-nitroaniline during the hydrolysis of 200 µM SAAPPpNA (S) catalysed by 100 nM α-CT (E) recorded after 15 mins of turbulent mixing of α-CT and SAAPPpNA (red line) and after 231 min of turbulent mixing of α-CT and SAAPPpNA (black line).

It can be seen from the Fig. 3.8, the absorbance at 410 nm varies with the change in settling time after the turbulent mixing of the enzyme and substrate in the mixing chamber of the stopped-flow instrument. Discrepancies in the amount of product formed were observed irrespective of the fact that both the experiments were carried out with constant concentrations of enzyme (100 nM) and substrate (200 µM). Thus, it was concluded that the actual absorbance values due to the product formation at 410 nm was concealed by the scattering of ATPS in the stopped-flow methodology and since, it was not possible to control the way these droplets are formed or their size upon mixing, reliable absorbance measurements of product formation could not be carried out. Hence, owing to the fact that the scattering contribution to the

absorbance signals varies with time and is not reproducible, a background correction was not possible to retrieve the true absorption values due to product formation.

Having learned the limitations of using the stopped-flow instrument in this case, it was decided to use fluorescence spectroscopy to monitor the kinetics of a hydrolysis reaction catalysed by α-CT. However, due to the lack of any intrinsic fluorophore in SAAPPpNA and its fast turnover to product formation, a new substrate, Ala-Ala-Phe-7-amido-4-methylcoumarin (AAF-AMC), was used which has a fluorescent reporter group, 7-amido-4-methylcoumarin (AMC) and a slower reaction kinetics (see Section 3.2). The model enzymatic system is shown below-

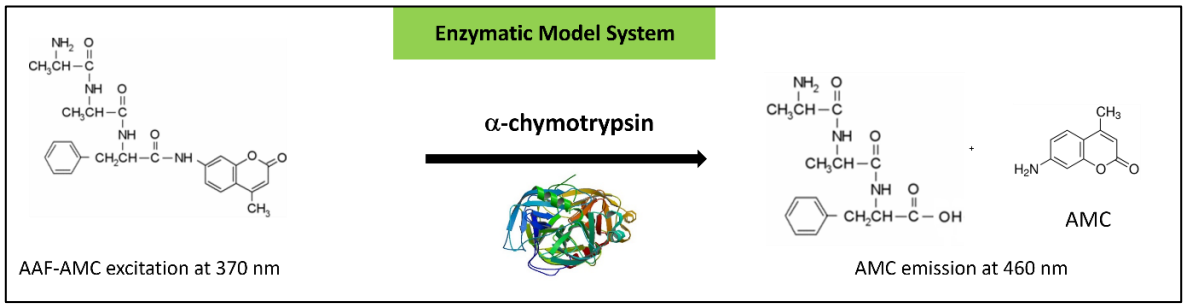

The excitation and emission wavelength of AMC are 370 nm and 460 nm, respectively. A scattering profile was recorded for AMC [121,165] in both buffer and ATPS to check for any scattering contribution resulting from the ATPS in the emission wavelength region of the product (Fig. 3.9).

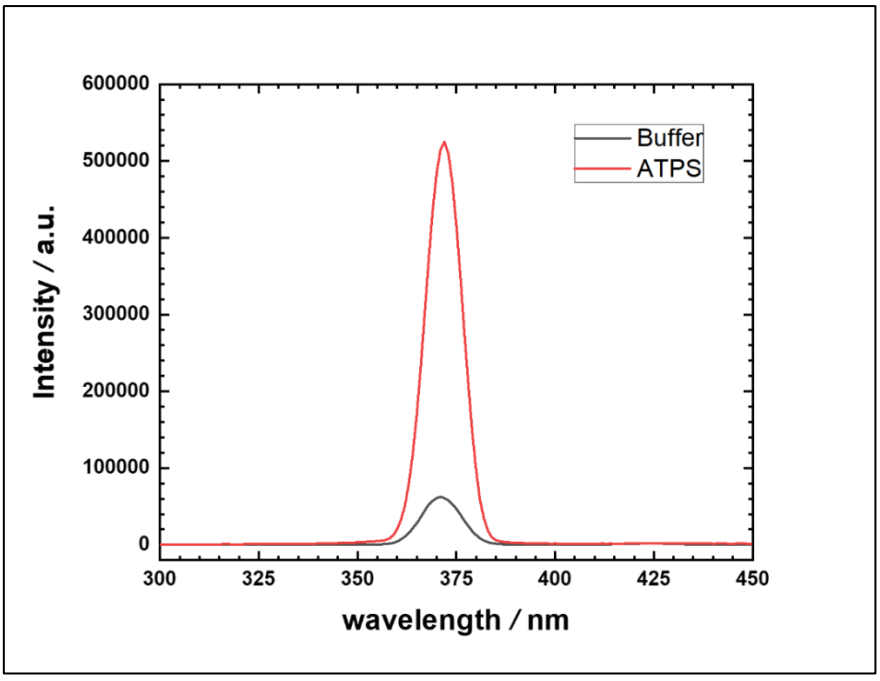

Figure 3.9. Scattering profile for AMC in buffer (black line) and ATPS (red line).

In fluorescence, the detector is at 90° and in this configuration, the scattering profile is a Gaussian curve [121]. As can be seen from Fig. 3.9, there was no scattering observed at 460 nm and maximum scattering was obtained around the excitation wavelength (370 nm), only. Hence, it was possible to record the fluorescence emission of product (AMC) at 460 nm as a function of time, without interferences from light scattering caused by the inhomogeneity of the ATPS.

3.5.3 Fluorescence spectroscopy study of the enzyme kinetics

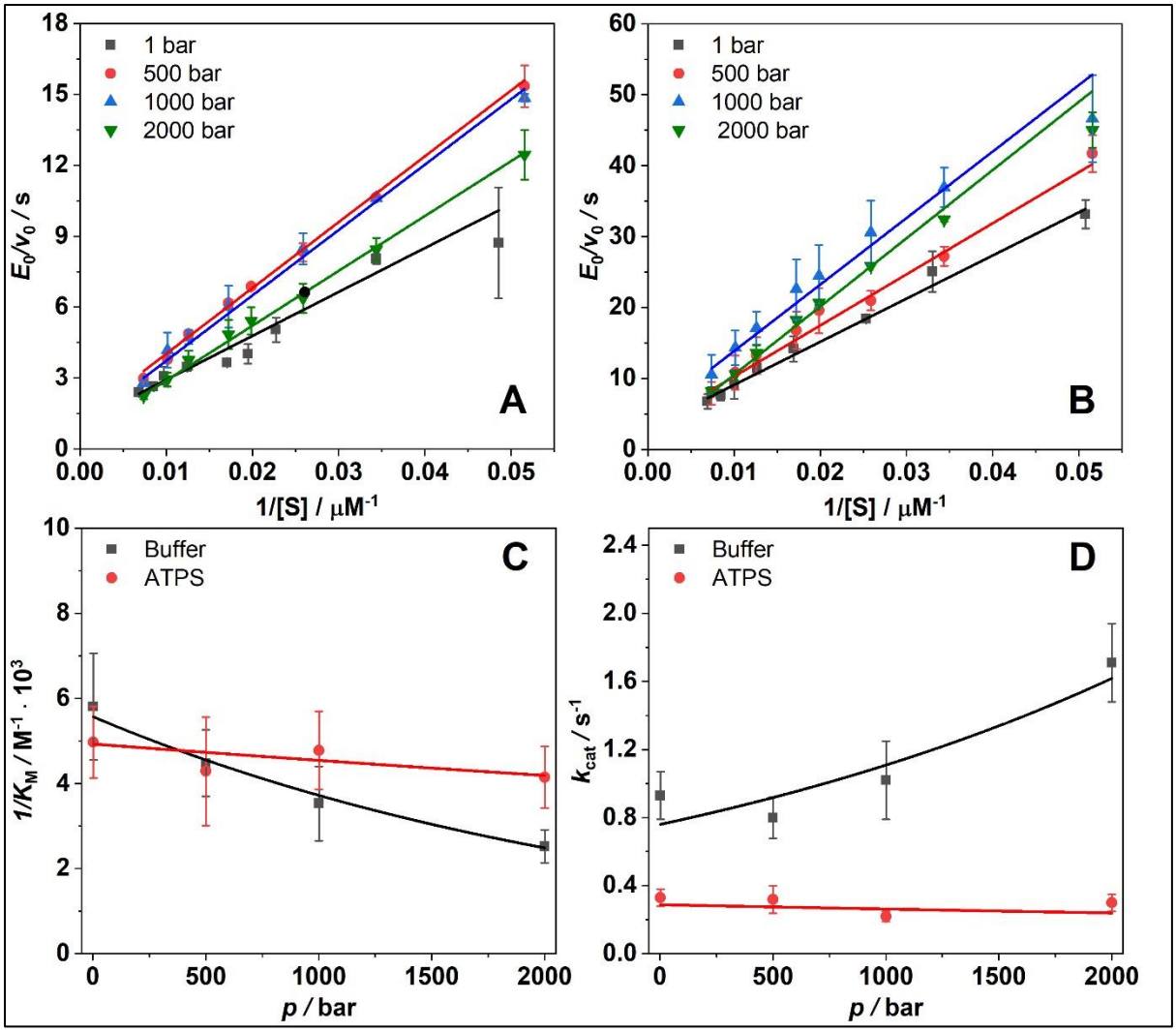

Figure 3.10. Lineweaver-Burk plots for the hydrolysis of AAF-AMC catalyzed by α-CT in (A) buffer and (B) ATPS. The colored lines represent the best fits of the experimental data according to Eq. 53. In (C) and (D), the dependences of $1/K_M$ and k_{cat} on pressure, p, are reported. The binding (ΔV_b) and the activation ($\Delta V^{\neq}$) volumes were calculated by fitting the experimental points to Eq. 52. E_0 and [S] are the total enzyme and substrate concentrations, respectively, v_0 is initial rate, K_M is the Michaelis-Menten constant and k_{cat} is the turnover number.

Fig. 3.10 shows the plot of E_0/v_0 vs. 1/[S] i.e., Lineweaver-Burk plots for the hydrolysis reaction of AAF-AMC catalysed by α-CT in buffer and in the ATPS. As have been mentioned in Section 3.3.3, all experiments were carried out at constant temperature of 20 °C and the pressure range from 1 bar to 2000 bar was explored both for buffer and the ATPS. The isoelectric point of the protein is 5.4, hence it is negatively charged in the buffer used. This reduces the risk of aggregation, which is higher in crowded media. The kinetic parameters that have been obtained from the linear fits of the data (section 3.3.3) have been summarised in Table 1.

	1 bar		**500 bar**		**1000 bar**		**2000 bar**	
Solvent	K_M **/ µM**	k_{cat} **/ s^{-1}**	K_M **/ µM**	k_{cat} **/ s^{-1}**	K_M **/ µM**	k_{cat} **/ s^{-1}**	K_M **/ µM**	k_{cat} **/ s^{-1}**
Buffer	172±37	0.93±0.14	223±39	0.80±0.12	283±70	1.02±0.23	396±61	1.71±0.23
Dex	87±6	1.00±0.05						
ATPS	201±34	0.33±0.05	233±69	0.32±0.08	209±40	0.22±0.03	241±42	0.30±0.05

Buffer: 0.1 M Tris-HCl and $CaCl_2$ 10 mM, pH 7.8
Dex: Dextran 10 kDa 30 wt%
ATPS: PEG 4.6 kDa 12.7 wt% and Dex 10 kDa 5.5 wt%

Table 1. Kinetic parameters for the hydrolysis of AAF-AMC catalysed by α-chymotrypsin at different pressures and at the temperature of 20 °C.

The K_M and k_{cat} values obtained for neat buffer at ambient pressure are in good agreement with the previously reported data [54]. Since the Dex-rich phase contains 30 wt% Dex and 3 wt% PEG (Section 3.4), kinetic measurements were also performed in pure 30 wt% Dex at ambient pressure to compare the values of the kinetic constants with other systems. The value of k_{cat} in 30 wt% Dex is similar to that in neat buffer, indicating no change in the turnover number of the enzyme. Generally, dextran solutions being viscous compared to buffer lead to the decrease in diffusion coefficient of the substrate and enzyme and thus, a decrease in k_{cat} is observed [57]. Since no such effect is seen in this case, it proves that the reaction is not diffusion controlled but is rather reaction-controlled. The K_M value decreases by nearly 50% with respect to buffer, indicating an increase in the enzyme-substrate affinity. This can be due to the crowding imposed by Dex due to its high concentration (30 wt%) which gives rise to a pronounced excluded volume effect leading to an increase in the effective concentration of the reactants

and the association rates [57]. This excluded volume effect might be the reason for the highest catalytic efficiency (k_{cat}/K_M) in Dex 30 wt% solution followed by buffer and ATPS.

The trend in the values for the catalytic constants in ATPS at ambient pressure were exactly the opposite to what was observed for the neat buffer solution. In ATPS, while the K_M remains nearly constant, the k_{cat} value decreased from 0.93 s^{-1} to 0.33 s^{-1}. Similar values of K_M in buffer and ATPS also proved that the reaction is not diffusion controlled and that both the enzyme and substrate partition in the same phase of the ATPS. The partitioning was further confirmed by phase contrast and fluorescence microscopy experiments.

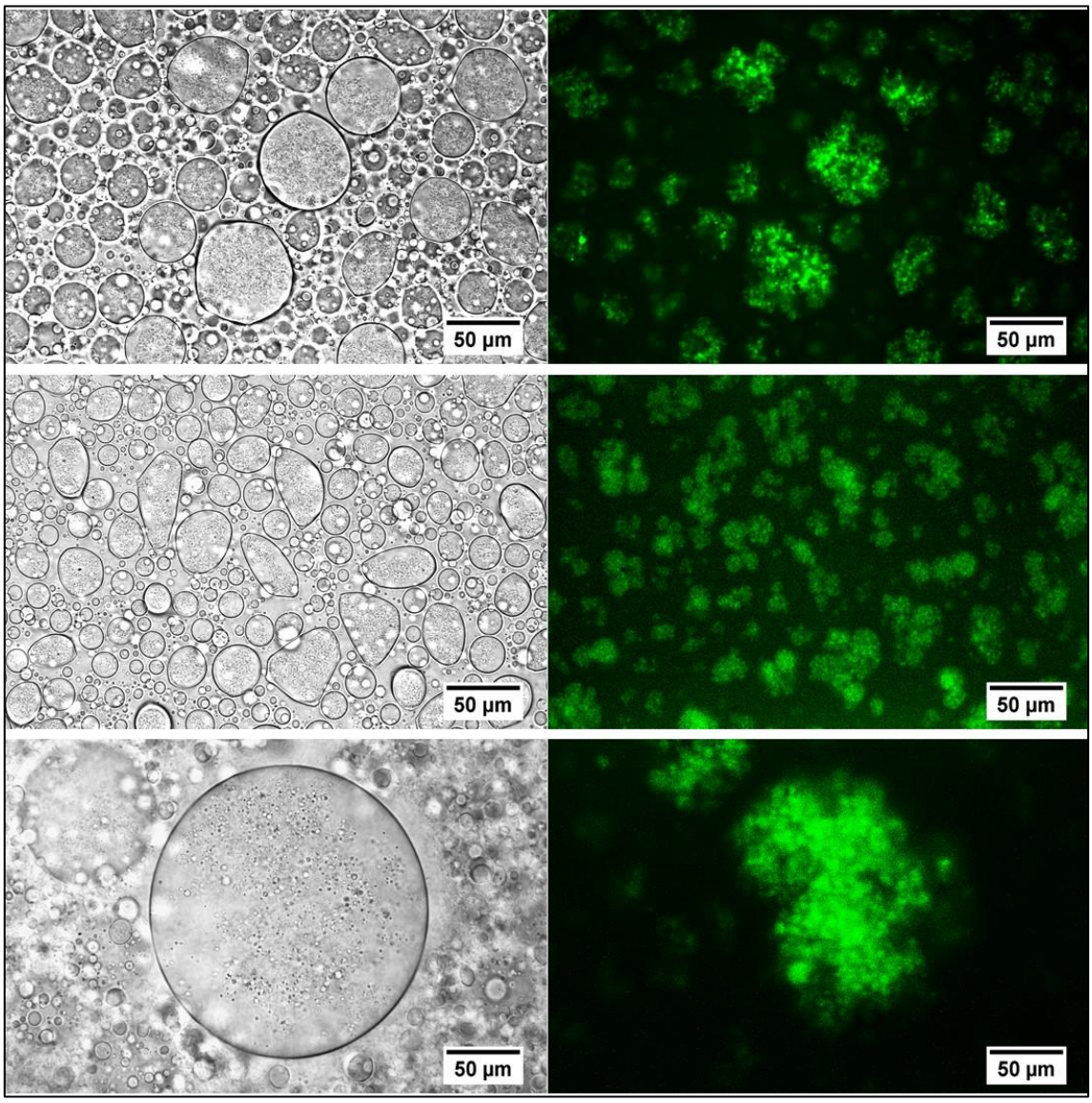

Figure 3.11. Phase contrast (left panels) and fluorescence (right panels) microscopy pictures of the ATPS (top) with rhodamine B-labeled dextran, (middle) danysl-α-CT and (bottom) AAF-AMC substrate (T = 20 °C, p = 1 bar). The size of the scale bar is 50 µm.

Fig. 3.11(top) depicts phase contrast microscopy pictures of the ATPS. The system is characterized by the presence of micrometer-sized droplets. Dextran was labeled with rhodamine B which showed that droplets are enriched with Dex, thus representing the Dex-rich droplets that are dispersed in the PEG-rich phase. Using dansyl-labeled α-CT (Fig. 3.11, middle) and taking advantage of the intrinsic fluorescence of the AAF-AMC substrate (Fig. 3.11, bottom), it was also shown that both the enzyme and the substrate partition in the same phase, i.e. the Dex-rich droplet phase. Though this same phase partitioning can explain the minor changes in the K_M value, it cannot account for the drastic decrease in the k_{cat} value as compared to the neat buffer system.

CD spectroscopy studies were performed to check any alterations in the conformation of the protein. Both the secondary and tertiary structure of α-CT are not significantly affected in the ATPS as can be seen from Fig. 3.12. Previously, high-pressure FTIR spectroscopy studies have shown that the enzyme is stable up to several kbar pressures [158]. Thus, the CD results rule out any possibility of the effect of structural changes on the kinetic constants values in the ATPS.

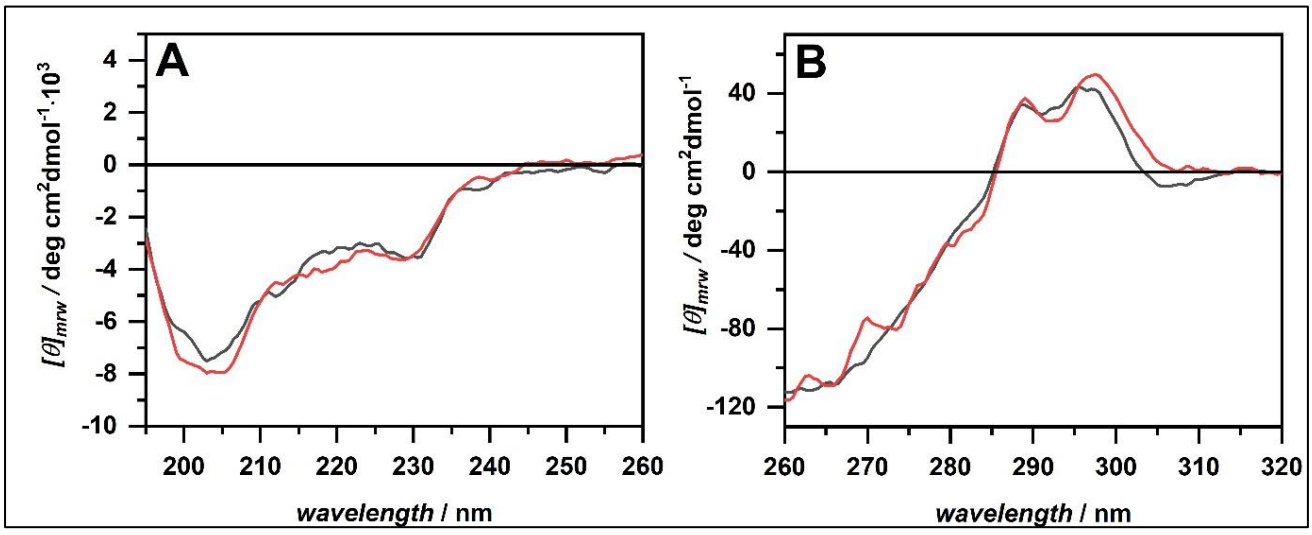

Figure 3.12. (A) Far-UV and (B) Near-UV circular dichroism spectra of α-chymotrypsin in buffer (black lines) and in the ATPS (red lines).

Comparing the k_{cat} value in ATPS with that of 30 wt% Dex clearly indicates that the steric crowding effect caused by high concentration of polymers is not the sole reason for the dramatic change in the turnover number. The probable reason for the ~70 % decrease in k_{cat} can be explained by a change in water activity owing to the markedly reduced water content in

the ATPS with respect to the bulk solution, as has been observed in osmotically stressed PEG systems [71]. Such changes in water activity may affect the rehydration and release kinetics of the products. To confirm such assumption, steady-state fluorescence spectroscopy was performed using dansyl-labeled α-CT in buffer, the ATPS and in 30 wt% Dex.

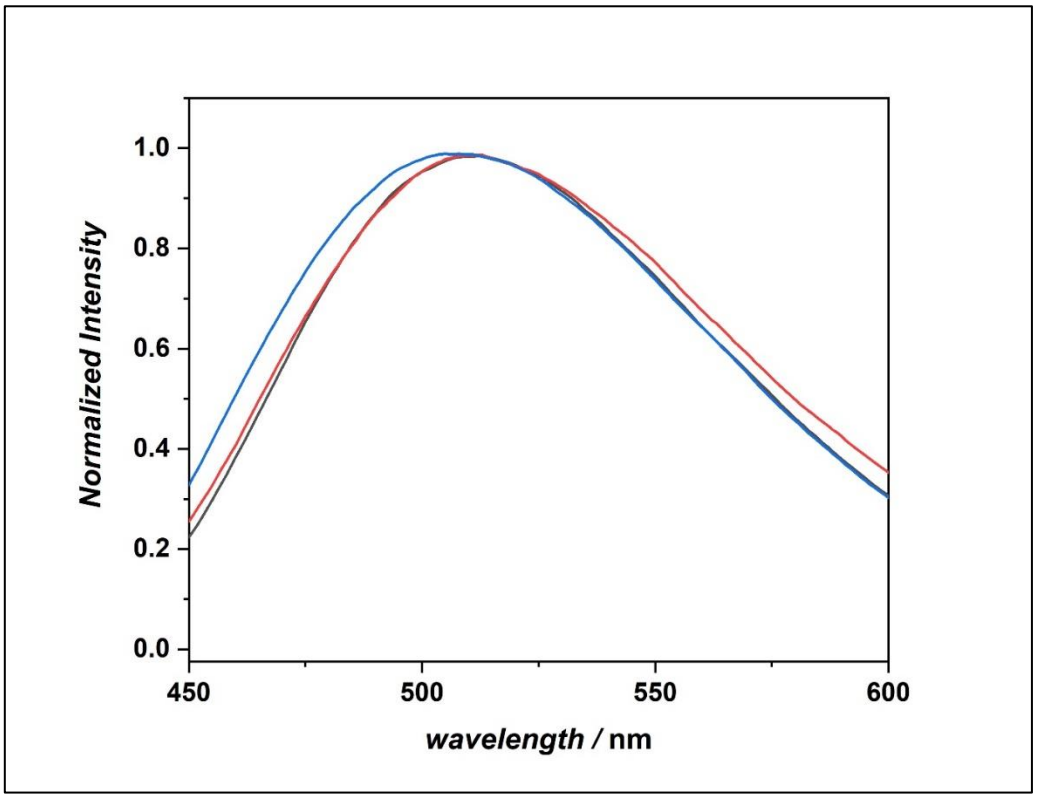

Figure 3.13. Normalized fluorescence emission spectra of Dansyl-α-chymotrypsin in buffer (black line), Dex 30 wt% (red line) and in the ATPS (blue line). The experiments were carried out at 20 °C using a 1-cm path length quartz cuvette.

The fluorophore used in this case, i.e., the dansyl group is sensitive to the change in polarity in its local environment and thus, is perfect to determine the change in hydration and water dynamics surrounding the enzyme. As is seen from Fig. 3.13, the center of mass (CM) in the fluorescence emission spectrum of the dansyl-labelled α-CT in buffer is located at 523 nm, similar to that of the position of the CM in 30 wt% Dex. This observation indicates that the crowding induced by the high concentration of Dex does not in any way change the hydration and the microenvironment surrounding the protein surface. On the other hand, a significant blue shift of the CM in ATPS was observed at 519 nm, revealing that the level of hydration and water dynamics close to the surface of the protein is markedly reduced. This change in the position of the CM for dansyl-labeled α-CT in the ATPS also supports the presumption that the decrease in k_{cat} is due to the change in hydration of the enzyme surface which affects the

catalytic activity of the enzyme [71]. The difference in the CM value between 30 wt% Dex and ATPS shows that the Dex 30 wt% phase has different physico-chemical properties than the Dex-rich droplet phase of the ATPS system, which in addition contains 3 wt% PEG molecules.

In the next step, the effect of high hydrostatic pressure (HHP) on the catalytic activity of α-CT in both buffer and ATPS was measured by means of steady-state fluorescence spectroscopy. In neat buffer, an increase in pressure lead to an increase in both k_{cat} and K_M. The K_M value increased from 172 μM at ambient pressure to 396 μM at 2000 bar, indicating that the pressure decreases the enzyme-substrate affinity. Similarly, the turnover number of the enzyme was accelerated from 0.93 s^{-1} at ambient pressure to 1.71 s^{-1} at 2000 bar. This increase in k_{cat} suggests the formation of a compact transition state of the enzyme-substrate complex, rendering the activation volume negative (Eq. 52) [66]. Following similar arguments, the increase of K_M should be related to an increase in the overall volume upon formation of the ES complex, i.e. upon substrate binding to the enzyme.

However, in the ATPS no significant effect of HHP was observed on the catalytic activity of the enzyme. By increasing the pressure up to 2000 bar, both the K_M and k_{cat} values remain essentially constant around 200 μM and 0.30 s^{-1}, respectively. These results indicate that the ATPS counterbalances the effect of pressure in modulating the kinetic constants of the α-CT catalyzed hydrolysis reaction. In an effort to rationalize these findings, the effect of HHP on the stability of ATPS system was explored using phase contrast and turbidity measurements.

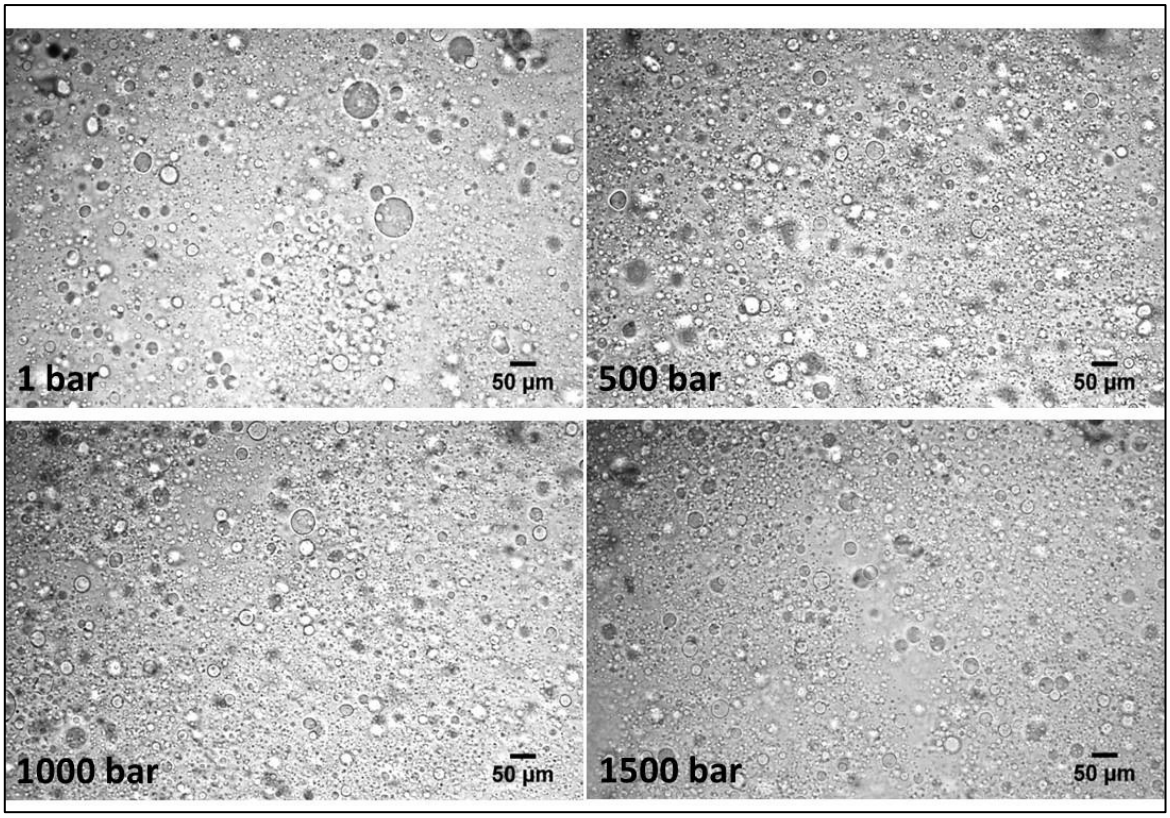

Figure 3.14. Phase contrast microscopy pictures of the ATPS at selected pressures. The experiments were performed at 20 °C. The size of the scale bar is 50 µm.

Fig. 3.14 showed that there was no significant change in the size and amount of the droplets in the whole pressure range covered which relates to the fact that HHP has no effect on the stability of the ATPS at room temperature. This is probably due to the absence of any significant void volume in this artificial ATPS. This is also supported by the turbidity measurement as shown in Fig. 3.15.

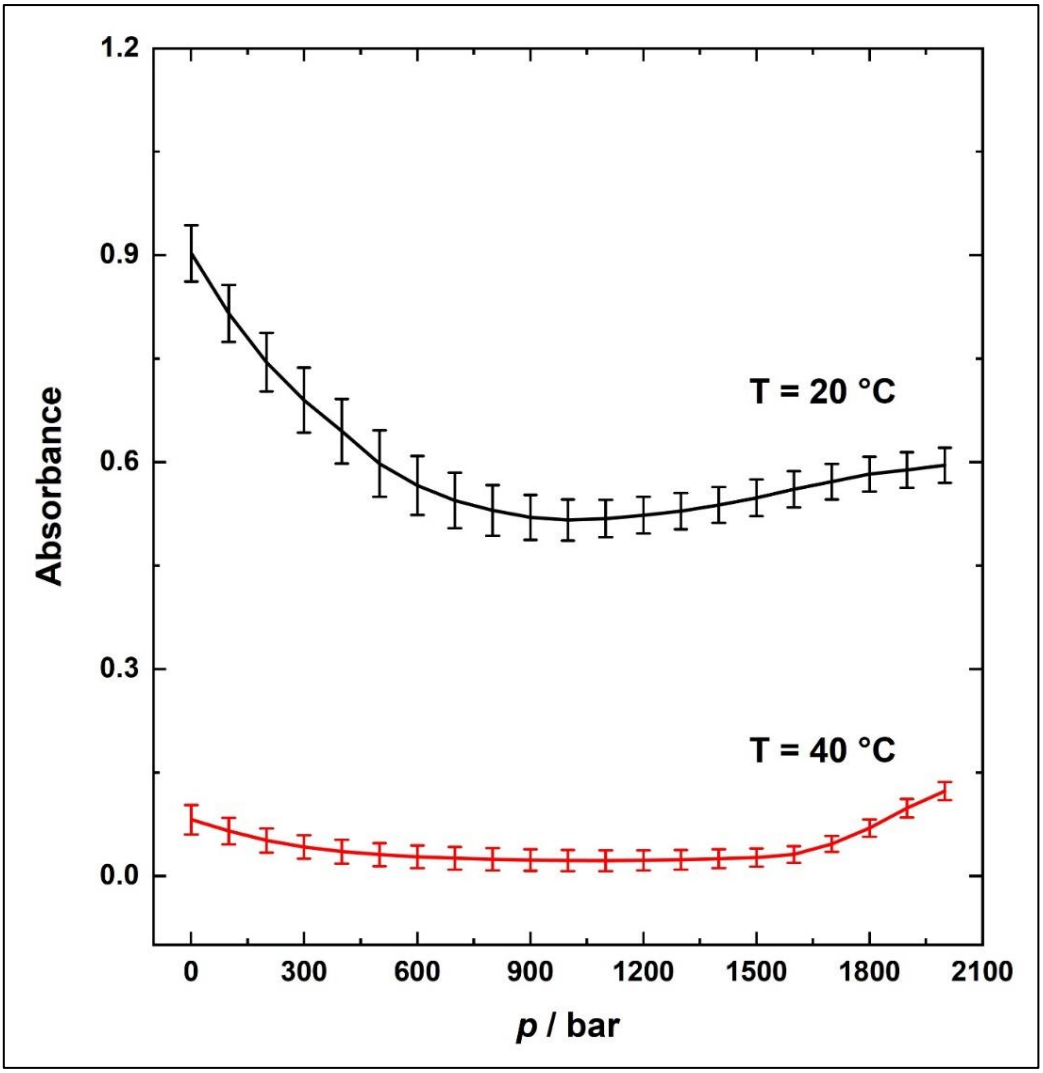

Figure 3.15. Changes in apparent absorbance (turbidity) with pressure of the ATPS at 20 °C (black line) and, as a reference, at 40 °C (red line). The employed PEG/Dex mixture is phase separated at 20 °C but not at 40 °C.

Fig. 3.15 shows that only minor changes were detected upon increasing the pressure at room temperature. Since it has been established from the phase diagram (Fig. 3.2) that this artificial ATPS is phase separated at 20 °C and moves towards the one-phase region at 40 °C and above, the absorbance (a measure of turbidity here) of the system at 40 °C is lower compared to 20 °C owing to its homogeneous nature. Since the ATPS lies at the boundary of the two- and one-phase system at 40 °C, the absorbance is close to zero at this temperature. However, as the ATPS is not completely homogeneous like the neat buffer system, it still shows some turbidity value over the entire pressure range explored. Thus, the counterbalancing effect of the ATPS on the kinetic parameters at 20 °C cannot be explained by changes of the structure of the ATPS at HHP.

To shed more light on the changes imposed by the ATPS, a volumetric analysis of the results was carried out. According to Eq. 52, from the pressure dependence of the kinetic and equilibrium constant it is possible to determine the partial volume changes for a given reaction. In particular, from the pressure dependence of $1/K_M$ and k_{cat}, the binding volume, ΔV_b, and the activation volume, $\Delta V^{\neq}$, of the enzyme reaction can be determined [158,159,160,243].The binding volume, ΔV_b, refers to the difference between the volume of the enzyme-substrate (ES) complex and the uncomplexed state (E+S), and the activation volume, $\Delta V^{\neq}$, at high substrate concentrations refers to the volume difference between the activated complex ($ES^{\neq}$) and the enzyme-substrate complex (ES).

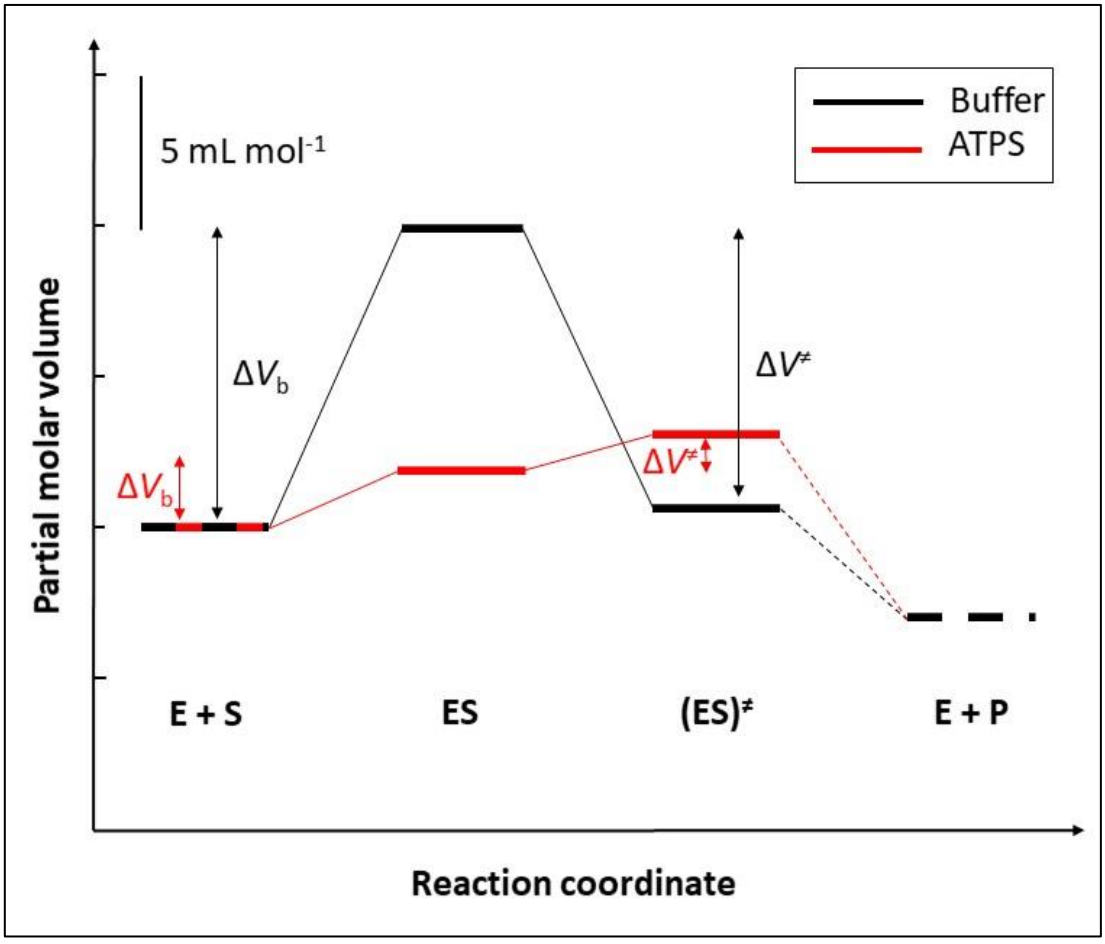

Figure 3.16. Schematic representation of the volume profile for the α-CT-catalyzed hydrolysis reaction of AAF-AMC substrate in buffer (black lines) and in the ATPS (red lines), with reference to V(E+S). The partial molar volume of the product state (E+P) cannot be given and is hence denoted as dashed line.

ΔV_b in fact was found to be positive, 9.8 ± 0.7 mL mol^{-1}, and $\Delta V^{\neq}$ to be negative, -9.2 ± 3.0 mL mol^{-1}, pointing to the decreased enzyme affinity and increased turnover number upon pressure

increase. The positive sign for ΔV_b indicates that the partial molar volume of the ES complex is slightly expanded with respect to the uncomplexed state, which might be due to the release of hydration water upon binding. The negative value of $\Delta V^{\neq}$ demonstrates that the volume occupied by the activated complex ($ES^{\neq}$) is smaller compared to the ES complex, which is hence more compressible than the activated state. Since the ΔV_b and $\Delta V^{\neq}$ values are of similar magnitude but of opposite sign, the enzymatic efficiency, k_{cat}/K_M, remains almost constant in the pressure range from 1 to 2000 bar. Conversely, in the ATPS, the two values, ΔV_b and $\Delta V^{\neq}$ (2.0 ± 0.9 and 2.2 ± 2.0 mL mol^{-1}, respectively) are both small and positive, making the kinetic constants in the ATPS rather insensitive to pressure. As hydration is a major contribution of the partial molar volume of proteins [215,243] the marked decrease in ΔV_b in the ATPS system with respect to the neat buffer solution is most likely related to the lower level of hydration of the reactants in the ATPS, i.e. also to a smaller volume-reducing electrostrictive effect of hydration water.

3.6 Conclusions

Generally, K_M and k_{cat} are known to depend in a complex way on solvent/cosolute/substrate/enzyme interactions, implicating that activities instead of concentrations of the reactants should be used in quantifying and predicting the kinetic constants [68,172]. In addition, substrate binding requires the (partial) dehydration of both the active site and the substrate, and product release requires rehydration of the enzyme and product molecules. Further, next to strong crowding, lower water activities may change the conformational flexibility of the enzyme and hence its function. Generally, a high flexibility is fostering enzymatic activity. Hence, water activity can be expected to affect both K_M and k_{cat}. Here it has been shown that simple steric crowding effects, such as in the presence of high concentrations of dextran, are not able to explain the kinetic constants in the ATPS. Additional contributions, such as changes in water activity and in reactant activity via non-specific weak interactions with ATPS components (e.g., hydrophobic substrates with PEG), must be invoked in explaining the results obtained. Certainly, depending on the substrate, other scenarios, such as product inhibition, could play a role as well [215]. By affecting the binding and activation volume, pressure is able to modify the kinetic parameters. In the case of α-CT, a significant increase of k_{cat} is observed at HHP. Remarkably, the effect of pressure on the kinetic parameters is alleviated in the ATPS, which is most likely related to changes in water activity and dynamics in the dense droplet phase of the ATPS. This indicates that the presence of PEG in the ATPS, i.e. the composition of the ATPS, has a marked effect on the properties of the droplet phase

and hence on the kinetic constants, rendering them rather robust to changes of pressure even up to the 2 kbar level compared to the neat buffer solution. These findings might be relevant for understanding cellular processes of piezophiles and might also have bearings on biotechnological applications using liquid-liquid phase separation and pressure in concert to modulate enzymatic reactions.

Chapter 4

Combined Effects of Aqueous Two-Phase System and High Hydrostatic Pressure on the Binding of BSA and ANS

4. Combined Effects of Aqueous Two-Phase System and High Hydrostatic Pressure on the Binding of BSA and ANS

Abstract

Molecular recognition or binding is one of the most important reasons for the proper functioning of cells. Binding of macromolecules depends on several factors, the most prominent being the various kinds of interactions that are present at the binding site. Pressure, on the other hand, effects the intra- and intermolecular interactions in a protein, leading either to its stabilisation or denaturation at higher pressure. This chapter focusses on the combined effect of ATPS and HHP on the binding of the plasma protein Bovine Serum Albumin (BSA) and the fluorophore 1-anilino-8-naphthalene (ANS) serving as ligand. The results indicate that ATPS being a highly crowded medium alters the affinity of various binding sites as compared to equivalent binding sites in neat buffer solution. The decrease in binding affinity with an increase in pressure in both buffer and ATPS suggests an unfavourable effect of pressure on the hydrophobic interaction between BSA and ANS which is the main driving force for binding.

Contributions

Dr. Rosario Oliva and Sudeshna Banerjee planned and carried out the experiments, Hasan Cinar performed the pressure-dependent phase contrast and turbidity measurements, Dr. Rosario Oliva developed the two theoretical models (Model 1 and Model 2) to analyse the data, Dr. Rosario Oliva, Sudeshna Banerjee and Hasan Cinar analysed the data, Dr. Rosario Oliva, Sudeshna Banerjee and Prof. Dr. Roland Winter interpreted the results.

4.1 Introduction

Molecular recognition is an important phenomenon in cells by which biomolecules interact among themselves or with other molecules via non-covalent interactions to form specific complex [27]. This phenomenon has two important characteristics: specificity and affinity. Specificity leads to the binding of a macromolecule with specific binding partner, whereas affinity determines that a high concentration of weakly interacting partners cannot replace the effect of a low concentration of the specific partner interacting with high affinity [39]. Proteins are a very important class of macromolecules and play a variety of roles in the cell, including biochemical (enzyme reactions), cell signalling and more [8,16,88]. All these works require the direct interaction of proteins with other biomolecules such as proteins, nucleic acids or small ligands. Thus, it is essential to know in-depth the factors effecting molecular binding for a better understanding of the cellular processes [16,118]. Apart from this, molecular recognition is an important step in drug design [245]. The effectiveness of a drug in the human body depends on its pharmacokinetics and pharmacodynamics [26]. Pharmacodynamics deals with the mechanism of drug action. A drug acts effectively inside the human body with an increase in its concentration till a certain limit after which it becomes toxic. The deciding factor for this limit is the binding affinity between the drug and the biological macromolecule, especially the plasma proteins [26]. Thus, knowledge of molecular binding may help in better drug design and delivery.

Serum albumins are the most abundant plasma proteins in human constituting about 60 % of the total serum content [81,249]. Of them, Bovine and Human Serum Albumins (BSA and HSA, respectively) are the most studied proteins. The main function of serum albumin is to transport a wide variety of fatty acids, hormones and metal ions [87,171]. Binding to BSA has been characterised by several molecular forces such as hydrophobic, hydrogen bonding and electrostatic interactions which are present in various binding sites [171]. 1-anilino-8-naphthalene (ANS) is a widely used fluorescent probe for biological studies, e.g., for studying conformational changes and folding-unfolding of proteins [9,97,98,202]. It is used extensively to characterise hydrophobic pockets in proteins since the fluorescence quantum yield of ANS in a polar solvent, such as water, is much less, and is significantly enhanced upon binding to the hydrophobic pockets of proteins [97,202]. The structure of ANS is shown in Fig. 4.1.

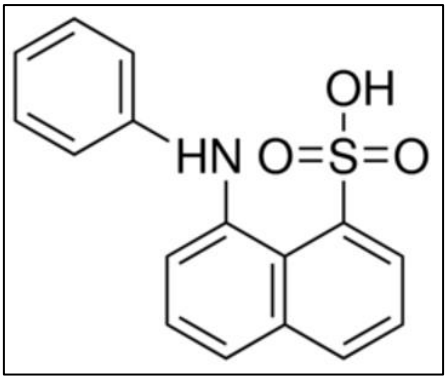

Figure 4.1. Structure of 1-anilino-8-naphthalene (ANS).

In this chapter, the binding of ANS to BSA has been studied in neat buffer (Tris buffer) and ATPS. As has been mentioned in Section 3.1, the ATPS serves as a primitive model for understanding membraneless organelles [188,223,235]. This synthetic ATPS is composed of two co-existing phases, one Dex-rich and the other is PEG-rich and it would be of great importance to reveal how crowding imposed by the ATPS affects the binding phenomenon, which might be helpful in explaining several biochemical reactions occurring in biological membraneless organelles and subsequent drug design for the human body. The effect of HHP on the binding has also been studied in this chapter. Several organisms have been discovered to thrive at extreme pressure conditions on earth [20,28,181], and the adaptability of their molecular machinery in such harsh situations is still under investigation [13,74,89,182]. Hence, the combined effect of HHP and ATPS has been studied on the binding of ANS to BSA to shed some light on the details of molecular binding in such crowded environment as well as in piezophiles.

4.2 Materials and methods

4.2.1 Materials

Lyophilized powder of the protein bovine serum albumin (BSA), the fluorophore 8-anilinonaphthalene-1-sulfonic acid (ANS), PEG of molecular weight 4.6 kDa and FITC-labeled BSA were purchased from Sigma Aldrich Chemical. Dex 10 kDa was purchased from Carl Roth. All the chemicals were used directly without any further purification. Solutions were prepared in pressure-stable Tris buffer (10 mM Tris-HCl, pH 7.4) and deionized water was used for buffer and the sample preparations.

4.2.2 Sample preparation

A stock solution of BSA was prepared by dissolving the protein in buffer. The exact concentration of the solution was determined by measuring the absorbance at 280 nm by means of UV/Vis spectroscopy (UV-1800 spectrometer from Shimadzu Corporation) and using a molar extinction coefficient of 43600 M^{-1} cm^{-1}. Similarly, a stock solution of the fluorophore ANS was prepared by dissolving it in water, and subsequent dilution in buffer was performed to determine the exact concentration. The concentration was determined by measuring the absorbance using an extinction coefficient of $\varepsilon(350) = 4950$ M^{-1} cm^{-1} [81].

4.2.3 Steady-state fluorescence spectroscopy

The binding dynamics was recorded using a K2 fluorometer from ISS, Inc. (Champaign, IL, USA) which is equipped with a xenon arc lamp as light source. The excitation and emission wavelengths were set at 350 nm and 468 nm, respectively, with the slit width set at 8 nm for both excitation and emission monochromators. The binding of ANS to BSA was monitored by recording the increase in fluorescence intensity due to the complex formation at 468 nm by scanning over a wavelength range of 420-520 nm. For analysing the fluorescence data obtained, two different models were developed. The first model (Model 1) was designed by assuming that all the binding sites of BSA are equivalent and independent of each other, whereas the second model (Model 2) assumed independent and non-equivalent sites. The detailed mathematical treatment of both the models is shown below. The temperature in all cases was kept constant at 25 °C using a circulating water bath and sufficient time was given for equilibration of the sample chamber. In all the experiments, the ANS concentration was kept constant at 5 μM. The BSA concentration was varied from 0 μM to 40 μM. The final volume of the solution was 1500 μL. In case of the pressure dependent measurements, the HHP cell system from ISS and quartz cuvettes were used. The pressure was controlled by means of a manual pump and water was used as pressurizing fluid. A pressure range from 1 bar to 2000 bar was explored. The ANS and BSA were mixed, vortexed and then filled into the sample cell which was sealed with DuraSeal™ laboratory stretch film and placed into the high-pressure vessel.

A Job's plot, also known as the method of continuous variation, is a very useful method for the characterization of products formed by an interaction of two species [194]. In this method, the mole fractions of both the species are varied while keeping their total concentration constant. In this case, in determining Job's plots at ambient pressure, the total concentration of ANS and

BSA was kept constant at 35 μM and the mole fraction of ANS (x_{ANS}) was varied from 1 to 0.05. The total volume of the solution was 100 μL. The fluorescence intensity of the BSA-ANS complex was measured and plotted versus the ANS molar fraction. Linear regression fittings were made at the two extremes of the curve. The cross point between the two linear plots provided the amount of ANS (molar fraction) for the binding stoichiometry of the fluorescent complex.

Model 1- equivalent and independent binding sites

The following equilibrium was considered. Ligand (L) binds to n sites of the protein P, forming an PL_n complex:

$$P + nL \rightleftarrows PL_n \quad (54)$$

Concentrations at time $t = 0$	$[P_0]$	$[L_0]$	0
at equilibrium	$[P_0\text{-}x]$	$[L_0\text{-}nx]$	$[x]$

where $[P_0]$ represents total protein concentration, $[L_0]$ total ligand concentration, $[x]$ is the amount of complex formed and n is the ratio of moles of ligand by moles of protein.

The microscopic binding constant K_b is defined as

$$K_b = \frac{[PL]}{[P][L]} = \frac{[x]}{[P_0 - x][L_0 - nx]} \quad (55)$$

$$\Rightarrow ([P_0][L_0] - n[x][P_0] - [x][L_0] + n[x]^2)K_b - [x] = 0 \quad (56)$$

Rearranging Eq. 56, a second order equation is obtained which can be represented as

$$ax^2 - bx + c = 0 \quad (57)$$

where $a = nK_b$, $b = (1 + n[P_0]K_b + [L_0]K_b)$ and $c = [P_0][L_0]K_b$.

Solving the second order Eq. 57 gives two solutions out of which one solution (x_1) is valid in this case (Eq. 58):

$$x_1 = -\frac{\sqrt{b^2 - 4ac} - b}{2a} \quad (58)$$

x_1 represents the amount of complex formed. The average number of ligands bound to the protein at any given time is defined by the parameter $\bar{v}$ [170]-

$$\bar{v} = \frac{moles\ of\ ligand\ bound}{moles\ of\ total\ protein\ concentration} = \frac{nx_1}{[P_0]} \quad (59)$$

The fractional saturation, θ, is given as the ratio of moles of complex formed to the moles of total protein concentration and is related to $\bar{v}$ as-

$$\theta = \frac{\bar{\nu}}{n} = \frac{x_1}{[P_0]} = \frac{\left(-\left(\sqrt{b^2-4ac}\right)-b\right)}{2a[P_0]} \quad (60)$$

Further, the fractional saturation can be correlated to the experimentally obtained fluorescence intensity as

$$\theta = \frac{\Delta F}{\Delta F_{max}} = \frac{F-F_0}{F_S-F_0} \quad (61)$$

where F is the fluorescence intensity of the complex formed, F_0 is the intensity of ANS alone in buffer or the ATPS, and F_S is the fluorescence intensity when the binding reaches saturation. Since the total protein $[P_0]$ and total ligand $[L_0]$ are known, equating Eq. 60 to Eq. 61 yields Eq. 62:

$$\Delta F = \frac{\left(-\left(\sqrt{b^2-4ac}\right)-b\right)}{2a[P_0]} \Delta F_{max} \quad (62)$$

Model 2 - Non-equivalent multiple and independent binding sites

The equilibrium for this model is represented as-

$$P + L' \rightleftharpoons PL' \qquad K_1 = \frac{[PL']}{[P][L']} \quad (63)$$

$$P + L'' \rightleftharpoons PL'' \qquad K_2 = \frac{[PL'']}{[P][L'']} \quad (64)$$

The total binding constant K is given by the summation of K_1 and K_2. Combining the above equilibria and solving the equation in a similar way as for model 1, $\bar{\nu}$ is given as

$$\bar{\nu} = \frac{n_1[PL']}{[P_0]} + \frac{n_2[PL'']}{[P_0]} = \frac{n_1[PL']+n_2[PL'']}{[P_0]} \quad (65)$$

The fractional saturation θ is given by:

$$\theta = \frac{1}{n_1+n_2}\left[\frac{\left(-\left(\sqrt{b_1^2-4a_1c_1}\right)-b_1\right)}{2a_1[P_0]} + \frac{\left(-\left(\sqrt{b_2^2-4a_2c_2}\right)-b_2\right)}{2a_2[P_0]}\right] \quad (66)$$

where: $a_1 = n_1K_1$ and $a_2 = n_2K_2$

$b_1 = (1 + n_1[P_0]K_1 + [L_0]K_2)$ and $b_2 = (1 + n_2[P_0]K_2 + [L_0]K_2)$

$c_1 = [P_0][L_0]K_1$ and $c_2 = [P_0][L_0]K_2$

4.2.4 Pressure dependent turbidity measurements

Pressure dependent turbidity measurements were carried out on a PerkinElmer Lambda 25 spectrophotometer with a home built high-pressure optical cell. Sapphire with a diameter of 20 mm and a thickness of 10 mm was used as window material. Pressure was applied using a high-pressure hand pump and was measured by a pressure sensor (Burster Präzisionsmesstechnik, Gernsbach). Water was used as pressurizing medium.

4.2.5 Pressure dependent microscopy measurements

Phase contrast and fluorescence microscopy experiments were also carried out using an Eclipse TE2000-U (Nikon Inc.) optical microscope with a Nikon CFI Plan Apo Lambda 10x objective coupled to an TIS DMK 23UX249 camera. FITC-labeled BSA and the intrinsic fluorophore property of ANS were used for fluorescence microscopy. For the pressure-dependent microscopy studies, a home-built high-pressure microscopy cell was used. The pressure was generated using a high-pressure hand pump using water as the pressure-transmitting fluid. Flat diamond windows were used as optical window materials on both sides.

4.3 Results and discussion

Steady state fluorescence experiments were performed to check the intensity of ANS alone in buffer and the ATPS at ambient pressure and at a temperature of 25 °C. From the Fig. 4.2 it is evident that ANS alone in buffer (blue line in A) or in the ATPS (black line in B) does not have any significant fluorescence intensity. It shows a strong increase in fluorescence intensity when complexed in the hydrophobic pockets of BSA as has been reported [97,202]. ATPS alone (blue line in B) too does not show any significant intensity due to scattering of droplets compared to the intensity of BSA-ANS complex. Due to the negligible intensity of pure ANS in buffer or ATPS, the F_0 value in Eq. 61 was assumed to be zero.

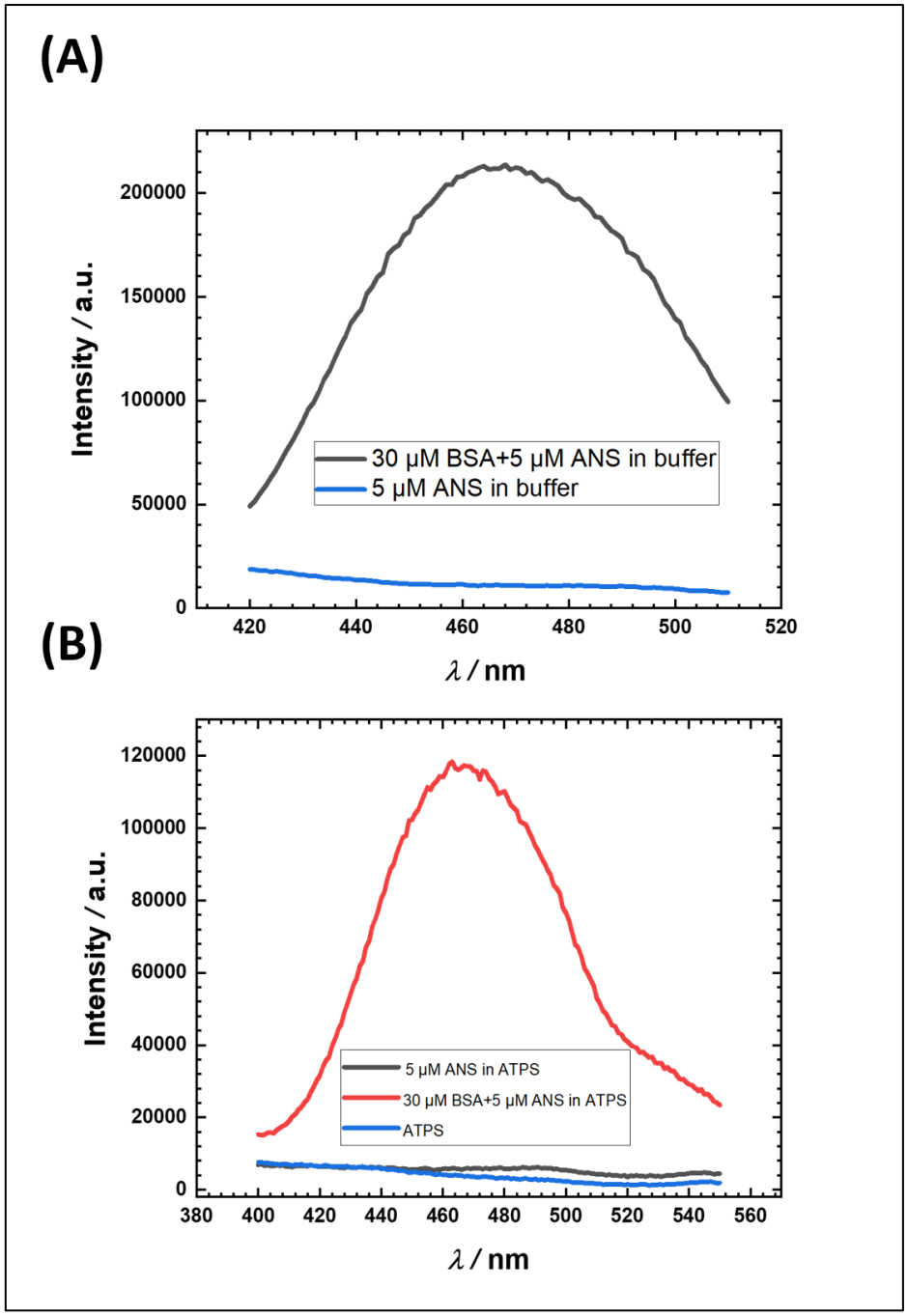

Figure 4.2. Fluorescence intensity of the neat ATPS and of 5 μM ANS in buffer (A) and the ATPS(B) and in complex with BSA.

Fig. 4.3 shows the binding curves (ΔF normalized vs $[BSA]_{total}$, see Section 4.2.3) of BSA and in the ANS in buffer (10 mM Tris-HCl, pH 7.8) and ATPS at a constant temperature of 25 °C and at ambient pressure. The ΔF values for both buffer and ATPS were normalized by dividing each value with their respective saturation value (ΔF value at the highest BSA concentration) for direct comparison. The binding constants obtained in buffer and in ATPS under various pressure conditions are summarised in Table 2 and Table 3, respectively.

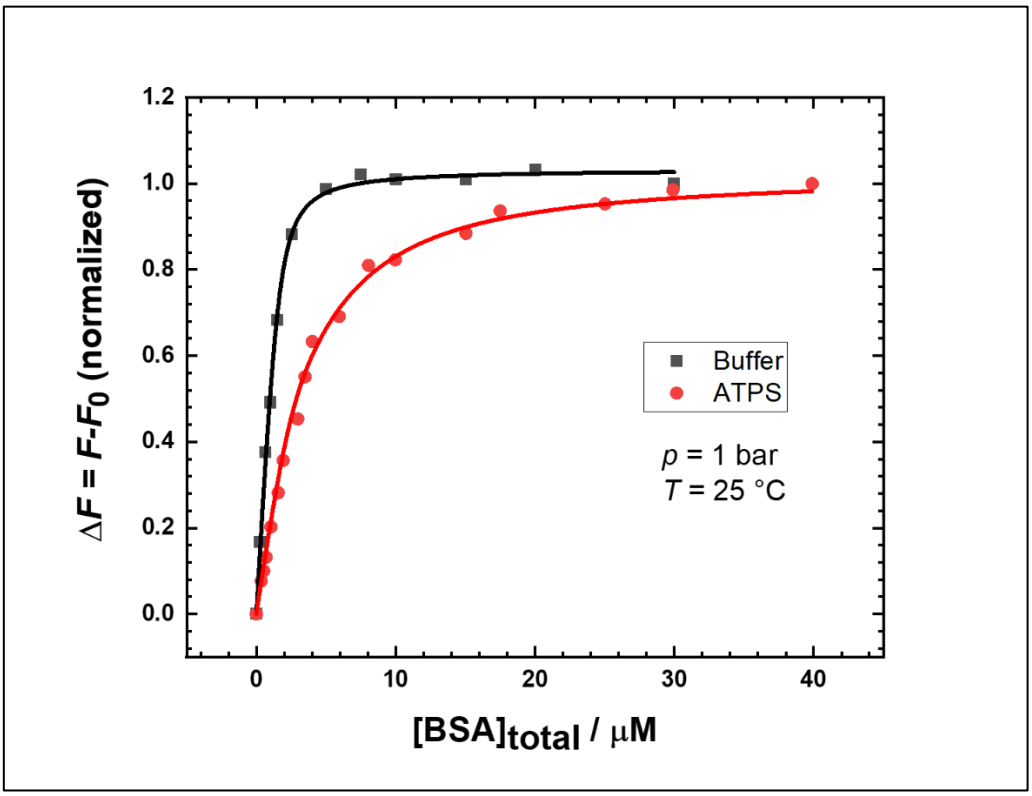

Figure 4.3 Binding isotherms for the binding of ANS to BSA in buffer (black squares) and in the ATPS (red dots) at ambient pressure. The colored lines represent the best fits of the experimental data according to Eq. 62.

Buffer (Table 2)

Pressure / bar	K_b (M^{-1}) *10^6	*n*
1	4.2±0.9	3.2±0.3
500	3.2±1.1	3.1±0.2
1000	2.8±0.9	3.1±0.2
1500	1.9±0.6	3.0±0.1
2000	1.2±0.4	2.9±0.1

ATPS (Table 3)

Pressure / bar	K_1 (M^{-1}) *10^6	*n*	K_2 (M^{-1}) *10^6	*n*	R^2
1	4.28	2	0.420	1	0.996530334
500	5.38	2,3	0.225	1,04	0.999295298
1000	0.415	2	0.224	1	0.999063336
1500	0.820	2	0.0898	1	0.998511903
2000	0.402	2	0.0994	1	0.998481566

Table. Binding parameters for the binding of ANS to BSA at different pressures and at a temperature of 25 °C in buffer (Table 2) and in the ATPS (Table 3).

As can be seen from Fig. 4.3, the shape of the binding curves of BSA and ANS in the ATPS and buffer exhibit striking differences. The binding constant (K_b) value of $4.2*10^6$ M^{-1} and the total number of binding sites (n) has been found to be 3 (Table 2) for binding in buffer at ambient pressure. These results were obtained by fitting the raw data (fluorescence intensity) using Model 1 (see Section 4.2.3 (A)) where it was assumed that all the sites are equivalent and independent of each other. Thus, the binding of ANS to one site on BSA does not in any way affect the binding to the remaining sites. The raw data were also fitted using the second binding model (Section 4.2.3 (B)) involving non-equivalent binding sites, but no good fits were obtained, suggesting that all the binding sites are probably equivalent. The K_b obtained in this case represents an average of all the microscopic binding constants for each of the three sites. However, the difference in the binding affinity between ANS and BSA in the three individual binding sites couldn't be distinguished using fluorescence. The reason for this may be very small differences between the binding constant values of the three sites, often techniques, such as NOIR titration, might be able to reveal these minor differences.

On the other hand, in the ATPS at ambient pressure, a significant change in the shape of the binding curve has been observed (Fig. 4.3). A steep rise of the curve has been detected till the BSA concentration of 8 μM followed by a more gradual increase for higher BSA concentrations (10-40 μM). The data were fitted using the non-equivalent model (Section 4.2.3 (B)) and two binding constants (K_1 and K_2) for two different classes of binding sites (n_1 and n_2) have been obtained (Table 3). The steeper part of the curve corresponds essentially to the behaviour of two binding sites ($n_1 = 2$) and the binding constant is given by K_1 which is equal to $4.28*10^6$ M^{-1}. Similar to the buffer data, K_1 is a microscopic binding constant representing the overall binding of both sites. The less prominent rise in the latter part of the binding curve with increase in BSA concentration is characterised by a binding constant K_2 of $0.420*10^6$ $M^{-1}$and $n_2 = 1$. Hence, K_2 embodies the microscopic binding constant of the third binding site. The total stoichiometry ($n_1+n_2 = n = 3$) is however preserved in the ATPS compared to that in the buffer. The relatively higher value of K_1 connotes stronger binding affinity between BSA and the ANS at two binding sites compared to the third one. Since K_1 is similar in magnitude to K_b in buffer solution, it can be said that the third binding site with binding constant K_2 is the most affected one by the ATPS. Though the exact reasons have not been completely understood, a few possible explanations can be suggested.

Numerous works on the investigation of ANS binding to BSA have been performed, yet no certainty about the binding stoichiometry and values of binding constants could be inferred. Some experiments report six binding modes whereas some state two [31,84,211,248]. The detection of two binding modes [3,5,246,274] in this experiment may be explained based on the BSA-like structure as proposed by Togashi and Ryder [81]. They used the Förster resonance energy transfer (FRET) method in donor-acceptor pair to determine the energy transfer efficiency between tryptophan residues (BSA) and ANS bound at different binding sites. It was assumed that the smaller Forster radius (6-12 Å) of the tryptophan residues [81] as compared to the distance between them in serum albumin (~36 Å) restricted the energy transfer between the tryptophan residues. Hence, the energy transfer efficiency was solely related to the degree of occupied binding sites which helped in calculating the distance of each donor centre to the different acceptor centres. These distances match well with the crystallographic studies of HSA complex [117] and hence, the approximation of BSA structure (Fig. 4.4) was proposed by Togashi and Ryder based on the crystal structure of HSA complexed with arachidonic acid obtained from the Protein Data Bank (ID: 1 gnj) [210].

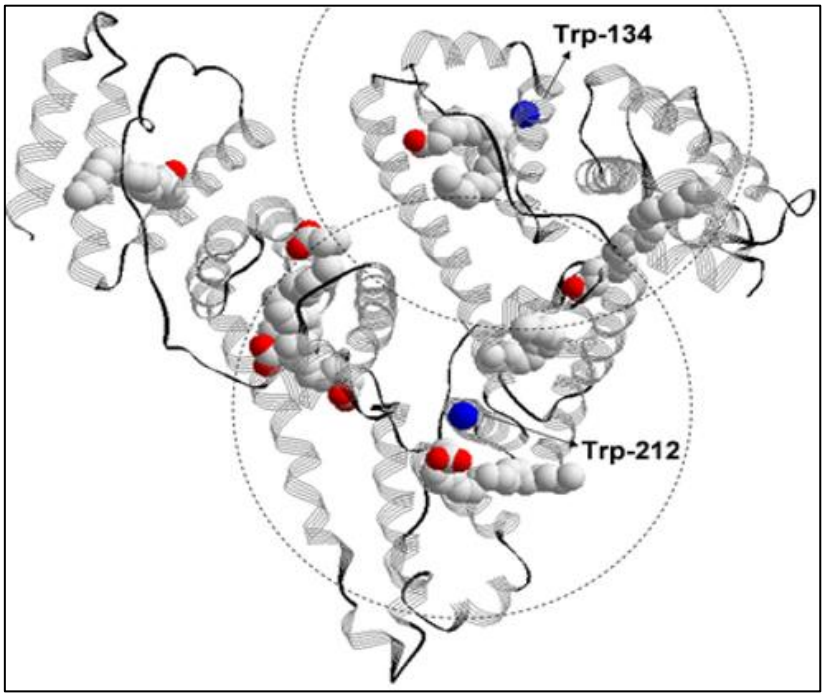

Figure 4.4. Three-dimensional representation of the "BSA-like" structure based on HSA complexed with arachidonic acid obtained from the Protein Data Bank (PDB ID: 1gnj) [4]. Dashed circles centred at the tryptophan residues limit the region for energy transfer efficiency greater than 50%. Adapted from [117].

As has been described in the literature [81], Trp-212 in BSA is believed to be located in a similar hydrophobic microenvironment as the single Trp-214 in HSA whereas Trp-134 is considered to be more exposed to the solvent i.e., water-accessible. It was found by Togashi

and Ryder that majority of binding sites are within the Forster radius limit close to Trp-214 and one binding site located very close to Trp-134. This might correspond to the two binding sites with binding constant K_1 obtained in this case in the ATPS. The third binding site with binding constant K_2 may be present close to Trp-134. Generally, several hydrophobic pockets on the surface of BSA bind the ANS aromatic rings with high affinity whereas binding of ANS to charged groups or hydrophobic clusters at the protein surface may reduce the affinity. ANS being a negatively charged molecule can bind strongly to cationic groups of polyamino acids (electrostatic interaction) [189,274]. Thus, the presence of negative or positive charged groups on the protein surface or in the hydrophobic pockets can alter the ANS binding to the protein [153,236,257]. The environment of Trp-134 might be more hydrophilic compared to Trp-212 due to its greater exposure to the solvent and since the hydrophobic interaction is the main driving force in the binding of ANS to BSA [115,246], Trp-134 binds to the ANS with lower affinity than the other two sites [187]. Several studies have shown that there exist electrostatic interactions between the sulfonate group of ANS and the polar patches in the hydrophobic cavities of BSA in the high-resolution structures of ANS complexed with BSA [8,73]. The more solvent exposed ANS molecules are reported to form complexes with BSA through hydrogen bonding or salt bridges between the sulfonate group and residues with hydrogen donor side chains [169,246]. Moreover, the exposure of aniline and naphthalene groups to the solvent allows an intermolecular electron-transfer reaction with the solvent that decreases the ANS fluorescence quantum yield [73,115,246]. Hence, from the binding curve of BSA with ANS in the ATPS it may be inferred that the two binding sites (n_1) may be present near the Trp-212 residue whereas the other binding site (n_2) might be located near to the Trp-134 residue.

Another possibility that might explain the two binding modes is the interaction of crowders with BSA. ATPS consists of two major synthetic crowders, PEG and Dextran. Though the critical concentration of the ATPS is 12.7 wt% PEG and 5.5 wt% Dex, the Dex-rich phase is composed of about 30 wt% Dex and about 3 wt% PEG, whereas the PEG-rich phase consists of about 14 wt% PEG and 2.5 wt% Dex (see section 3.4). To better understand the partitioning of BSA and ANS in the ATPS, fluorescence microscopy experiments were carried out.

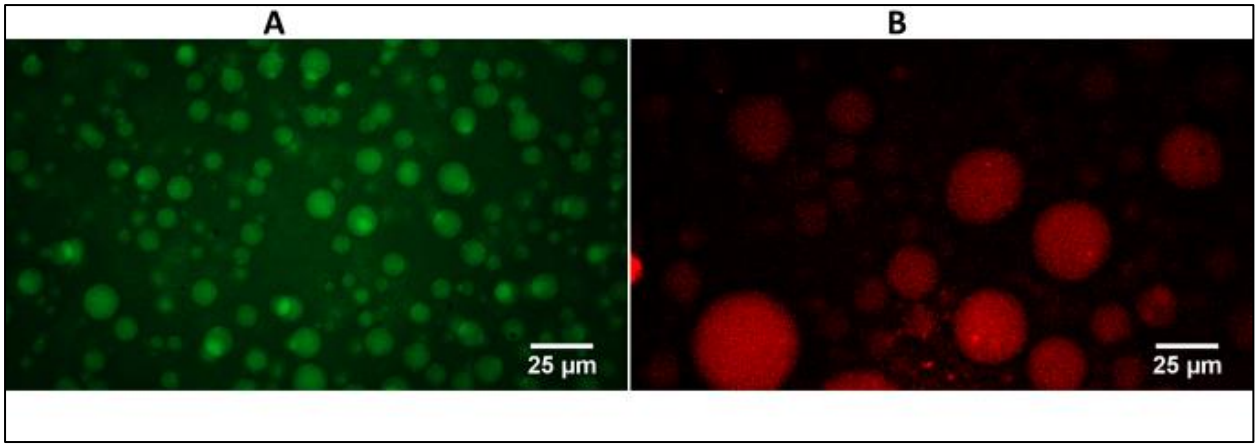

Figure 4.5. Fluorescence microscopy pictures of FITC-labeled BSA (A) and ANS (B). The size of the scale bar is 25 µm.

Fig. 4.5 depicts the presence of micrometer-sized droplets in the system. As has been shown in section 3.5.3, these droplets are enriched with Dex, thus representing the Dex-rich droplets that are dispersed in the PEG-rich phase. Using FITC labelled BSA (Fig. 4.5) and taking advantage of the intrinsic fluorescence of ANS [155], it has been shown that both ANS and BSA partition in the same phase i.e., in the Dex-rich droplet phase. Due to this partitioning, the Dex/protein ratio can be considered to be high which might affect the conformationally dynamics and stability of BSA. It has been suggested that the formation of hydrogen bonds between the hydroxyl groups of the Dex and the tryptophan residues located on the surface of BSA might lead to partial destabilisation of the protein and additional exposure of the hydrophobic residues to the surface of BSA [280]. This increase in solvent exposure might lead to a decrease of the fluorescence intensity as has been discussed above. The interaction of Dex with the binding sites might also lead to the occlusion of sites, which might be the reason for the lowering in binding constant. The strength of interaction between BSA and Dex depends on the orientation of the molecules, i.e., the accessibility of the binding sites to the surrounding Dex molecules.

A further interaction that could lead to two binding modes in the ATPS is the interaction between the more hydrophobic PEG and BSA. As has been mentioned in section 3.5.3, the presence of 3 wt% PEG in the 30 wt% Dex-rich phase makes a difference in the physico-chemical properties of the system, hence might be expected to alter the binding behaviour as well. The interaction of PEG with BSA has been studied extensively [64,164]. According to some reported results, the effect of PEG of M.W. 4.7 kDa, which is nearly similar to the one being used in this experiment (4.6 kDa), is quite significant [64]. The effect is generally brought in by the binding of PEG to the protein, which might lead to some PEG-induced conformational

change of the protein. The moderate chain length of PEG 4.6 kDa provides an added advantage for a better conformational adaptation of the PEG molecules onto the hydrophobic patches present on the BSA surface through van der Waals interactions [8]. This soft interaction might stimulate the occlusion of binding sites and thus, some binding sites of ANS might find it difficult to bind to BSA in the presence of PEG, depending on the surface hydrophobicity of the interaction site. In crowded media such as ATPS, the accessibility of the crowders and ANS to the hydrophobic patches situated on the surface of BSA may be unique in their own way and give rise to the different binding modes as observed here.

Effect of HHP on the binding behaviour

The effect of HHP on the binding of ANS to BSA in both buffer and the ATPS has been studied by means of high-pressure steady-state fluorescence spectroscopy.

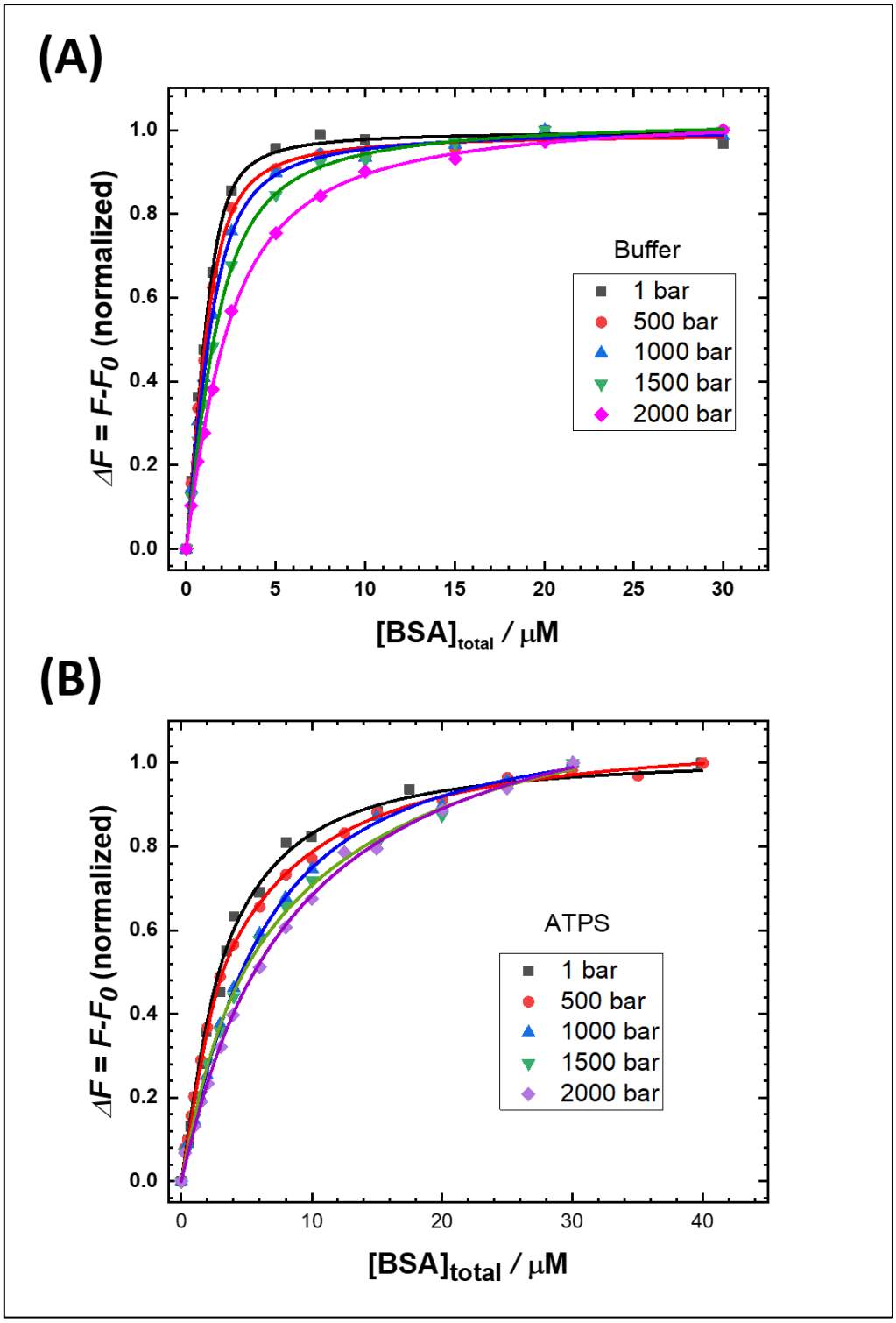

Figure 4.6. Binding isotherm plots of ANS to BSA in (A) neat buffer solution and (B) ATPS in the pressure range of 1-2000 bar. ΔF was calculated by fitting the raw data to Eq. 62.

In neat buffer, an increase in pressure leads to the decrease in binding constant, K_b. The value of K_b drops from $4.2*10^6$ M^{-1} at ambient pressure to $1.2*10^6$ M^{-1} at 2000 bar. The binding stoichiometry remains constant at n=3. The decrease in K_b indicates that the volume of the

complexed state is larger than the uncomplexed state which could be due to unfavourable pressure effects on the hydrophobic interaction and/or concomitant increase in void volume and/or changes in hydration upon binding. From the Fig. 4.6(A) and Table 2, it can be inferred that HHP does not favour ANS binding to BSA, i.e., the binding affinity decreases with pressure.

The same trend is followed in the ATPS, but the extent to which HHP affects the binding affinity alters from one binding site to another. Table 3 illustrates the effect of HHP on the two binding constants (K_1 and K_2). Both K_1 and K_2 decrease with increase in HHP but the effect is more pronounced in case of K_1. The value of K_1 decreases from $4.28*10^6$ M^{-1} at ambient pressure to $0.402*10^6$ M^{-1} at 2000 bar. The K_2-value, on the other hand, decreases from $0.420*10^6$ M^{-1} at ambient pressure to $0.0994*10^6$ M^{-1} at 2000 bar. The strong decrease in K_1 is due to a larger ΔV_b value, probably due to a larger void volume in the binding pocket. The n_2 binding site, due to its greater exposure to the solvent, might experience a smaller pressure effect as compared to n_1 due to the specific hydrophobic pockets in n_1. To see if BSA has an effect on the structure of the ATPS, turbidity measurements at HHP was carried out.

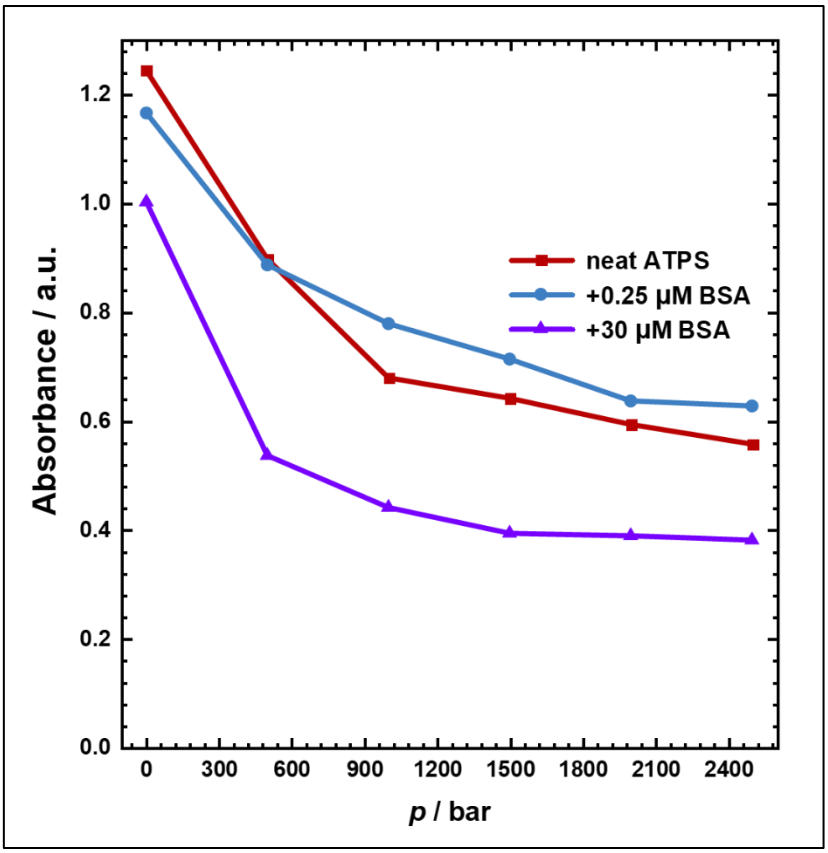

Figure 4.7. Changes in apparent absorbance (turbidity) with pressure of the ATPS at 25 °C (red line), 30 µM BSA dissolved in the ATPS (violet line) and 0.25 µM BSA dissolved in the ATPS (blue line). All the three systems are phase separated at 25 °C.

Fig. 4.7 shows that though there is a decrease in turbidity for the ATPS alone and the ATPS with varying concentrations of BSA with increase in pressure at room temperature, the effect is not very different. The decrease in turbidity might be due to changes in droplet size and an increasing tendency towards macroscopic phase separation upon pressurization. The decrease of the turbidity is more prominent in the system consisting of 30 μM BSA dissolved in ATPS as compared to the other two. This might be due to the excluded volume effect at the high BSA concentration which might fasten the process of complete phase separation and thus decrease in turbidity.

To check the stability of the neat ATPS and the ATPS containing BSA under pressure, phase contrast and fluorescence microscopy experiments were also carried out.

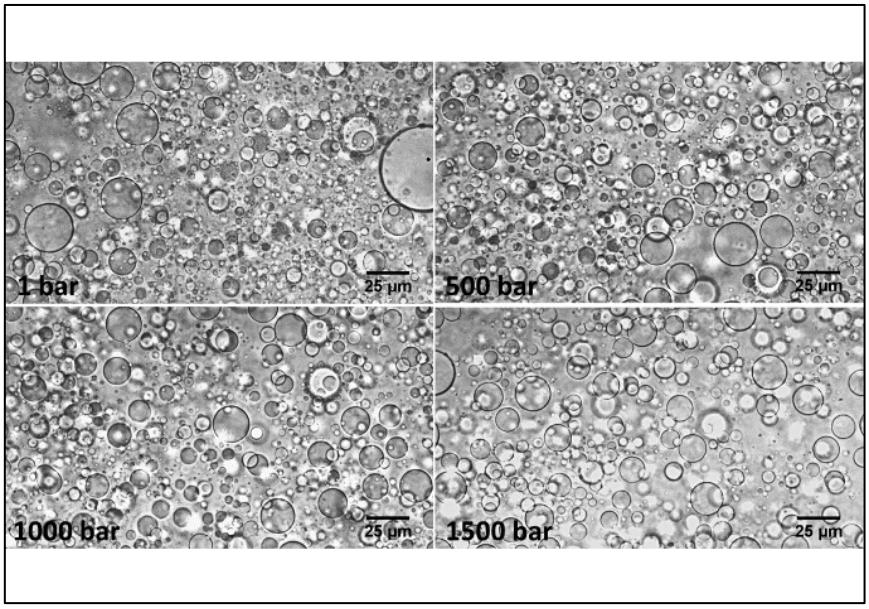

Figure 4.8. Phase contrast microscopy pictures of the ATPS at selected pressures. The experiments were performed at 25 °C. The size of the scale bar is 25 µm

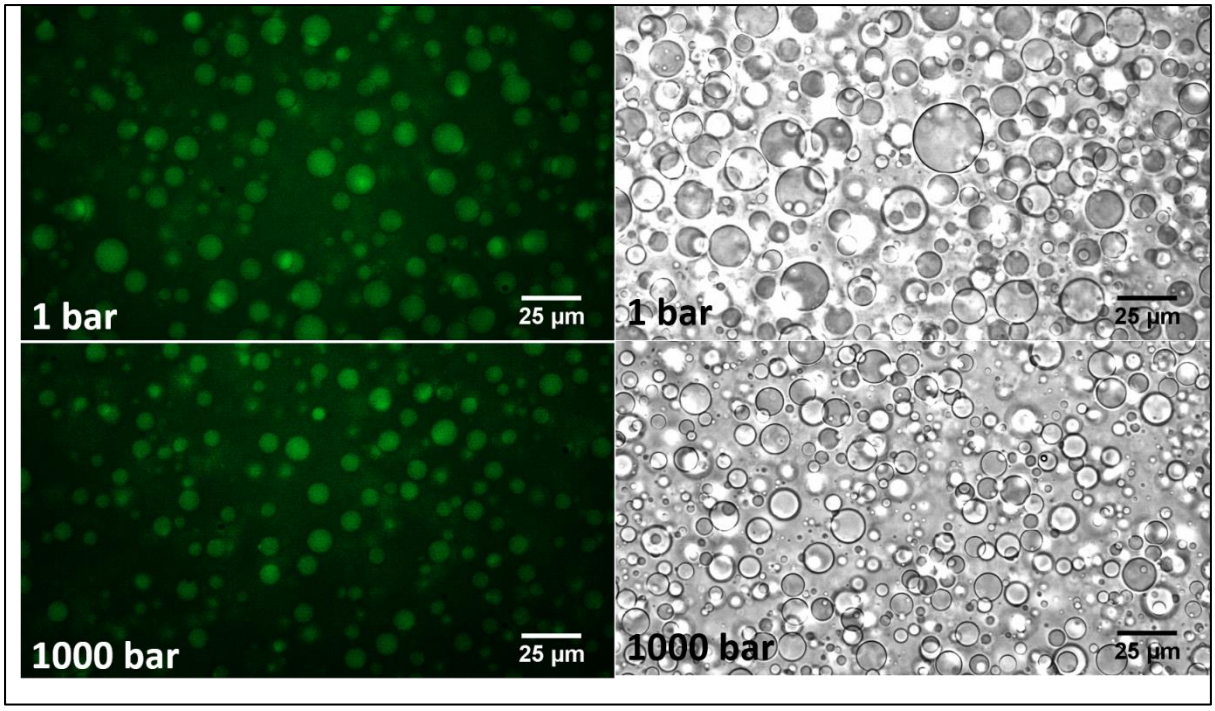

Figure 4.9. Phase contrast (right panels) and fluorescence (left panels) microscopy pictures of the FITC-labeled BSA in the ATPS (T = 25 °C, p = 1 bar). The size of the scale bar is 25 µm.

Fig. 4.8 and Fig. 4.9 clearly indicate that HHP has no marked effect on the stability of the ATPS and the ATPS with BSA at room temperature. The amount and the size of the droplets do not seem to change significantly in the whole pressure range covered. To get more insights into the pressure effect, a volumetric analysis of the results was carried out. According to Eq. 51, from the pressure dependence of the binding constant, the binding volume ΔV_b can be determined. ΔV_b is the difference in volume the between complexed and the uncomplexed state. Fig. 4.10 illustrates the pressure effect on ΔV_b in both neat buffer and the ATPS.

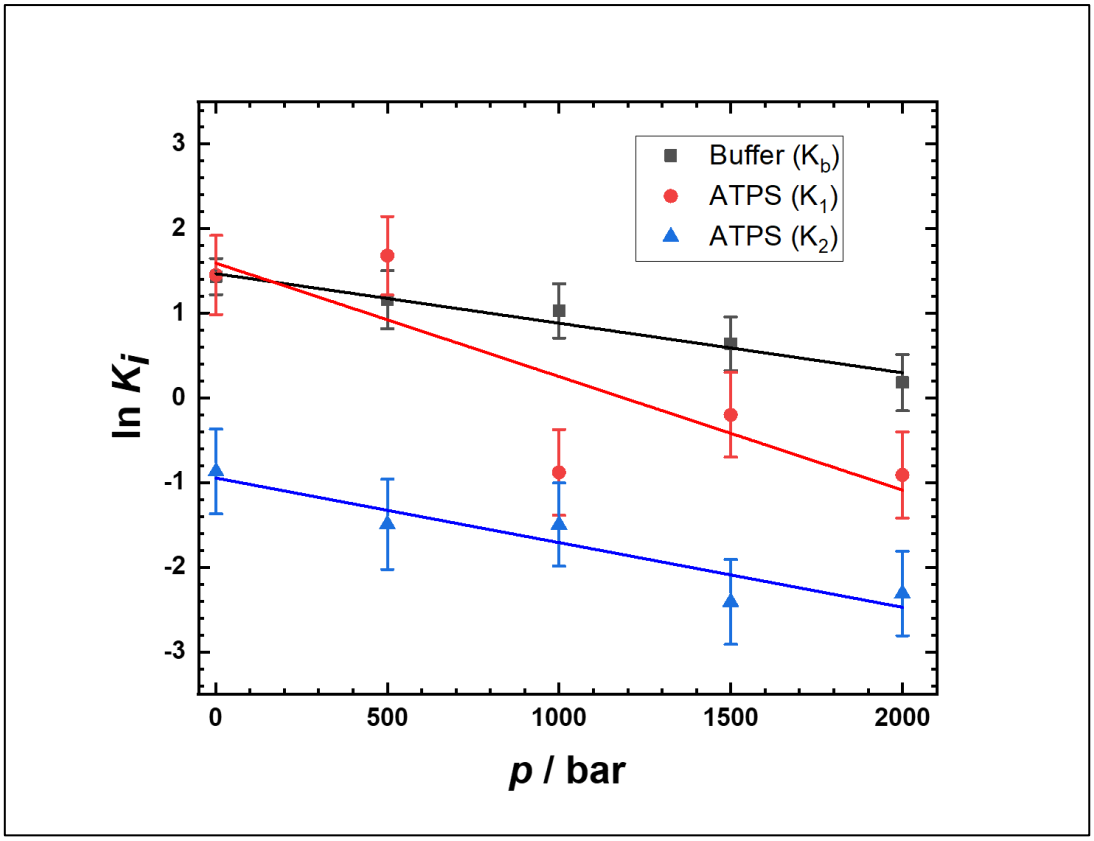

Figure 4.10. Schematic representation of $K_i(p)$ of ANS binding to BSA in buffer (black line) and the two different binding modes in the ATPS (red and blue line). The slope of the fitted lines represents $-\Delta V_b / RT$.

The positive ΔV_b value in all three cases might be due to two factors, a positive volume change upon loss of water molecules due to binding of ANS to BSA in the binding site, which is referred to as hydration volume, and / or a positive volume change upon formation of void volume at the binding sites upon ANS binding. For buffer, ΔV_b was estimated to be 14.5±1.5 mL mol^{-1}. In case of K_2 i.e., the one with a weaker binding affinity in the ATPS, if exclusively an electrostatic interaction would be considered, then with the increase in pressure the dissociation of ion pairs and contraction of solvent molecules around the ion pairs (electrostriction) would have been favoured at high pressure due to an overall volume decrease, but even in this case a positive ΔV_b of 18.9±4.1 mL mol^{-1} was found. Thus, it seems that similar to K_1 and K_b, the hydrophobic interaction is a dominating factor leading to the positive ΔV_b value observed. Else, different void volumes and / or hydration changes dominate over the different binding modes. The maximum positive change in ΔV_b was observed for K_1 which is equals to 33.2±12.5 mL mol^{-1}. Since the degree to which each of these forces (electrostatic, hydrophobic) affect the binding are not known, there is a possibility that the opposing effect of electrostatic and hydrophobic at high pressure might be the reason for a smaller increase in ΔV_b

in n_2 compared to that in n_1, but the differences observed might as well be related to differences in hydration and void volume of the different binding sites upon binding.

Jobs plot

The continuous variation method or Job plot is commonly employed for the determination of the stoichiometry of complex chemical entities [78,194]. To obtain a conclusive view on the stoichiometry of the bound complex formed between ANS and BSA, a Jobs plot was performed both in neat buffer and ATPS at ambient pressure.

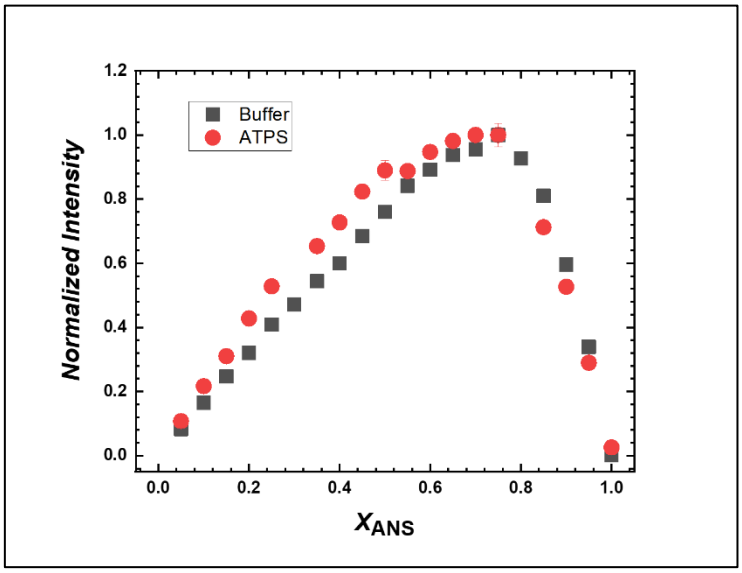

Figure 4.11. Jobs plot in buffer (black dots) and the ATPS (red dots).

The maxima in Fig. 4.11 appear at about x_{ANS} = 0.75 in both neat buffer and the ATPS indicating the binding stoichiometry to be 3, which matches well with the fluorescence data reported above. In case of the ATPS, a small inflection around x_{ANS} = 0.5 is observed. This additional inflection point might be related to changes in the equivalency of binding sites in the ATPS system which is densely packed with synthetic crowders [194].

4.4 Conclusions

From the steady-state fluorescence data and Jobs plot, it is evident that the total number of binding sites on the surface of BSA in both neat buffer and ATPS equals to 3. In neat buffer, the microscopic binding constants could not be distinguished by the fluorescence method employed and thus, it ends up giving an average of all 3 microscopic binding constants (K_b). On the contrary, in the ATPS, two different binding modes were perceived due to major

differences in the strength of interaction between BSA and ANS. The results suggested that two (n_1) of the three binding sites are present more towards the protein core with a pronounced hydrophobic microenvironment and hence, have a stronger binding affinity. The third one (n_2) is more exposed to the solvent and thus binding to this site may have an additional effect of electrostatic interaction along with the hydrophobic one. Hence, the binding affinity at this site might be governed by the fine balance between these two forces. At HHP, the general trend is a decrease in binding constants for both neat buffer solution and the ATPS due to positive values for the binding volume, ΔV_b, which is different for the two binding sites, however. While in buffer, a consistent decrease in K_b has been observed, in the ATPS the decrease in K_1 corresponding to n_1 is much more prominent than the decrease in K_2. The difference in ΔV_b values might be due to differences in hydration and void volume upon ligand binding. These results also demonstrate that pressure-dependent experiments are able to reveal differences in binding sites of ligands, owing to the extreme accuracy but which volume changes can be determined using this methodology. The ΔV_b values determined here are on the order of one water molecule only.

Bibliography

1. Zimmerman, S. B. & Trach, S. O. Estimation of macromolecule concentrations and excluded volume effects for the cytoplasm of Escherichia coli. *Journal of Molecular Biology* **222**, 599–620 (1991).

2. Wu, Y.-T., Lin, D.-Q. & Zhu, Z.-Q. Thermodynamics of aqueous two-phase systems—the effect of polymer molecular weight on liquid–liquid equilibrium phase diagrams by the modified NRTL model. *Fluid Phase Equilibria* **147**, 25–43 (1998).

3. Weber, G. Polarization of the Fluorescence of Macromolecules. *Biochem. J.* **51**, 145-155 (1952).

4. Wang, P., Yu, I., Feig, M. & Sugita, Y. Influence of protein crowder size on hydration structure and dynamics in macromolecular crowding. *Chemical Physics Letters* **671**, 63–70 (2017).

5. Togashi, D. M. & Ryder, A. G. Assessing protein–surface interactions with a series of multi-labeled BSA using fluorescence lifetime microscopy and Förster Energy Resonance Transfer. *Biophysical Chemistry* **152**, 55–64 (2010).

6. Teresa Cunha, M., Cabral, J. M. S., Tjerneld, F. & Raquel Aires-Barros, M. Effect of salts and surfactants on the partitioning of Fusarium solani pisi cutinase in aqueous two-phase systems of thermoseparating ethylene oxide/propylene oxide random copolymer and hydroxypropyl starch. *Bioseparation* **9**, 203–209 (2000).

7. Strulson, C. A., Molden, R. C., Keating, C. D. & Bevilacqua, P. C. RNA catalysis through compartmentalization. *Nat. Chem.* **4**, 941–946 (2012).

8. Steinbrecher, T. & Labahn, A. Towards accurate free energy calculations in ligand protein-binding studies. *Curr. Med. Chem.* **17**, 767–785 (2010).

9. Slavík, J. Anilinonaphthalene sulfonate as a probe of membrane composition and function. *Biochem. Biophys. Acta* **694**, 1–25 (1982).

10. Schnell, S. & Turner, T. E. Reaction kinetics in intracellular environments with macromolecular crowding: simulations and rate laws. *Progress in Biophysics and Molecular Biology* **85**, 235–260 (2004).

11. Salamanca, M. H., Merchuk, J. C., Andrews, B. A. & Asenjo, J. A. On the kinetics of phase separation in aqueous two-phase systems. *Journal of Chromatography B: Biomedical Sciences and Applications* **711**, 319–329 (1998).

12. Ruiz-Ruiz, F., Benavides, J., Aguilar, O. & Rito-Palomares, M. Aqueous two-phase affinity partitioning systems: current applications and trends. *Journal of Chromatography A* **1244**, 1–13 (2012).

13. Robb, F. T. & Clark, D. S. Adaptation of proteins from hyperthermophiles to high pressure and high temperature. *J. Mol. Microbiol. Biotechnol.* **1**, 101–105 (1999).

14. Raja, S., Murty, V. R., Thivaharan, V., Rajasekar, V. & Ramesh, V. Aqueous Two Phase Systems for the Recovery of Biomolecules – A Review. *SCIT* **1**, 7–16 (2012).

15. Pastor, I. *et al.* Effect of crowding by Dextrans in enzymatic reactions. *Biophysical Chemistry* **185**, 8–13 (2014).

16. Ozbabacan, S. E. A., Gursoy, A., Keskin, O. & Nussinov, R. Conformational ensembles, signal transduction and residue hot spots: Application to drug discovery. *Current opinion in drug discovery & development* **13**, 527-537 (2010).

17. Minton, A. P. Implications of macromolecular crowding for protein assembly. *Current Opinion in Structural Biology* **10**, 34–39 (2000).

18. Messens, W., Van Camp, J. & Huyghebaert, A. The use of high pressure to modify the functionality of food proteins. *Trends in Food Science & Technology* **8**, 107–112 (1997).

19. Merchuk, J. C., Andrews, B. A. & Asenjo, J. A. Aqueous two-phase systems for protein separation Studies on phase inversion. *Journal of Chromatography B: Biomedical Sciences and Applications* **711**, 285-293 (1998).

20. Kunugi, S., Fujiwara, S., Kidokoro, S., Endo, K. & Hanzawa, S. Single-point amino acid substitutions at the 119th residue of thermolysin and their pressure-induced activation. *FEBS Letters* **462**, 231–235 (1999).

21. Knight, C. G. Fluorimetric assays of proteolytic enzymes. *Meth. Enzymol.* **248**, 18–34 (1995).

22. Kelly, S. M., Jess, T. J. & Price, N. C. How to study proteins by circular dichroism. *Biochimica et Biophysica Acta (BBA) - Proteins and Proteomics* **1751**, 119–139 (2005).

23. Kaul, A. The Phase Diagram. *Aqueous Two-Phase Systems: Methods and Protocols: Methods and Protocols*. 11–21 (2000).

24. Johansson, H.-O., Persson, J. & Tjerneld, F. Thermoseparating water/polymer system: A novel one-polymer aqueous two-phase system for protein purification. *BIOTECHNOLOGY AND BIOENGINEERING* **66**, 247-257 (1999).

25. Johansson, G. Effects of salts on the partition of proteins in aqueous polymeric biphasic systems. *Acta Chem. Scand., B, Org. Chem. Biochem.* **28**, 873–882 (1974).

26. Jasińska, A., Ferguson, A., Mohamed, W. S. & Szreder, T. The study of interactions between ibuprofen and bovine serum albumin. *Food Chem. Biotechnol.* **73** (2009).

27. Janin, J. Protein-protein recognition. *Progress in Biophysics and Molecular Biology* **64**, 145–166 (1995).

28. Jaenicke, R. Enzymes Under Extremes of Physical Conditions. *Annu. Rev. Biophys. Bioeng.* **10**, 1–67 (1981).

29. Heremans, L. & Heremans, K. Pressure effects on the Raman spectrum of proteins: stability of the salt bridge in trypsin and elastase. *Journal of Molecular Structure* **214**, 305–314 (1989).

30. Heremans, L. & Heremans, K. Raman spectroscopic study of the changes in secondary structure of chymotrypsin: effect of pH and pressure on the salt bridge. *Biochimica et Biophysica Acta (BBA) - Protein Structure and Molecular Enzymology* **999**, 192–197 (1989).

31. Hazra, P., Chakrabarty, D., Chakraborty, A. & Sarkar, N. Probing protein-surfactant interaction by steady state and time-resolved fluorescence spectroscopy. *Biochemical and Biophysical Research Communications* **314**, 543–549 (2004).

32. Hachem, F., Andrews, B. A. & Asenjo, J. A. Hydrophobic partitioning of proteins in aqueous two-phase systems. *Enzyme and Microbial Technology* **19**, 507–517 (1996).

33. Gunduz, U. Evaluation of viscosities of aqueous two-phase systems containing protein. *Journal of Chromatography B* **807**, 157–161 (2004).

34. Gao, M. & Winter, R. Kinetic Insights into the Elongation Reaction of Actin Filaments as a Function of Temperature, Pressure, and Macromolecular Crowding. *Chemphyschem* **16**, 3681–3686 (2015).

35. Forciniti, D., Hall, C. K. & Kula, M. R. Interfacial tension of polyethyleneglycol-dextran-water systems: influence of temperature and polymer molecular weight. *Journal of Biotechnology* **16**, 279–296 (1990).

36. Flory, P. J. Statistical Mechanics of Swelling of Network Structures. *The Journal of Chemical Physics* **18**, 108–111 (1950).

37. Dubin, P., Bock, J., Davis, R., Schulz, D. N. & Thies, C. *Macromolecular Complexes in Chemistry and Biology*, (2012).

38. Dix, J. A. & Verkman, A. S. Crowding Effects on Diffusion in Solutions and Cells. *Annu. Rev. Biophys.* **37**, 247–263 (2008).

39. Demchenko, A. P. Recognition between flexible protein molecules: induced and assisted folding. *J. Mol. Recognit.* **14**, 42-61 (2001).

40. Dai, J., Zhang, Y. & Xiu, Z. Salting-out Extraction of 2,3-Butanediol from Jerusalem artichoke-based Fermentation Broth. *Chinese Journal of Chemical Engineering* **19**, 682–686 (2011).

41. Carlsson, M., Linse, P. & Tjerneld, F. Temperature-dependent protein partitioning in two-phase aqueous polymer systems. *Macromolecules* **26**, 1546–1554 (1993).

42. Brooks, D. E., Sharp, K. A. & Fisher, D. Theoretical Aspects of Partitioning. in *Partitioning in Aqueous Two-Phase System* 11–84 (1985).

43. Aumiller, W. M. & Keating, C. D. Experimental models for dynamic compartmentalization of biomolecules in liquid organelles: Reversible formation and partitioning in aqueous biphasic systems. *Adv Colloid Interface Sci* **239**, 75–87 (2017).

44. Asenjo, J. A. & Andrews, B. A. Aqueous two-phase systems for protein separation: Phase separation and applications. *Journal of Chromatography A* **1238**, 1–10 (2012).

45. Albertsson, P. Å. Fractionation of particles and macromolecules in aqueous two-phase systems. *Biochemical Pharmacology* **5**, 351–358 (1961).

46. Alberti, S. The wisdom of crowds: regulating cell function through condensed states of living matter. *J. Cell Sci.* **130**, 2789–2796 (2017).

47. Abbott, N. L., Blankschtein, D. & Hatton, T. A. On protein partitioning in two-phase aqueous polymer systems. *Bioseparation* **1**, 191–225 (1990).

48. Grilo, A. L., Aires-Barros, M. R. & Azevedo, A. M. Partitioning in Aqueous Two-Phase Systems: Fundamentals, Applications and Trends. *Separation & Purification Reviews* **45**, 68–80 (2016).

49. 'KinetAsyst' Stopped-Flow Systems. *TgK Scientific Stopped-Flow Solutions*

50. Hermans, J & Lentz, B. Thermodynamics of Molecular Interactions. *Equilibria and Kinetics of Biological Macromolecules*, 185–196 (2013).

51. Lakowicz, J. R. Basic Principles of Fluorescence Spectroscopy. *Handbook of Fluorescence Spectroscopy and Imaging*, 1–30 (2011).

52. Kaul, H. *Aqueous Two-Phase Systems: Methods and Protocols*, (2000).

53. Zimmerman, S. B. & Minton, A. P. Macromolecular Crowding: Biochemical, Biophysical, and Physiological Consequences. *Annu. Rev. Biophy. Biomol. Struc.* **22**, 27-64 (1993).

54. Zimmerman, M., Ashe, B., Yurewicz, E. C. & Patel, G. Sensitive assays for trypsin, elastase, and chymotrypsin using new fluorogenic substrates. *Analytical Biochemistry* **78**, 47–51 (1977).

55. Zijlstra, G. M., Michielsen, M. J. F., de Gooijer, C. D., van der Pol, L. A. & Tramper, J. Hybridoma and CHO Cell Partitioning in Aqueous Two-Phase Systems. *Biotechnol. Prog.* **12**, 363–370 (1996).

56. Zhu, J.-H., Wei, D.-Z., Cao, X.-J., Liu, Y.-Q. & Yuan, Z.-Y. Partitioning behaviour of cephalexin and 7-aminodeacetoxicephalosporanic acid in PEG/ammonium sulfate aqueous two-phase systems. *Journal of Chemical Technology & Biotechnology* **76**, 1194–1200 (2001).

57. Zhou, H.-X., Rivas, G. & Minton, A. P. Macromolecular Crowding and Confinement: Biochemical, Biophysical, and Potential Physiological Consequences. *Annual Review of Biophysics* **37**, 375–397 (2008).

58. Zhou, H. X. & Szabo, A. Theory and simulation of the time-dependent rate coefficients of diffusion-influenced reactions. *Biophysical Journal* **71**, 2440–2457 (1996).

59. Zaslavsky, Ferreira & Uversky. Driving Forces of Liquid–Liquid Phase Separation in Biological Systems. *Biomolecules* **9**, 1-5 (2019).

60. Zafarani-Moattar, M. T., Hamzehzadeh, S. & Nasiri, S. A new aqueous biphasic system containing polypropylene glycol and a water-miscible ionic liquid. *Biotechnol. Progress* **28**, 146–156 (2012).

61. Yang, L., Dordick, J. S. & Garde, S. Hydration of Enzyme in Nonaqueous Media Is Consistent with Solvent Dependence of Its Activity. *Biophysical Journal* **87**, 812–821 (2004).

62. Xiao, J.-X., Sivars, U. & Tjerneld, F. Phase behavior and protein partitioning in aqueous two-phase systems of cationic–anionic surfactant mixtures. *Journal of Chromatography B: Biomedical Sciences and Applications* **743**, 327–338 (2000).

63. Wu, J., Yang, J. T. & Wu, C.-S. C. β-II conformation of all-β proteins can be distinguished from unordered form by circular dichroism. *Analytical Biochemistry* **200**, 359–364 (1992).

64. Wu, J. *et al.* Binding characteristics between polyethylene glycol (PEG) and proteins in aqueous solution. *J. Mater. Chem. B* **2**, 2983–2992 (2014).

65. Wohlgemuth, R. Biocatalysis—key to sustainable industrial chemistry. *Current Opinion in Biotechnology* **21**, 713–724 (2010).

66. Winter, R. Interrogating the Structural Dynamics and Energetics of Biomolecular Systems with Pressure Modulation. *Annu. Rev. Biophys.* **48**, 441–463 (2019).

67. Williams, M. A., Goodfellow, J. M. & Thornton, J. M. Buried waters and internal cavities in monomeric proteins. *Protein Sci.* **3**, 1224–1235 (1994).

68. Wangler, A. *et al.* Co-solvent effects on reaction rate and reaction equilibrium of an enzymatic peptide hydrolysis. *Phys. Chem. Chem. Phys.* **20**, 11317–11326 (2018).

69. Vöpel, T. & Makhatadze, G. I. Enzyme Activity in the Crowded Milieu. *PLoS ONE* **7**, 3-8 (2012).

70. Voloshin, V. P., Medvedev, N. N., Smolin, N., Geiger, A. & Winter, R. Disentangling Volumetric and Hydrational Properties of Proteins. *J. Phys. Chem. B* **119**, 1881–1890 (2015).

71. Verma, P. K., Rakshit, S., Mitra, R. K. & Pal, S. K. Role of hydration on the functionality of a proteolytic enzyme α-chymotrypsin under crowded environment. *Biochimie.* **93**, 1424–1433 (2011).

72. Vázquez-Villegas, P. *et al.* Factorial and Economic Evaluation of an Aqueous Two-Phase Partitioning Pilot Plant for Invertase Recovery From Spent Brewery Yeast. *Front. Chem.* **6**, 454 (2018).

73. Varela, A. S., Macho, M. I. S. & Miñones, J. Spectrofluorimetric Study of the Binding of 1-Anilinonaphthalene-8-Sulfonate to Bovine Serum Albumin. *Journal of Pharmaceutical Sciences* **81**, 842–844 (1992).

74. Vanlint, D. *et al.* Rapid Acquisition of Gigapascal-High-Pressure Resistance by Escherichia coli. *mBio.* **2**, e00130-10 (2011).

75. van den Berg, B. Effects of macromolecular crowding on protein folding and aggregation. *The EMBO Journal* **18**, 6927–6933 (1999).

76. Van Berlo, M., Luyben, K. Ch. A. M. & van der Wielen, L. A. M. Poly(ethylene glycol)–salt aqueous two-phase systems with easily recyclable volatile salts. *Journal of Chromatography B: Biomedical Sciences and Applications* **711**, 61–68 (1998).

77. Urry, D. W. Absorption, circular dichroism and optical rotatory dispersion of polypeptides, proteins, prosthetic groups and biomembranes. *New Comprehensive Biochemistry* **11**, 275–346 (1985).

78. Ulatowski, F., Dąbrowa, K., Bałakier, T. & Jurczak, J. Recognizing the Limited Applicability of Job Plots in Studying Host–Guest Interactions in Supramolecular Chemistry. *J. Org. Chem.* **81**, 1746–1756 (2016).

79. Towell, J. F. & Manning, M. C. Analysis of protein structure by circular dichroism spectroscopy. *Techniques and Instrumentation in Analytical Chemistry* **14**, 175–205 (1994).

80. Tokuriki, N. Protein folding by the effects of macromolecular crowding. *Protein Science* **13**, 125–133 (2004).

81. Togashi, D. M.; Ryder, A. G. A Fluorescence Analysis of ANS Bound to Bovine Serum Albumin: Binding Properties Revisited by Using Energy Transfer. *J. Fluoresc.* **18**, 519–526 (2008).

82. Tanaka, N., Mitani, D. & Kunugi, S. Pressure-Induced Perturbation on the Active Site of β-Amylase Monitored from the Sulfhydryl Reaction. *Biochemistry* **40**, 5914–5920 (2001).

83. Tanaka, N. *et al.* Pressure Effect on the Conformational Fluctuation of Apomyoglobin in the Native State. *Biochemistry* **39**, 12063–12068 (2000).

84. Takehara, K., Yuki, K., Shirasawa, M., Yamasaki, S. & Yamada, S. Binding Properties of Hydrophobic Molecules to Human Serum Albumin Studied by Fluorescence Titration. *Anal. Sci.* **25**, 115–120 (2009).

85. Takahashi, S. & Sugimoto, N. Effect of Pressure on the Stability of G-Quadruplex DNA: Thermodynamics under Crowding Conditions. *Angew. Chem. Int. Ed.* **52**, 13774–13778 (2013).

86. Sukenik, S., Sapir, L., Gilman-Politi, R. & Harries, D. Diversity in the mechanisms of cosolute action on biomolecular processes. *Faraday Discuss.* **160**, 225–237 (2013).

87. Sudlow, G., Birkett, D. J. & Wade, D. N. The Characterization of Two Specific Drug Binding Sites on Human Serum Albumin. *Mol. Pharmacol.* **11**, 824–832 (1975).

88. Strogatz, S. H. Exploring complex networks. *Nature* **410**, 268–276 (2001).

89. Somero, G. N. Adaptations to High Hydrostatic Pressure. *Annu. Rev. Physiol.* **54**, 557–577 (1992).

90. Silva, M. E. & Franco, T. T. Liquid-liquid extraction of biomolecules in downstream processing - A review paper. *Braz. J. Chem. Eng.* **17**, 1–17 (2000).

91. Silva, J. L. *et al.* High-Pressure Chemical Biology and Biotechnology. *Chem. Rev.* **114**, 7239–7267 (2014).

92. Silva, J. L. & Weber, G. Pressure Stability of Proteins. *Annu. Rev. Phys. Chem.* **44**, 89–113 (1993).

93. Shoup, D. & Szabo, A. Role of diffusion in ligand binding to macromolecules and cell-bound receptors. *Biophysical Journal* **40**, 33–39 (1982).

94. Sharp, K. A. Analysis of the size dependence of macromolecular crowding shows that smaller is better. *Proc. Natl. Acad. Sci. U. S. A.* **112**, 7990–7995 (2015).

95. Sharma, R. & Bahadur, P. Effect of different additives on the cloud point of a polyethylene oxide-polypropylene oxide-polyethylene oxide block copolymer in aqueous solution. *J. Surfact. Deterg.* **5**, 263–268 (2002).

96. Senske, M. *et al.* Protein Stabilization by Macromolecular Crowding through Enthalpy Rather Than Entropy. *J. Am. Chem. Soc.* **136**, 9036–9041 (2014).

97. Sen, D. & Mandal, D. K. Pea lectin unfolding reveals a unique molten globule fragment chain. *Biochimie.* **93**, 409–417 (2011).

98. Semisotnov, G. V. *et al.* Study of the molten globule intermediate state in protein folding by a hydrophobic fluorescent probe. *Biopolymers* **31**, 119–128 (1991).

99. Seeliger, J., Werkmüller, A. & Winter, R. Macromolecular Crowding as a Suppressor of Human IAPP Fibril Formation and Cytotoxicity. *PLoS ONE* **8**, 26-32 (2013).

100. Schmidt, A. S., Andrews, B. A. & Asenjot, J. A. Correlations for the partition behavior of proteins in aqueous two-phase systems: Effect of overall protein concentration. *Biotechnol. Bioeng.* **50**, 617-626 (1996).

101. Schmid, F.-X. Biological Macromolecules: UV-visible Spectrophotometry. *eLS* 0003142 (2001).

102. Schellman, J. A. Protein Stability in Mixed Solvents: A Balance of Contact Interaction and Excluded Volume. *Biophysical Journal* **85**, 108–125 (2003).

103. Sarkar, M., Lu, J. & Pielak, G. J. Protein Crowder Charge and Protein Stability. *Biochemistry* **53**, 1601–1606 (2014).

104. Sapir, L. & Harries, D. Is the depletion force entropic? Molecular crowding beyond steric interactions. *Current Opinion in Colloid & Interface Science* **20**, 3–10 (2015).

105. Salabat, A. The influence of salts on the phase composition in aqueous two-phase systems: experiments and predictions. *Fluid Phase Equilibria* **187–188**, 489–498 (2001).

106. Saad-Nehme, J., Silva, J. L. & Meyer-Fernandes, J. R. Osmolytes protect mitochondrial F0F1-ATPase complex against pressure inactivation. *Biochimica et Biophysica Acta (BBA) - Protein Structure and Molecular Enzymology* **1546**, 164–170 (2001).

107. Rodgers, K. K. & Sligarj, S. G. Mapping Electrostatic Interactions in Macromolecular Associations. *J. Mol. Biol.* **221**, 1453–1460 (1991).

108. Roche, J. *et al.* Cavities determine the pressure unfolding of proteins. *Proc. Natl. Acad. Sci. U. S. A.* **109**, 6945–6950 (2012).

109. Robinson, C. R. & Sligar, S. G. Hydrostatic and osmotic pressure as tools to study macromolecular recognition. in *Methods in Enzymology* **259**, 395–427 (1995).

110. Rivas, G. & Minton, A. P. Macromolecular Crowding In Vitro, In Vivo, and In Between. *Trends in Biochemical Sciences* **41**, 970–981 (2016).

111. Rivas, G., Ferrone, F. & Herzfeld, J. Life in a crowded world. *EMBO Rep.* **5**, 23–27 (2004).

112. Rivalain, N., Roquain, J. & Demazeau, G. Development of high hydrostatic pressure in biosciences: Pressure effect on biological structures and potential applications in Biotechnologies. *Biotechnology Advances* **28**, 659–672 (2010).

113. Reddy, P. M., Venkatesu, P. & Bohidar, H. B. Influence of Polymer Molecular Weight and Concentration on Coexistence Curve of Isobutyric Acid + Water. *J. Phys. Chem. B* **115**, 12065–12075 (2011).

114. Ralston, G. B. Effects of 'crowding' in protein solutions. *J. Chem. Educ.* **67**, 857 (1990).

115. Povarova, O. I., Kuznetsova, I. M. & Turoverov, K. K. Differences in the Pathways of Proteins Unfolding Induced by Urea and Guanidine Hydrochloride: Molten Globule State and Aggregates. *PLoS ONE* **5**, 1-4 (2010).

116. Politi, R. & Harries, D. Enthalpically driven peptide stabilization by protective osmolytes. *Chem. Commun.* **46**, 6449-6451 (2010).

117. Petitpas, I., Grüne, T., Bhattacharya, A. A. & Curry, S. Crystal structures of human serum albumin complexed with monounsaturated and polyunsaturated fatty acids. *Journal of Molecular Biology* **314**, 955–960 (2001).

118. Perozzo, R., Folkers, G. & Scapozza, L. Thermodynamics of Protein–Ligand Interactions: History, Presence, and Future Aspects. *Journal of Receptors and Signal Transduction* **24**, 1–52 (2004).

119. Perez, B., Malpiedi, L. P., Tubío, G., Nerli, B. & de Alcântara Pessôa Filho, P. Experimental determination and thermodynamic modeling of phase equilibrium and protein partitioning in aqueous two-phase systems containing biodegradable salts. *The Journal of Chemical Thermodynamics* **56**, 136–143 (2013).

120. Patra, S. *et al.* Exploring the effects of cosolutes and crowding on the volumetric and kinetic profile of the conformational dynamics of a poly dA loop DNA hairpin: a single-molecule FRET study. *Nucleic Acids Research* **47**, 981–996 (2019).

121. Oster, Gerald. The Scattering of Light and its Applications to Chemistry. *Chem. Rev.* **43**, 319–365 (1948).

122. Oliveranappa, A., Lagomarsino, G., Andrews, B. & Asenjo, J. Effect of electrostatic energy on partitioning of proteins in aqueous two-phase systems. *Journal of Chromatography B* **807**, 81–86 (2004).

123. Oliveira, A. C., Gaspar, L. P., Da Poian, A. T. & Silva, J. L. Arc Repressor will not Denature Under Pressure in the Absence of Water. *Journal of Molecular Biology* **240**, 184–187 (1994).

124. Ohmae, E., Murakami, C., Gekko, K. & Kato, C. *Review Pressure Effects on Enzyme Functions* **7**, 19-23 (2007).

125. Ockenga, W. Phase Contrast- **making unstained phase objects visible. Univ. Philipps (2011).**

126. Northrop, D. B. Effects of high pressure on enzymatic activity. *Biochimica et Biophysica Acta- Protein Struct. Mol. Enzymol.* **1595**, 71–79 (2002).

127. Ni, Y., Zhu, R. & Kokot, S. Competitive binding of small molecules with biopolymers: a fluorescence spectroscopy and chemometrics study of the interaction of aspirin and ibuprofen with BSA. *Analyst* **136**, 4794-4801 (2011).

128. Nakano, S., Miyoshi, D. & Sugimoto, N. Effects of Molecular Crowding on the Structures, Interactions, and Functions of Nucleic Acids. *Chem. Rev.* **114**, 2733–2758 (2014).

129. Mozhaev, V. V., Heremans, K., Frank, J., Masson, P. & Balny, C. High pressure effects on protein structure and function. *Proteins: Structure, Function, and Bioinformatics* **24**, 81–91 (1996).

130. Mozhaev, V. V., Heremans, K., Frank, J., Masson, P. & Balny, C. Exploiting the effects of high hydrostatic pressure in biotechnological applications. *Trends in Biotechnology* **12**, 493–501 (1994).

131. Mozhaev, V. V., Lange, R., Kudryashova, E. V. & Balny', C. Application of high hydrostatic pressure for increasing activity and stability of enzymes. *BIOTECHNOLOGY AND BIOENGINEERING* **52**, 320-331 (1996).

132. Morild, E. The Theory of Pressure Effects on Enzymes. *Advances in Protein Chemistry* **34**, 93–166 (1981).

133. Mombelli, E. *et al.* The Role of Phenylalanine 31 in Maintaining the Conformational Stability of Ribonuclease P2 from Sulfolobus solfataricus under Extreme Conditions of Temperature and Pressure. *Biochemistry* **36**, 8733–8742 (1997).

134. Molino, J. V. D., Viana Marques, D. de A., Júnior, A. P., Mazzola, P. G. & Gatti, M. S. V. Different types of aqueous two-phase systems for biomolecule and bioparticle extraction and purification. *Biotechnol. Progress* **29**, 1343–1353 (2013).

135. Mohana-Borges, R., Lima Silva, J. & de Prat-Gay, G. Protein Folding in the Absence of Chemical Denaturants: Reversible Pressure Denaturation of the Noncovalent Complex Formed by the Association of Two Protein Fragments. *J. Biol. Chem.* **274**, 7732–7740 (1999).

136. Mittal, S., Chowhan, R. K. & Singh, L. R. Macromolecular crowding: Macromolecules friend or foe. *Biochimica et Biophysica Acta (BBA) - General Subjects* **1850**, 1822–1831 (2015).

137. Minton, A. P. Quantitative assessment of the relative contributions of steric repulsion and chemical interactions to macromolecular crowding. *Biopolymers* **99**, 239–244 (2013).

138. Minton, A. P. Macromolecular crowding. *Current Biology* **16**, 269–271 (2006).

139. Minton, A. P. Models for Excluded Volume Interaction between an Unfolded Protein and Rigid Macromolecular Cosolutes: Macromolecular Crowding and Protein Stability Revisited. *Biophysical Journal* **88**, 971–985 (2005).

140. Minton, A. P. The Influence of Macromolecular Crowding and Macromolecular Confinement on Biochemical Reactions in Physiological Media. *J. Biol. Chem.* **276**, 10577–10580 (2001).

141. Minton, A. P. Molecular crowding: Analysis of effects of high concentrations of inert cosolutes on biochemical equilibria and rates in terms of volume exclusion. *Methods in Enzymology* **295**, 127–149 (1998).

142. Minton, A. P. Macromolecular crowding and molecular recognition. *J. Mol. Recognit.* **6**, 211–214 (1993).

143. Minton, A. P. Excluded volume as a determinant of macromolecular structure and reactivity. *Biopolymers* **20**, 2093–2120 (1981).

144. Minton, A. P. Excluded volume as a determinant of protein structure and stability. *Biophysical Journal* **32**, 77–79 (1980).

145. Minton, A. P. Influence of excluded volume upon macromolecular and associations in ‘crowded’ media. *Curr. Opin. Biotechnol.* **8**, 65–69 (1997).

146. Minton, A. P. How can biochemical reactions within cells differ from those in test tubes? *Journal of Cell Science* **119**, 2863-2869 (2006).

147. Minton, A. P. Protein folding: Thickening the broth. *Current Biology* **10**, R97–R99 (2000).

148. Meurer, F., Do, H. T., Sadowski, G. & Held, C. Standard Gibbs energy of metabolic reactions: II. Glucose-6-phosphatase reaction and ATP hydrolysis. *Biophysical Chemistry* **223**, 30–38 (2017).

149. Meurer, F., Bobrownik, M., Sadowski, G. & Held, C. Standard Gibbs Energy of Metabolic Reactions: I. Hexokinase Reaction. *Biochemistry* **55**, 5665–5674 (2016).

150. Mei, L.-H., Lin, D.-Q. & Zhu, Z.-Q. Densities and Viscosities of Polyethylene Glycol + Salt + Water Systems at 20 °C. *J. Chem. Eng. Data* **40**, 1168–1171 (1995).

151. McGuffee, S. R. & Elcock, A. H. Diffusion, Crowding & Protein Stability in a Dynamic Molecular Model of the Bacterial Cytoplasm. *PLOS Computational Biology* **6**, e1000694 (2010).

152. Mazzola, P. G. *et al.* Liquid–liquid extraction of biomolecules: an overview and update of the main techniques. *Journal of Chemical Technology & Biotechnology* **83**, 143–157 (2008).

153. Matulis, D. & Lovrien, R. 1-Anilino-8-Naphthalene Sulfonate Anion-Protein Binding Depends Primarily on Ion Pair Formation. *Biophysical Journal* **74**, 422–429 (1998).

154. Masson, P. Hydration change during the aging of phosphorylated human butyrylcholinesterase : importance of residues aspartate-70 and glutamate-197 in the water network as probed by hydrostatic and osmotic pressures. *Biochem. J.* **343**, 361–369 (1999).

155. Marty, A., Boiret, M. & Deumie, M. How to illustrate ligand-protein binding in a class experiment: An elementary fluorescent assay. *J. Chem. Educ.* **63**, 365-366 (1986).

156. Manavalan, P. & Johnson, W. C. Sensitivity of circular dichroism to protein tertiary structure class. *Nature* **305**, 831–832 (1983).

157. Ma, B. & Nussinov, R. Structured Crowding and Its Effects on Enzyme Catalysis. *Dynamics in Enzyme Catalysis* **337**, 123–137 (2013).

158. Luong, T. Q. & Winter, R. Combined pressure and cosolvent effects on enzyme activity – a high-pressure stopped-flow kinetic study on α-chymotrypsin. *Phys. Chem. Chem. Phys.* **17**, 23273–23278 (2015).

159. Luong, T. Q., Kapoor, S. & Winter, R. Pressure-A Gateway to Fundamental Insights into Protein Solvation, Dynamics, and Function. *ChemPhysChem* **16**, 3555–3571 (2015).

160. Luong, T. Q. *et al.* Hydrostatic Pressure Increases the Catalytic Activity of Amyloid Fibril Enzymes. *Angew. Chem. Int. Ed.* **55**, 12412–12416 (2016).

161. Luby-Phelps, K., Castle, P. E., Taylor, D. L. & Lanni, F. Hindered diffusion of inert tracer particles in the cytoplasm of mouse 3T3 cells. *Proc. Natl. Acad. Sci. U.S.A.* **84**, 4910–4913 (1987).

162. Liu, C., Kamei, D. T., King, J. A., Wang, D. I. C. & Blankschtein, D. Separation of proteins and viruses using two-phase aqueous micellar systems. *Journal of Chromatography B: Biomedical Sciences and Applications* **711**, 127–138 (1998).

163. Levin, A. Anwendung von Druck zur Untersuchung der Wechselwirkungen zwischen Proteinen und Polyelektrolytgrenzflächen sowie Modellbiomembranen. (2019)

164. Lai, J., Yan, H., Liu, Y. & Huang, Y. Effects of PEG molecular weight on its interaction with albumin. *Chin. J. Polym. Sc.i* **33**, 1373–1379 (2015).

165. Ladokhin, A. S., Jayasinghe, S. & White, S. H. How to Measure and Analyze Tryptophan Fluorescence in Membranes Properly, and Why Bother? *Analytical Biochemistry* **285**, 235–245 (2000).

166. Ladbury, J. E. & Chowdhry, B. Z. Sensing the heat: the application of isothermal titration calorimetry to thermodynamic studies of biomolecular interactions. *Chemistry & Biology* **3**, 791–801 (1996).

167. Kuznetsova, I., Turoverov, K. & Uversky, V. What Macromolecular Crowding Can Do to a Protein. *Int. J. Mol. Sci.* **15**, 23090–23140 (2014).

168. Kuznetsova, I. M., Zaslavsky, B. Y., Breydo, L., Turoverov, K. K. & Uversky, V. N. Beyond the Excluded Volume Effects: Mechanistic Complexity of the Crowded Milieu. *Molecules* **20**, 1377–1409 (2015).

169. Kuznetsova, I. M., Sulatskaya, A. I., Povarova, O. I. & Turoverov, K. K. Reevaluation of ANS Binding to Human and Bovine Serum Albumins: Key Role of Equilibrium Microdialysis in Ligand – Receptor Binding Characterization. *PLoS ONE* **7**, 1-9 (2012).

170. Kuriyan, J., Konforti, B. & Wemmer, D. 'Molecular Recognition: The Thermodynamics of Binding'. *The Molecules of Life: Physical and Chemical Principles* 531–580 (2013).

171. Kragh-Hansen, U., Chuang, V. T. G. & Otagiri, M. Practical Aspects of the Ligand-Binding and Enzymatic Properties of Human Serum Albumin. *Biol. Pharm. Bull.* **25**, 695–704 (2002).

172. Knierbein, M. *et al.* Combined co-solvent and pressure effect on kinetics of a peptide hydrolysis: an activity-based approach. *Phys. Chem. Chem. Phys.* **21**, 22224–22229 (2019).

173. Klostermeier, D. & Rudolph, M. G. Biophysical Chemistry, (2017).

174. King, J. T., Arthur, E. J., Brooks, C. L. & Kubarych, K. J. Crowding Induced Collective Hydration of Biological Macromolecules over Extended Distances. *J. Am. Chem. Soc.* **136**, 188–194 (2014).

175. Keating, C. D. Aqueous Phase Separation as a Possible Route to Compartmentalization of Biological Molecules. *Acc. Chem. Res.* **45**, 2114–2124 (2012).

176. Kauzmann, W. Thermodynamics of unfolding. *Nature* **325**, 763–764 (1987).

177. Kauzmann, W. Some Factors in the Interpretation of Protein Denaturation. *Advances in Protein Chemistry* **14**, 1–63 (1959).

178. Jurado, E., Camacho, F., Luzón, G. & Vicaria, J. M. Kinetic models of activity for β-galactosidases: influence of pH, ionic concentration and temperature. *Enzyme and Microbial Technology* **34**, 33–40 (2004).

179. Johansson, H.-O., Karlström, G., Tjerneld, F. & Haynes, C. A. Driving forces for phase separation and partitioning in aqueous two-phase systems. *Journal of Chromatography B: Biomedical Sciences and Applications* **711**, 3–17 (1998).

180. Johansson, G. Partitioning procedures and techniques: Small molecules and macromolecules. *Methods in Enzymology* **228**, 28–42 (1994).

181. Jaenicke, R. & Závodszky, P. Proteins under extreme physical conditions. *FEBS Letters* **268**, 344–349 (1990).

182. Jaenicke, R. & Böhm, G. The stability of proteins in extreme environments. *Current Opinion in Structural Biology* **8**, 738–748 (1998).

183. Jaenicke, R. Stability and stabilization of globular proteins in solution. *Journal of Biotechnology* **79**, 193–203 (2000).

184. Iyer, P. V. & Ananthanarayan, L. Enzyme stability and stabilization—Aqueous and non-aqueous environment. *Process Biochemistry* **43**, 1019–1032 (2008).

185. Iqbal, M. *et al.* Aqueous two-phase system (ATPS): an overview and advances in its applications. *Biol. Proced. Online* **18**, 1-18 (2016).

186. Inagaki, F. *et al.* Exploring deep microbial life in coal-bearing sediment down to ~2.5 km below the ocean floor. *Science* **349**, 420–424 (2015).

187. I. Kurganov, B. Analysis of negative cooperativity for glutamate dehydrogenase. *Biophysical Chemistry* **87**, 185–199 (2000).

188. Hyman, A. A., Weber, C. A. & Jülicher, F. Liquid-Liquid Phase Separation in Biology. *Annu. Rev. Cell Dev. Biol.* **30**, 39–58 (2014).

189. Hulme, E. C. & Trevethick, M. A. Ligand binding assays at equilibrium: validation and interpretation: Equilibrium binding assays. *British Journal of Pharmacology* **161**, 1219–1237 (2010).

190. Huggins, M. L. Theory of Solutions of High Polymers [1]. *J. Am. Chem. Soc.* **64**, 1712–1719 (1942).

191. Huggins, M. L. Some Properties of Solutions of Long-chain Compounds. *J. Phys. Chem.* **46**, 151–158 (1942).

192. Huddleston, J. *et al.* The molecular basis of partitioning in aqueous two-phase systems. *Trends in Biotechnology* **9**, 381–388 (1991).

193. Huang, K.-Y. *et al.* Stability of Protein-Specific Hydration Shell on Crowding. *J. Am. Chem. Soc.* **138**, 5392–5402 (2016).

194. Huang, C. Y. Determination of binding stoichiometry by the continuous variation method: The job plot. *Methods in Enzymology* **87**, 509–525 (1982).

195. Homouz, D., Perham, M., Samiotakis, A., Cheung, M. S. & Wittung-Stafshede, P. Crowded, cell-like environment induces shape changes in aspherical protein. *Proc. Natl. Acad. Sci. U. S. A.* **105**, 11754–11759 (2008).

196. Held, C., Tsurko, E. N., Neueder, R., Sadowski, G. & Kunz, W. Cation Effect on the Water Activity of Ternary (*S*)-Aminobutanedioic Acid Magnesium Salt Solutions at 298.15 and 310.15 K. *J. Chem. Eng. Data* **61**, 3190–3199 (2016).

197. Held, C. *et al.* Cosolvent and pressure effects on enzyme-catalysed hydrolysis reactions. *Biophysical Chemistry* **252**, 106209 (2019).

198. Hei, D. J. & Clark, D. S. Pressure Stabilization of Proteins from Extreme Thermophiles. *Applied and Environmental Microbiology* **60**, 932–939 (1994).

199. Hazael, R., Meersman, F., Ono, F. & McMillan, P. F. Pressure as a Limiting Factor for Life. *Life (Basel)* **6**, 1-8 (2016).

200. Hatti-Kaul, R. Aqueous two-phase systems. *Mol. Biotechnol.* **19**, 269–277 (2001).

201. Hatters, D. M., Minton, A. P. & Howlett, G. J. Macromolecular Crowding Accelerates Amyloid Formation by Human Apolipoprotein C-II. *J. Biol. Chem.* **277**, 7824–7830 (2002).

202. Haskard, C. A. & Li-Chan, E. C. Y. Hydrophobicity of Bovine Serum Albumin and Ovalbumin Determined Using Uncharged (PRODAN) and Anionic (ANS $^{-}$) Fluorescent Probes. *J. Agric. Food Chem.* **46**, 2671–2677 (1998).

203. Harada, R., Sugita, Y. & Feig, M. Protein Crowding Affects Hydration Structure and Dynamics. *J. Am. Chem. Soc.* **134**, 4842–4849 (2012).

204. Han, J. & Herzfeld, J. Macromolecular diffusion in crowded solutions. *Biophys. J.* **65**, 1155–1161 (1993).

205. Halling, P. J. What can we learn by studying enzymes in non–aqueous media? *Phil. Trans. R. Soc. Lond. B* **359**, 1287–1297 (2004).

206. Hall, D. & Minton, A. P. Macromolecular crowding: qualitative and semiquantitative successes, quantitative challenges. *Biochimica et Biophysica Acta (BBA) - Proteins and Proteomics* **1649**, 127–139 (2003).

207. Gross, M. & Jaenicke, R. Proteins under pressure. *European Journal of Biochemistry* **221**, 617–630 (1994).

208. Gnutt, D., Gao, M., Brylski, O., Heyden, M. & Ebbinghaus, S. Excluded-Volume Effects in Living Cells. *Angew. Chem. Int. Ed.* **54**, 2548–2551 (2015).

209. Gilman-Politi, R. & Harries, D. Unraveling the Molecular Mechanism of Enthalpy Driven Peptide Folding by Polyol Osmolytes. *J. Chem. Theory Comput.* **7**, 3816–3828 (2011).

210. Ghuman, J. *et al.* Structural Basis of the Drug-binding Specificity of Human Serum Albumin. *Journal of Molecular Biology* **353**, 38–52 (2005).

211. Georgiou, M. E., Georgiou, C. A. & Koupparis, M. A. Automated Flow Injection Gradient Technique for Binding Studies of Micromolecules to Proteins Using Potentiometric Sensors: Application to Bovine Serum Albumin with Anilinonaphthalenesulfonate Probe and Drugs. *Anal. Chem.* **71**, 2541–2550 (1999).

212. Gekko, K. & Hasegawa, Y. Compressibility-structure relationship of globular proteins. *Biochemistry* **25**, 6563–6571 (1986).

213. Garlid, K. D. The State of Water in Biological Systems. *International Review of Cytology* **192**, 281–302 (1999).

214. García-Pérez, A. I. *et al.* Molecular Crowding and Viscosity as Determinants of Translational Diffusion of Metabolites in Subcellular Organelles. *Archives of Biochemistry and Biophysics* **362**, 329–338 (1999).

215. Gao, M. *et al.* Crowders and Cosolvents—Major Contributors to the Cellular Milieu and Efficient Means to Counteract Environmental Stresses. *ChemPhysChem* **18**, 2951–2972 (2017).

216. Gao, M. *et al.* Modulation of human IAPP fibrillation: cosolutes, crowders and chaperones. *Phys. Chem. Chem. Phys.* **17**, 8338–8348 (2015).

217. Galazka, V. Changes in protein-protein and protein-polysaccharide interactions induced by high pressure. *Food Chemistry* **57**, 393–398 (1996).

218. Fulton, A. B. How crowded is the cytoplasm? *Cell* **30**, 345–347 (1982).

219. Frye, K. J. & Royer, C. A. The kinetic basis for the stabilization of staphylococcal nuclease by xylose. *Protein Sci* **6**, 789–793 (1997).

220. Forciniti, D., Hall, C. K. & Kula, M. R. Analysis of polymer molecular weight distributions in aqueous two-phase systems. *Journal of Biotechnology* **20**, 151–161 (1991).

221. Forciniti, D., Hall, C. K. & Kula, M.-R. Influence of polymer molecular weight and temperature on phase composition in aqueous two-phase systems. *Fluid Phase Equilibria* **61**, 243–262 (1991).

222. Feig, M., Yu, I., Wang, P., Nawrocki, G. & Sugita, Y. Crowding in Cellular Environments at an Atomistic Level from Computer Simulations. *J. Phys. Chem. B* **121**, 8009–8025 (2017).

223. Falahati, H. & Haji-Akbari, A. Thermodynamically driven assemblies and liquid–liquid phase separations in biology. *Soft Matter* **15**, 1135–1154 (2019).

224. Ellis, R. J. Macromolecular crowding: obvious but underappreciated. *Trends in Biochemical Sciences* **26**, 597–604 (2001).

225. Ellis, R. J. & Hartl, F. U. Principles of protein folding in the cellular environment. *Current Opinion in Structural Biology* **9**, 102–110 (1999).

226. Ellis, R. J. Macromolecular crowding: an important but neglected aspect of the intracellular environment. *Curr. Opin. Struct. Biol.* **11**, 114–119 (2001).

227. Elcock, A. H. Models of macromolecular crowding effects and the need for quantitative comparisons with experiment. *Current Opinion in Structural Biology* **20**, 196–206 (2010).

228. Eisenmenger, M. J. & Reyes-De-Corcuera, J. I. High pressure enhancement of enzymes: A review. *Enzyme and Microbial Technology* **45**, 331–347 (2009).

229. Ebbinghaus, S. *et al.* An extended dynamical hydration shell around proteins. *Proceedings of the National Academy of Sciences* **104**, 20749–20752 (2007).

230. Du, X. *et al.* Insights into Protein–Ligand Interactions: Mechanisms, Models, and Methods. *Int. J. Mol. Sci.* **17**, 1-37 (2016).

231. Diamond, A. D. & Hsu, J. T. Fundamental studies of biomolecule partitioning in aqueous two-phase systems. *Biotechnol. Bioeng.* **34**, 1000–1014 (1989).

232. Davis, B. W. *et al.* Colocalization and Sequential Enzyme Activity in Aqueous Biphasic Systems: Experiments and Modeling. *Biophysical Journal* **109**, 2182–2194 (2015).

233. Daniel, I., Oger, P. & Winter, R. Origins of life and biochemistry under high-pressure conditions. *Chem. Soc. Rev.* **35**, 858-875 (2006).

234. Czeslik, C., Luong, T. Q. & Winter, R. Enzymatic activity under pressure. *MRS Bull.* **42**, 738–742 (2017).

235. Crowe, C. D. & Keating, C. D. Liquid–liquid phase separation in artificial cells. *Interface Focus* **8**, 20180032 (2018).

236. Collini, M., D'Alfonso, L. & Baldini, G. New insight on b-lactoglobulin binding sites by 1-anilinonaphthalene-8-sulfonate fluorescence decay. *Protein Sci.* **9**, 1968-1974 (2000).

237. Cohen, L. M., Eiteman, M. A. & Gainer, J. L. A Model to Predict the Partition Coefficients of Amino Acids in PEG/Salt Aqueous Two-Phase Systems. *Separation Science and Technology* **30**, 225–237 (1995).

238. Cioni, P. & Strambini, G. B. Pressure Effects on Protein Flexibility Monomeric Proteins. *Journal of Molecular Biology* **242**, 291–301 (1994).

239. Cinar, S., Cinar, H., Chan, H. S. & Winter, R. Pressure-Sensitive and Osmolyte-Modulated Liquid–Liquid Phase Separation of Eye-Lens γ-Crystallins. *J. Am. Chem. Soc.* **141**, 7347–7354 (2019).

240. Cinar, H., Cinar, S., Chan, H. S. & Winter, R. Pressure-Induced Dissolution and Reentrant Formation of Condensed, Liquid-Liquid Phase-Separated Elastomeric α-Elastin. *Chem. Eur. J.* **24**, 8286–8291 (2018).

241. Chen, C., Loe, F., Blocki, A., Peng, Y. & Raghunath, M. Applying macromolecular crowding to enhance extracellular matrix deposition and its remodeling in vitro for tissue engineering and cell-based therapies. *Advanced Drug Delivery Reviews* **63**, 277–290 (2011).

242. Chen, C. R. & Makhatadze, G. I. Molecular determinant of the effects of hydrostatic pressure on protein folding stability. *Nat. Commun.* **8**, 1–9 (2017).

243. Chalikian, T. V. Volumetric Properties of Proteins. *Annu. Rev. Biophys. Biomol. Struct.* **32**, 207–235 (2003).

244. Chalikian, T. V. Structural Thermodynamics of Hydration. *J. Phys. Chem. B* **105**, 12566–12578 (2001).

245. Chaires, J. B. Calorimetry and Thermodynamics in Drug Design. *Annu. Rev. Biophys.* **37**, 135–151 (2008).

246. Cattoni, D. I., Kaufman, S. B. & Flecha, F. L. G. Kinetics and thermodynamics of the interaction of 1-anilino-naphthalene-8-sulfonate with proteins. *Biochimica et Biophysica Acta (BBA) - Proteins and Proteomics* **1794**, 1700–1708 (2009).

247. Carlson, A. Factors Influencing the Use of Aqueous Two-Phase Partition for Protein Purification. *Separation Science and Technology* **23**, 785–817 (1988).

248. Cardamone, M. & Puri, N. K. Spectrofluorimetric assessment of the surface hydrophobicity of proteins. *Biochemical Journal* **282**, 589–593 (1992).

249. Calderon, C., Abuin, E., Lissi, E. & Montecinos, R. Effect of Human Serum Albumin on the Kinetics of 4-Methylumbelliferyl-β-D-N-N′-N″ Triacetylchitotrioside Hydrolysis Catalyzed by Hen Egg White Lysozyme. *Protein J.* **30**, 367–373 (2011).

250. Cabezas, H. Theory of phase formation in aqueous two-phase systems. *Journal of Chromatography B: Biomedical Sciences and Applications* **680**, 3–30 (1996).

251. Burg, M. B. Macromolecular Crowding as a Cell Volume Sensor. *Cell Physiol. Biochem.* **10**, 251–256 (2000).

252. Bujalowski, W. & Lohman, T. M. A general method of analysis of ligand-macromolecule equilibria using a spectroscopic signal from the ligand to monitor binding. Application to Escherichia coli single-strand binding protein-nucleic acid interactions. *Biochemistry* **26**, 3099–3106 (1987).

253. Bru, R. & Walde, P. Product inhibition of α-chymotrypsin in reverse micelles. *European Journal of Biochemistry* **199**, 95–103 (1991).

254. Bronowska, A. K. Thermodynamics of Ligand-Protein Interactions: Implications for Molecular Design. *Thermodynamics - Interaction Studies - Solids, Liquids and Gases* (2011)

255. Breydo, L. *et al.* The crowd you're in with: Effects of different types of crowding agents on protein aggregation. *Biochimica et Biophysica Acta (BBA) - Proteins and Proteomics* **1844**, 346–357 (2014).

256. Boonyaratanakornkit, B. B., Park, C. B. & Clark, D. S. Pressure effects on intra- and intermolecular interactions within proteins. *Biochimica et Biophysica Acta (BBA) - Protein Structure and Molecular Enzymology* **1595**, 235–249 (2002).

257. Bismuto, E., Gratton, E. & Lamb, D. C. Dynamics of ANS Binding to Tuna Apomyoglobin Measured with Fluorescence Correlation Spectroscopy. *Biophysical Journal* **81**, 3510–3521 (2001).

258. Berthod, A., Ruiz-Ángel, M. J. & Carda-Broch, S. Ionic liquids in separation techniques. *Journal of Chromatography A* **1184**, 6–18 (2008).

259. Berry, J., Brangwynne, C. P. & Haataja, M. Physical principles of intracellular organization via active and passive phase transitions. *Rep. Prog. Phys.* **81**, 046601 (2018).

260. Berezhkovskii, A. M. & Szabo, A. Theory of Crowding Effects on Bimolecular Reaction Rates. *J. Phys. Chem. B* **120**, 5998–6002 (2016).

261. Benton, L. A., Smith, A. E., Young, G. B. & Pielak, G. J. Unexpected Effects of Macromolecular Crowding on Protein Stability. *Biochemistry* **51**, 9773–9775 (2012).

262. Benavides, J., Rito-Palomares, M. & Asenjo, J. A. Aqueous Two-Phase Systems. *Comprehensive Biotechnology*, 697–713 (2011).

263. Batra, J., Xu, K. & Zhou, H.-X. Nonadditive effects of mixed crowding on protein stability. *Proteins* **77**, 133–138 (2009).

264. Baskir, J. N., Hatton, T. A. & Suter, U. W. Protein partitioning in two-phase aqueous polymer systems. *Biotechnol. Bioeng.* **34**, 541–558 (1989).

265. Baskir, J. N., Hatton, T. A. & Suter, U. W. Thermodynamics of the separation of biomaterials in two-phase aqueous polymer systems: effect of the phase-forming polymers. *Macromolecules* **20**, 1300–1311 (1987).

266. Barciszewski, J., Jurczak, J., Porowski, S., Specht, T. & Erdmann, V. A. The role of water structure in conformational changes of nucleic acids in ambient and high-pressure conditions: Nucleic acids at high pressure. *European Journal of Biochemistry* **260**, 293–307 (2001).

267. Banik, R. M., Santhiagu, A., Kanari, B., Sabarinath, C. & Upadhyay, S. N. Technological aspects of extractive fermentation using aqueous two-phase systems. *World J. Microbiol. Biotechnol.* **19**, 337–348 (2003).

268. Banani, S. F., Lee, H. O., Hyman, A. A. & Rosen, M. K. Biomolecular condensates: organizers of cellular biochemistry. *Nat. Rev. Mol. Cell Biol.* **18**, 285–298 (2017).

269. Bamberger, S., Brooks, D. E., Sharp, K. A., Van Alstine, J. M. & Webber, T. J. Preparation of Phase Systems and Measurement of Their Physicochemical Properties. *Partitioning in Aqueous Two-Phase System*, 85–130 (1985).

270. Balny, C., Mozhaev, V. V. & Lange, R. Hydrostatic Pressure and Proteins: Basic Concepts and New Data. *Comparative Biochemistry and Physiology Part A: Physiology* **116**, 299–304 (1997).

271. Balny, C. & Masson, P. Effects of high pressure on proteins. *Food Reviews International* **9**, 611–628 (1993).

272. Ball, P. Water as an Active Constituent in Cell Biology. *Chem. Rev.* **108**, 74–108 (2008).

273. Balcells, C. *et al.* MACROMOLECULAR CROWDING UPON IN-VIVO- LIKE ENZYME-KINETICS: EFFECT OF ENZYME- OBSTACLE SIZE RATIO. *New Journal of Chemistry* **24**, 3-16 (2015).

274. Bagatolli, L. A. *et al.* Two distinguishable fluorescent modes of 1-anilino-8-naphthalenesulfonate bound to human albumin. *J. Fluoresc.* **6**, 33–40 (1996).

275. Aumiller, W. M., Davis, B. W., Hatzakis, E. & Keating, C. D. Interactions of Macromolecular Crowding Agents and Cosolutes with Small-Molecule Substrates: Effect on Horseradish Peroxidase Activity with Two Different Substrates. *J. Phys. Chem. B* **118**, 10624–10632 (2014).

276. Atkins, P & Paula, J. de. Physical Chemistry, Oxford University Press, **9** (2009).

277. Asenjo, J. A. & Andrews, B. A. Aqueous two-phase systems for protein separation: A perspective. *Journal of Chromatography A* **1218**, 8826–8835 (2011).

278. Asenjo, J. A., Mistry, S. L., Andrews, B. A. & Merchuk, J. C. Phase separation rates of aqueous two-phase systems: Correlation with system properties. *Biotechnol. Bioeng.* **79**, 217–223 (2002).

279. Asakura, S. & Oosawa, F. On Interaction between Two Bodies Immersed in a Solution of Macromolecules. *The Journal of Chemical Physics* **22**, 1255–1256 (1954).

280. Antonov, Y. A. & Wolf, B. A. Calorimetric and Structural Investigation of the Interaction between Bovine Serum Albumin and High Molecular Weight Dextran in Water. *Biomacromolecules* **6**, 2980–2989 (2005).

281. Andrews, B. A. & Asenjo, J. A. Theoretical and Experimental Evaluation of Hydrophobicity of Proteins to Predict their Partitioning Behavior in Aqueous Two Phase Systems: A Review. *Separation Science and Technology* **45**, 2165–2170 (2010).

282. Andrews, B. A., Schmidt, A. S. & Asenjo, J. A. Correlation for the partition behavior of proteins in aqueous two-phase systems: Effect of surface hydrophobicity and charge. *Biotechnol. Bioeng.* **90**, 380–390 (2005).

283. Alberty, R. A. Thermodynamics of the binding of ligands by macromolecules. *Biophysical Chemistry* **62**, 141–159 (1996).

284. Albertsson, P.-Å. History of Aqueous Polymer Two-Phase Partition. *Partitioning in Aqueous Two-Phase Syste*, 1–10 (1985).

285. Albertsson, P.-Å. Partition of Cell Particles and Macromolecules in Polymer Two-Phase Systems. *Advances in Protein Chemistry* **24**, 309–341 (1970).

286. Alberti, S., Gladfelter, A. & Mittag, T. Considerations and Challenges in Studying Liquid-Liquid Phase Separation and Biomolecular Condensates. *Cell* **176**, 419–434 (2019).

287. Akasaka, K., Nagahata, H., Maeno, A. & Sasaki, K. Pressure acceleration of proteolysis: A general mechanism. *BIOPHYSICS* **4**, 29–32 (2008).

288. Aguzzi, A. & Altmeyer, M. Phase Separation: Linking Cellular Compartmentalization to Disease. *Trends in Cell Biology* **26**, 547–558 (2016).

289. Abe, F., Kato, C. & Horikoshi, K. Pressure-regulated metabolism in microorganisms. *Trends Microbiol.* **7**, 447–453 (1999).

Eidesstattliche Versicherung (Affidavit)

Banerjee, Sudeshna
Name, Vorname
(Surname, first name)

199457
Matrikel-Nr.
(Enrolment number)

Belehrung:

Wer vorsätzlich gegen eine die Täuschung über Prüfungsleistungen betreffende Regelung einer Hochschulprüfungsordnung verstößt, handelt ordnungswidrig. Die Ordnungswidrigkeit kann mit einer Geldbuße von bis zu 50.000,00 € geahndet werden. Zuständige Verwaltungsbehörde für die Verfolgung und Ahndung von Ordnungswidrigkeiten ist der Kanzler/die Kanzlerin der Technischen Universität Dortmund. Im Falle eines mehrfachen oder sonstigen schwerwiegenden Täuschungsversuches kann der Prüfling zudem exmatrikuliert werden, § 63 Abs. 5 Hochschulgesetz NRW.

Die Abgabe einer falschen Versicherung an Eides statt ist strafbar.

Wer vorsätzlich eine falsche Versicherung an Eides statt abgibt, kann mit einer Freiheitsstrafe bis zu drei Jahren oder mit Geldstrafe bestraft werden, § 156 StGB. Die fahrlässige Abgabe einer falschen Versicherung an Eides statt kann mit einer Freiheitsstrafe bis zu einem Jahr oder Geldstrafe bestraft werden, § 161 StGB.

Die oben stehende Belehrung habe ich zur Kenntnis genommen:

Official notification:

Any person who intentionally breaches any regulation of university examination regulations relating to deception in examination performance is acting improperly. This offence can be punished with a fine of up to EUR 50,000.00. The competent administrative authority for the pursuit and prosecution of offences of this type is the chancellor of the TU Dortmund University. In the case of multiple or other serious attempts at deception, the candidate can also be unenrolled, Section 63, paragraph 5 of the Universities Act of North Rhine-Westphalia.

The submission of a false affidavit is punishable.

Any person who intentionally submits a false affidavit can be punished with a prison sentence of up to three years or a fine, Section 156 of the Criminal Code. The negligent submission of a false affidavit can be punished with a prison sentence of up to one year or a fine, Section 161 of the Criminal Code.

I have taken note of the above official notification.

Dortmund,
Ort, Datum
(Place, date)

Unterschrift
(Signature)

Titel der Dissertation:
(Title of the thesis):

Role of Aqueous Two-Phase Systems in Modulating the Kinetics and Dynamics of Biological Processes.

Ich versichere hiermit an Eides statt, dass ich die vorliegende Dissertation mit dem Titel selbstständig und ohne unzulässige fremde Hilfe angefertigt habe. Ich habe keine anderen als die angegebenen Quellen und Hilfsmittel benutzt sowie wörtliche und sinngemäße Zitate kenntlich gemacht.
Die Arbeit hat in gegenwärtiger oder in einer anderen Fassung weder der TU Dortmund noch einer anderen Hochschule im Zusammenhang mit einer staatlichen oder akademischen Prüfung vorgelegen.

I hereby swear that I have completed the present dissertation independently and without inadmissible external support. I have not used any sources or tools other than those indicated and have identified literal and analogous quotations.

The thesis in its current version or another version has not been presented to the TU Dortmund University or another university in connection with a state or academic examination.*

*Please be aware that solely the German version of the affidavit ("Eidesstattliche Versicherung") for the PhD thesis is the official and legally binding version.

Ort, Datum
(Place, date)

Unterschrift
(Signature)

Copyright Clearance Center Marketplace™

Royal Society of Chemistry - License Terms and Conditions

Order Date	15-Jan-2020
Order license ID	1013573-1
ISSN	1364-548X
Type of Use	Republish in a thesis/dissertation
Publisher	ROYAL SOCIETY OF CHEMISTRY
Portion	Chapter/article

LICENSED CONTENT

Publication Title	Chemical communications	**Country**	United Kingdom of Great Britain and Northern Ireland
Author/Editor	Royal Society of Chemistry (Great Britain)	**Rightsholder**	Royal Society of Chemistry
Date	01/01/1996	**Publication Type**	e-Journal
Language	English		

REQUEST DETAILS

Portion Type	Chapter/article	**Rights Requested**	Main product
Page range(s)	1-4	**Distribution**	Worldwide
Total number of pages	4	**Translation**	Original language of publication
Format (select all that apply)	Print, Electronic	**Copies for the disabled?**	No
Who will republish the content?	Author of requested content	**Minor editing privileges?**	No
Duration of Use	Life of current edition	**Incidental promotional use?**	No
Lifetime Unit Quantity	Up to 499	**Currency**	EUR

NEW WORK DETAILS

Title	Role of Aqueous Two-Phase Systems in Modulating the Kinetics and Dynamics of Biological Processes	**Institution name**	TU Dortmund University
		Expected presentation date	2020-02-03
Instructor name	Roland Winter		

ADDITIONAL DETAILS

Order reference number	N/A	**The requesting person / organization to appear on the license**	Sudeshna Banerjee

REUSE CONTENT DETAILS

Title, description or numeric reference of the portion(s)	Modulation of enzymatic activity by aqueous two-phase systems and pressure – rivalry between kinetic constants	**Title of the article/chapter the portion is from**	N/A
		Author of portion(s)	Royal Society of Chemistry (Great Britain)
Editor of portion(s)	N/A	**Issue, if republishing an article from a serial**	N/A

Volume of serial or monograph	N/A	**Publication date of portion**	1996-01-01
Page or page range of portion	1-4		

PUBLISHER SPECIAL TERMS AND CONDITIONS

Permission is granted as long as the article is fully acknowledged and a link is given back to the article on our Platform. Please go to rsc.li/permissions for details. Please note that if the material specified above or any part of it appears with credit or acknowledgement to a third party then you must also secure permission from that third party before reproducing that material.

CCC Republication Terms and Conditions

1. Description of Service; Defined Terms. This Republication License enables the User to obtain licenses for republication of one or more copyrighted works as described in detail on the relevant Order Confirmation (the "Work(s)"). Copyright Clearance Center, Inc. ("CCC") grants licenses through the Service on behalf of the rightsholder identified on the Order Confirmation (the "Rightsholder"). "Republication", as used herein, generally means the inclusion of a Work, in whole or in part, in a new work or works, also as described on the Order Confirmation. "User", as used herein, means the person or entity making such republication.

2. The terms set forth in the relevant Order Confirmation, and any terms set by the Rightsholder with respect to a particular Work, govern the terms of use of Works in connection with the Service. By using the Service, the person transacting for a republication license on behalf of the User represents and warrants that he/she/it (a) has been duly authorized by the User to accept, and hereby does accept, all such terms and conditions on behalf of User, and (b) shall inform User of all such terms and conditions. In the event such person is a "freelancer" or other third party independent of User and CCC, such party shall be deemed jointly a "User" for purposes of these terms and conditions. In any event, User shall be deemed to have accepted and agreed to all such terms and conditions if User republishes the Work in any fashion.

3. Scope of License; Limitations and Obligations.

    3.1. All Works and all rights therein, including copyright rights, remain the sole and exclusive property of the Rightsholder. The license created by the exchange of an Order Confirmation (and/or any invoice) and payment by User of the full amount set forth on that document includes only those rights expressly set forth in the Order Confirmation and in these terms and conditions, and conveys no other rights in the Work(s) to User. All rights not expressly granted are hereby reserved.

    3.2. General Payment Terms: You may pay by credit card or through an account with us payable at the end of the month. If you and we agree that you may establish a standing account with CCC, then the following terms apply: Remit Payment to: Copyright Clearance Center, 29118 Network Place, Chicago, IL 60673-1291. Payments Due: Invoices are payable upon their delivery to you (or upon our notice to you that they are available to you for downloading). After 30 days, outstanding amounts will be subject to a service charge of 1-1/2% per month or, if less, the maximum rate allowed by applicable law. Unless otherwise specifically set forth in the Order Confirmation or in a separate written agreement signed by CCC, invoices are due and payable on "net 30" terms. While User may exercise the rights licensed immediately upon issuance of the Order Confirmation, the license is automatically revoked and is null and void, as if it had never been issued, if complete payment for the license is not received on a timely basis either from User directly or through a payment agent, such as a credit card company.

    3.3. Unless otherwise provided in the Order Confirmation, any grant of rights to User (i) is "one-time" (including the editions and product family specified in the license), (ii) is non-exclusive and non-transferable and (iii) is subject to any and all limitations and restrictions (such as, but not limited to, limitations on duration of use or circulation) included in the Order Confirmation or invoice and/or in these terms and conditions. Upon completion of the licensed use, User shall either secure a new permission for further use of the Work(s) or immediately cease any new use of the Work(s) and shall render inaccessible (such as by deleting or by removing or severing links or other locators) any further copies of the Work (except for copies printed on paper in accordance with this license and still in User's stock at the end of such period).

    3.4. In the event that the material for which a republication license is sought includes third party materials (such as photographs, illustrations, graphs, inserts and similar materials) which are identified in such material as having been used by permission, User is responsible for identifying, and seeking separate

licenses (under this Service or otherwise) for, any of such third party materials; without a separate license, such third party materials may not be used.

3.5. Use of proper copyright notice for a Work is required as a condition of any license granted under the Service. Unless otherwise provided in the Order Confirmation, a proper copyright notice will read substantially as follows: "Republished with permission of [Rightsholder's name], from [Work's title, author, volume, edition number and year of copyright]; permission conveyed through Copyright Clearance Center, Inc. " Such notice must be provided in a reasonably legible font size and must be placed either immediately adjacent to the Work as used (for example, as part of a by-line or footnote but not as a separate electronic link) or in the place where substantially all other credits or notices for the new work containing the republished Work are located. Failure to include the required notice results in loss to the Rightsholder and CCC, and the User shall be liable to pay liquidated damages for each such failure equal to twice the use fee specified in the Order Confirmation, in addition to the use fee itself and any other fees and charges specified.

3.6. User may only make alterations to the Work if and as expressly set forth in the Order Confirmation. No Work may be used in any way that is defamatory, violates the rights of third parties (including such third parties' rights of copyright, privacy, publicity, or other tangible or intangible property), or is otherwise illegal, sexually explicit or obscene. In addition, User may not conjoin a Work with any other material that may result in damage to the reputation of the Rightsholder. User agrees to inform CCC if it becomes aware of any infringement of any rights in a Work and to cooperate with any reasonable request of CCC or the Rightsholder in connection therewith.

4. Indemnity. User hereby indemnifies and agrees to defend the Rightsholder and CCC, and their respective employees and directors, against all claims, liability, damages, costs and expenses, including legal fees and expenses, arising out of any use of a Work beyond the scope of the rights granted herein, or any use of a Work which has been altered in any unauthorized way by User, including claims of defamation or infringement of rights of copyright, publicity, privacy or other tangible or intangible property.

5. Limitation of Liability. UNDER NO CIRCUMSTANCES WILL CCC OR THE RIGHTSHOLDER BE LIABLE FOR ANY DIRECT, INDIRECT, CONSEQUENTIAL OR INCIDENTAL DAMAGES (INCLUDING WITHOUT LIMITATION DAMAGES FOR LOSS OF BUSINESS PROFITS OR INFORMATION, OR FOR BUSINESS INTERRUPTION) ARISING OUT OF THE USE OR INABILITY TO USE A WORK, EVEN IF ONE OF THEM HAS BEEN ADVISED OF THE POSSIBILITY OF SUCH DAMAGES. In any event, the total liability of the Rightsholder and CCC (including their respective employees and directors) shall not exceed the total amount actually paid by User for this license. User assumes full liability for the actions and omissions of its principals, employees, agents, affiliates, successors and assigns.

6. Limited Warranties. THE WORK(S) AND RIGHT(S) ARE PROVIDED "AS IS". CCC HAS THE RIGHT TO GRANT TO USER THE RIGHTS GRANTED IN THE ORDER CONFIRMATION DOCUMENT. CCC AND THE RIGHTSHOLDER DISCLAIM ALL OTHER WARRANTIES RELATING TO THE WORK(S) AND RIGHT(S), EITHER EXPRESS OR IMPLIED, INCLUDING WITHOUT LIMITATION IMPLIED WARRANTIES OF MERCHANTABILITY OR FITNESS FOR A PARTICULAR PURPOSE. ADDITIONAL RIGHTS MAY BE REQUIRED TO USE ILLUSTRATIONS, GRAPHS, PHOTOGRAPHS, ABSTRACTS, INSERTS OR OTHER PORTIONS OF THE WORK (AS OPPOSED TO THE ENTIRE WORK) IN A MANNER CONTEMPLATED BY USER; USER UNDERSTANDS AND AGREES THAT NEITHER CCC NOR THE RIGHTSHOLDER MAY HAVE SUCH ADDITIONAL RIGHTS TO GRANT.

7. Effect of Breach. Any failure by User to pay any amount when due, or any use by User of a Work beyond the scope of the license set forth in the Order Confirmation and/or these terms and conditions, shall be a material breach of the license created by the Order Confirmation and these terms and conditions. Any breach not cured within 30 days of written notice thereof shall result in immediate termination of such license without further notice. Any unauthorized (but licensable) use of a Work that is terminated immediately upon notice thereof may be liquidated by payment of the Rightsholder's ordinary license price therefor; any unauthorized (and unlicensable) use that is not terminated immediately for any reason (including, for example, because materials containing the Work cannot reasonably be recalled) will be subject to all remedies available at law or in equity, but in no event to a payment of less than three times the Rightsholder's ordinary license price for the most closely analogous licensable use plus Rightsholder's and/or CCC's costs and expenses incurred in collecting such payment.

8. Miscellaneous.

8.1. User acknowledges that CCC may, from time to time, make changes or additions to the Service or to these terms and conditions, and CCC reserves the right to send notice to the User by electronic mail or

otherwise for the purposes of notifying User of such changes or additions; provided that any such changes or additions shall not apply to permissions already secured and paid for.

8.2. Use of User-related information collected through the Service is governed by CCC's privacy policy, available online here: https://marketplace.copyright.com/rs-ui-web/mp/privacy-policy

8.3. The licensing transaction described in the Order Confirmation is personal to User. Therefore, User may not assign or transfer to any other person (whether a natural person or an organization of any kind) the license created by the Order Confirmation and these terms and conditions or any rights granted hereunder; provided, however, that User may assign such license in its entirety on written notice to CCC in the event of a transfer of all or substantially all of User's rights in the new material which includes the Work(s) licensed under this Service.

8.4. No amendment or waiver of any terms is binding unless set forth in writing and signed by the parties. The Rightsholder and CCC hereby object to any terms contained in any writing prepared by the User or its principals, employees, agents or affiliates and purporting to govern or otherwise relate to the licensing transaction described in the Order Confirmation, which terms are in any way inconsistent with any terms set forth in the Order Confirmation and/or in these terms and conditions or CCC's standard operating procedures, whether such writing is prepared prior to, simultaneously with or subsequent to the Order Confirmation, and whether such writing appears on a copy of the Order Confirmation or in a separate instrument.

8.5. The licensing transaction described in the Order Confirmation document shall be governed by and construed under the law of the State of New York, USA, without regard to the principles thereof of conflicts of law. Any case, controversy, suit, action, or proceeding arising out of, in connection with, or related to such licensing transaction shall be brought, at CCC's sole discretion, in any federal or state court located in the County of New York, State of New York, USA, or in any federal or state court whose geographical jurisdiction covers the location of the Rightsholder set forth in the Order Confirmation. The parties expressly submit to the personal jurisdiction and venue of each such federal or state court.If you have any comments or questions about the Service or Copyright Clearance Center, please contact us at 978-750-8400 or send an e-mail to support@copyright.com.

v 1.1